Evolution and function of RHO cell polarity signalling in plants

Hugh Mulvey

St Edmund Hall

Department of Plant Sciences

University of Oxford

Thesis submitted for the degree of Doctor of Philosophy

Trinity 2022

Evolution and function of RHO cell polarity signalling in plants

Hugh Mulvey

St Edmund Hall

Department of Plant Sciences

University of Oxford

Thesis submitted for the degree of Doctor of Philosophy

Trinity 2022

Abstract

Since their origin from a unicellular ancestor 630–890 million years ago, the streptophytes, which comprise streptophyte algae and land plants, have evolved mechanisms to develop morphologically complex body plans. Much remains unknown about how such mechanisms evolved and how they regulate plant morphogenesis. To start, I hypothesise that cell polarity signalling, which can spatially regulate fundamental cellular processes like growth and division, contributed to morphological evolution in the streptophytes. In this context, the aim of this thesis is to investigate the evolution and function of RHO Of Plant (ROP) signalling, the plant specific form of the ancient eukaryotic RHO cell polarity signalling. First, I report phylogenetic and sequence analyses resulting in the discovery that ROP signalling genes became established early in the streptophyte lineage, during the period when multicellular filamentous body plans are believed to have evolved from unicellular/colonial forms. Second, by functionally characterising the single *ROP* gene in the liverwort *Marchantia polymorpha*, I demonstrate that ROP protein regulates the morphogenesis of complex plant tissues by controlling cell growth, division, and possibly adhesion. Finally, through a series of cross-species complementation experiments with *M. polymorpha rop* mutants, I show that ROP function has remained largely conserved since the time land plants last shared a common ancestor with the filamentous streptophyte algae, *Klebsormidium nitens.* Collectively, the findings from this thesis reveal that an ancient signalling mechanism which became established early in the streptophyte lineage is required for the morphogenesis of complex tissues in extant land plants. They also indicate a potential role of ROP signalling function in the morphological evolution of early streptophytes.

Acknowledgements

I would first like to thank my primary supervisor, Professor Liam Dolan, for proposing an exciting project and giving me the opportunity to put my own stamp on it. I have greatly appreciated his continuous guidance and encouragement.

I would also like to thank my second supervisor, Professor Jane Langdale, for invaluable feedback and helpful advice on my work.

My thanks also go to everyone who has been part of the Dolan group over the past four years, for help in the lab and generous feedback during lab meetings. In the Oxford group, special thanks to Dr Anna Thamm for advice on molecular cloning, Dr Sandy Hetherington for teaching me phylogenetics, and Helen Prescott and Lida Chen for running the lab. In the Vienna group, special thanks to Kathi Jandrasits and Dr Magda Mosiolek for managing lab matters. I am also very grateful to Kathi for taking excellent care of my plants.

Former colleagues at Oxford also helped me enormously, especially Dr Charlotte Kirchhelle, who taught me so much about microscopy and image analysis. Thank you, also, to Professor Hugh Dickinson for showing me how to use the scanning electron microscope and for helpful discussions about my project, which I greatly enjoyed and miss here in Vienna.

Meanwhile, in Vienna, I have benefited greatly from the BioOptics Facility, and I thank Dr Pawel Pasierbek and Dr Alberto Moreno Cencerrado for their constant help on the confocal microscopes, and Dr Thomas Lendl for advice on image analysis. I would also like to acknowledge the GMI lab support team for helping us move from Oxford to Vienna, and the media kitchen for preparing media.

I am grateful, too, to the Haseloff lab for sharing the OpenPlant toolkit and the plasma membrane reporter line.

I thank the UKRI Biotechnology and Biological Sciences Research Council (BBSRC) and the European Research Council (ERC) for funding my studies. I am also thankful to Professor Gail Preston for her work with the Interdisciplinary Bioscience DTP and for providing continued support after the move to Vienna.

Finally, I would like to thank my family – my mother, for letting me live with her in Oxford, rent-free, meals included, and for keeping my spirits up through tough times, and my father, for his encouragement and years of effort to teach me English, before and after I left Japan aged 13, without which I probably would not have been able to write this thesis.

Thank you all.

Table of Contents

List of figures

Chapter 1: General introduction

1.1 Body plan complexity generally increased during streptophyte evolution, the genetic basis of which is poorly understood

1.1.1 Morphological complexity evolved independently in different lineages

Life on Earth exhibits diverse forms – from relatively simple unicellular organisms, like bacteria, yeast, and some algae, to complex multicellular organisms like animals and land plants with elaborate morphology. Morphological complexity evolved independently in different eukaryotic lineages (Knoll, 2011). Just within plants, broadly defined here to encompass all Archaeplastida, complex multicellular body plans evolved independently in rhodophytes (red algae), chlorophytes, and streptophytes (Umen, 2014). How complex organisms evolved from simple unicellular ancestors, and the genetic basis for these transitions, is an outstanding question in evolutionary developmental biology (Carroll, 2008). My thesis will specifically focus on the streptophytes, the lineage which includes the morphologically most complex plants, the land plants.

1.1.2 Defining plant morphological (body plan) complexity

First, I will define some aspects of "complexity" in the context of plant morphological (body plan) evolution, because there is no consensus definition of "complexity" (Adami, 2002). There are different levels of morphological complexity, both in overall form and composition.

- Overall form: A unicellular organism is less complex than a multicellular organism. Within multicellular organisms, a filamentous body plan, where cells are linked in a linear chain with a single axis (1D) is the least complex. This is followed by branching filaments, a 2D mat or sheet like body plan, composed of a single cell layer, and a 3D body plan, composed of multiple cell layers, in increasing order of complexity.
- Composition: Multicellular organisms can be composed of different cell types. The number of cell types can be considered a measure of morphological complexity (Valentine et al., 1994). Composition can also be considered at the tissue or organ level – body plan complexity increases with the number of tissue and organ types which make up the body.

The overall form of an organism and its composition are not independent of each other because the way in which the different cells/tissues/organs are arranged determines the final form of an organism. This spatial organisation is what allows division of labour, greatly increasing the functional capabilities of morphologically complex organisms. Therefore, morphological complexity refers to both the overall form of an organism as well as its composition, and different levels of morphological complexity exists.

1.1.3 Phylogenetic relationships within plants have been clarified recently because of the availability of extensive sequence data and advanced phylogenetic models

To study how morphological traits evolved, comparative approaches are widely used whereby traits of different extant species are compared to make inferences about their most recent or last common ancestor (Delaux et al., 2019). To make meaningful inferences, having an accurate understanding of the phylogenetic relationship between different species is a prerequisite (Puttick et al., 2018). Many of the phylogenies for the major plant lineages proposed in the past are now considered inaccurate. It is only in the last few years, thanks to increased availability of genomic/transcriptomic sequence data from a broad taxa and advanced phylogenetic models, that plant species relationships have been resolved with greater certainty (Donoghue et al., 2021). This has aided in making more robust inferences about the evolution of morphological traits such as the stomata (Harris et al., 2020). It is therefore imperative to establish an accurate understanding of plant phylogeny before studying how morphological complexity evolved in the streptophytes. Below, I summarise our current understanding of phylogenetic relationship within the Archaeplastida.

1.1.4 The Streptophyta comprises the paraphyletic streptophyte algae and the monophyletic land plants

The Archaeplastida are organisms with primary plastids. They originated through the primary endosymbiosis between a photosynthetic cyanobacterium and a heterotrophic eukaryotic host 1.6–2.1 billion years ago (Sánchez-Baracaldo et al., 2017). The Archaeplastida comprises three main lineages – the rhodophytes (red algae), the glaucophytes, and the Viridiplantae (the green plants).

The Viridiplantae and glaucophytes form a sister group relationship based on recent nuclear phylogenomic studies (Irisarri et al., 2022; Leebens-Mack et al., 2019). The Viridiplantae thought to have first emerged 670–972 million years ago (mya), are split into chlorophyte and streptophyte clades (Morris et al., 2018). The chlorophytes consist entirely of algae, whilst the streptophytes consist of the paraphyletic streptophyte algae and the monophyletic land plants. Within the land plants, which emerged 475–515 mya, the monophyly of tracheophytes (vascular plants) has been long accepted, however, its precise relationship to the bryophytes has remained unclear until recently (Morris et al., 2018). Based on recent phylogenomic studies, the current consensus is that bryophytes are monophyletic and liverworts and mosses form a sister group relationship (Harris et al., 2020; Leebens-Mack et al., 2019; Puttick et al., 2018). Within the streptophyte algae, the Zygnematales are considered the closet relatives to land plants, contrary to some previous beliefs (Morris et al., 2018). Streptophyte algae most distantly related to land plants belong to the *Mesostigma* and *Chlorokybus* lineages. The phylogenetic relationship of these two linages has also been debated in the past, some suggesting that *Chlorokybus* are more closely related to land plants than *Mesostigma*, but the current consensus is that these two lineages form a monophyletic group and hence are equally distantly related to land plants (Irisarri et al., 2021; Lemieux et al., 2007). To summarise, many phylogenetic relationships within plants have been recently clarified, which allows us to make inferences about trait evolution with greater confidence.

1.1.5 Innovations associated with complex streptophyte body plan evolution mostly emerged after the divergence of Klebsormidiales

There has been a general increase in morphological complexity within the streptophytes, with lineages more closely related to land plants showing greater level of morphological complexity (Fig. 1.01). The exception is the Zygnematales lineage, where morphological complexity has been secondarily lost (Rensing, 2020). This suggests that morphological complexity increased in the streptophyte lineage in a stepwise manner. Assessing the presence/absence of cellular features in extant streptophytes from different lineages have allowed inferences to be made about innovations which facilitated body plant evolution, some of which I have annotated in Fig. 1.01.

The transition from a unicellular/colonial to a filamentous body plan likely involved alterations in cell growth mechanisms and cell wall composition, to restrict cell growth to a single axis and to allow cells to remain adhered after division. Unlike cells of *Mesostigma* and *Chlorokybus* which are globular, *Klebsormidium* cells are more cuboidal and grow by polarised diffuse growth, as observed in other streptophytes (Buschmann, 2020). *Mesostigma* and *Klebsormidium* also clearly differ in their cell coverings, the former having calcified scales instead of a cellulosic cell wall (Manton & Ettl, 1965). However, there is currently limited indication of cell wall compositional differences between *Chlorokybus* and *Klebsormidium* (Mikkelsen et al., 2021; O'Rourke et al., 2015). Both have limited cellulose content, which contrasts with that of Charales, Coleochaetales and Zygnematales, which have land plant like cell walls (Sørensen et al., 2011). It is also unknown if cellulose synthase complexes in *Chlorokybus* and Klebsormidiales form a rosette confirmation like in Charales, Coleochaetales, Zygnematales, and land plants, or a linear confirmation like in chlorophytes (Haigler & Roberts, 2019). Therefore, there is a poor understanding of innovations which mediated the transition from a unicellular/colonial to a filamentous body plan in the streptophytes.

There are many cellular innovations which are predicted to have evolved after the divergence of the Klebsormidiales and before the divergence of the Charales. The most notable is the phragmoplast, which gives the name to the monophyletic clade comprising Charales, Coleochaetales, Zygnematales, and land plants (Phragmoplastophyta). The transition from the cleavage mechanism to a phragmoplast based cytokinesis is believed to have given ancestral streptophytes greater control over cell division orientation (Buschmann & Zachgo, 2016; Pickett-Heaps et al., 1999). The ability to alter cell division orientation likely contributed to the formation of parenchymatous tissue as seen in extant Coleochaetales. It may also be responsible for the advent of asymmetric cell division, which is associated with cell differentiation. Cell differentiation of vegetative cells is observed in the Phragmoplastophyta but not in the other streptophyte lineages (Graham et al., 2000). For example, rhizoids and seta cells are specialised cells found in *Chara* and *Coleochaete*, respectively (Buschmann, 2020). Finally, the innovation of

plasmodesmata allowed neighbouring cells to communicate, share resources and coordinate (Graham et al., 2000; Mikhailyuk et al., 2014). Therefore, there are numerous innovations thought to have evolved in the last common ancestor of Phragmoplastophyta which likely contributed to the evolution of morphological complexity. However, the genetic basis for these innovations is not understood.

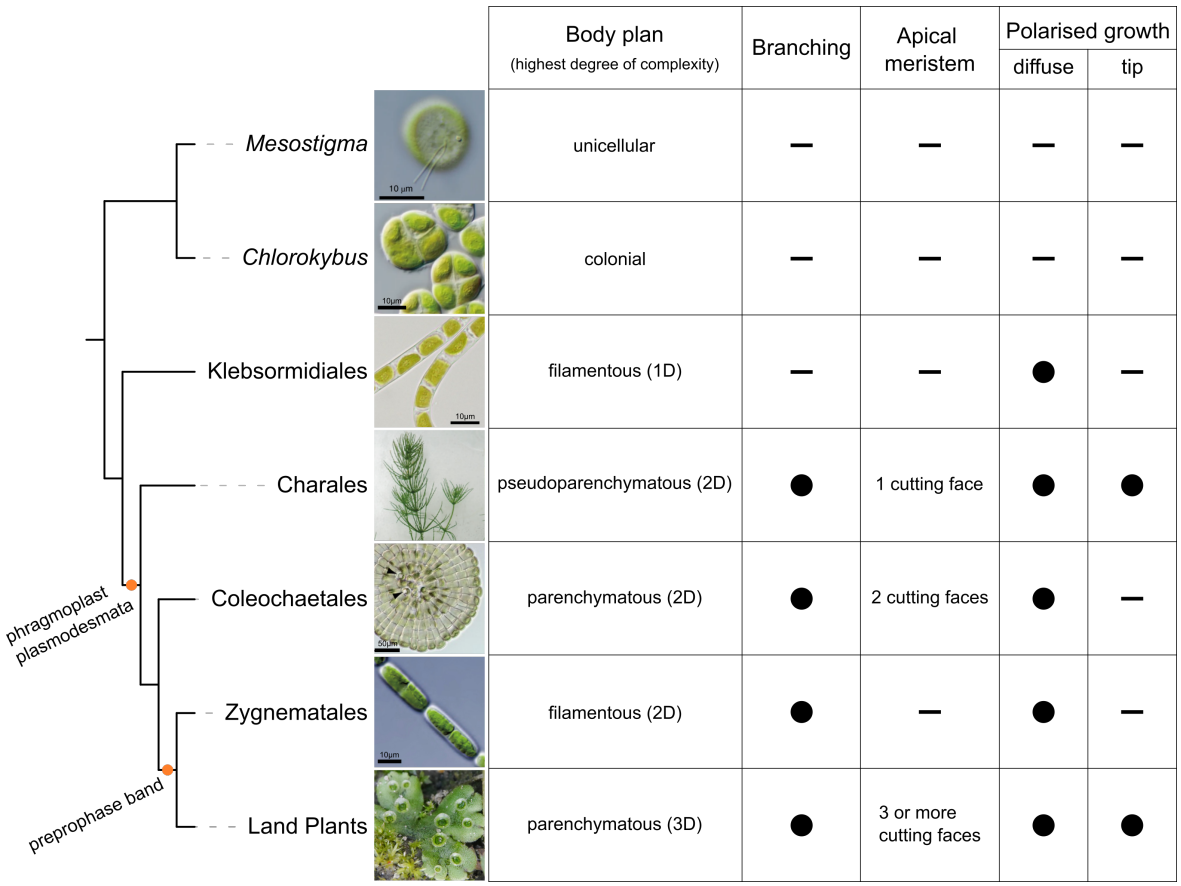

Body plan (highest degree of complexity)	Branching	Apical meristem	Polarised growth	
			diffuse	tip
unicellular	—	—	—	—
colonial	—	—	—	—
filamentous (1D)	—	—	●	—
pseudoparenchymatous (2D)	●	1 cutting face	●	●
parenchymatous (2D)	●	2 cutting faces	●	—
filamentous (2D)	●	—	●	—
parenchymatous (3D)	●	3 or more cutting faces	●	●

Figure 1.01 Morphological complexity generally increased in the streptophyte lineage which gave rise to the land plants

Current consensus on the phylogenetic relationship within the streptophytes based on Leebens-Mack et al., 2019 and Puttick et al., 2018. Cellular innovations associated with the emergence of the Phragmoplastophyta as well as with the last common ancestor of land plants and Zygenmatales are marked on respective nodes. In the table, circle represents presence of the trait, whilst horizontal bar represents lack of evidence for the given trait. For lineages in which apical meristems have been described, the maximum number of cutting faces reported is noted. Images are from the following sources: *Mesostigma viride* and *Chlorokybus atmophyticus* (Wang et al., 2020); *Klebsormidium nitens* (genome project website), *Chara* (Barbosa et al., 2021), *Coleochaete orbicularis* (Graham et al., 2012), *Mesotaenium endlicherianum* (S. Cheng et al., 2019), *Marchantia polymorpha* (ukrbin.com).

1.1.6 Genetic basis for land plant body plan evolution is starting to be understood

Within the streptophytes, the distinguishing morphological feature of land plants is their complex 3D body plan derived from an apical stem cell with three or more cutting faces (Buschmann, 2020; Graham et al., 2000; Moody, 2020). Apical stem cells with up to two cutting faces have been identified in streptophyte algae, but ones with three or more cutting faces are unique to land plants. To gain insight into the genetic basis of the 2D to 3D transition, the moss *Physcomitrium patens* has attracted attention, as gametophore initiation during its development represents a transition from a 2D to a 3D body plan (Harrison, 2017; Moody, 2019). The APB transcription factors are considered master regulators of the 2D–3D transition, as these are expressed in the gametophore apical cells and the loss of APB function abolishes gametophore initiation (Aoyama et al., 2012). Numerous other genes such as Pp*DEK1*, Pp*NOG1* and those involved in CLAVATA signalling have been implicated in the transition to 3D growth in *P. patens* (Moody et al., 2018; Perroud et al., 2014; Whitewoods et al., 2018). Gametophore development is arrested or defective when these genes are mutated due to defects in cell division orientation, highlighting the importance of regulating cell division orientation for the morphogenesis of complex 3D tissues. Thus, through studies in *P. patens*, a genetic understanding for the evolution of 3D body plans is starting to be developed.

To summarise, there has been a general increase in morphological complexity in the streptophyte lineage leading to the land plants. Based on comparative studies of extant streptophyte species, some cellular innovations potentially associated with the evolution of morphological complexity have been suggested, however, the genetic basis of these is poorly understood, especially for innovations in early streptophytes.

1.2 Cell polarity signalling was likely critical for evolution of morphological complexity in the streptophytes

Based on our current understanding of body plan evolution in streptophytes reviewed above, enhanced control over cell growth and division patterns was likely important for increasing

morphological complexity. For example, the innovation of the phragmoplast may have allowed alterations in cell division orientation and asymmetric cell divisions to take place. However, the phragmoplast is only part of the machinery which executes cytokinesis and on its own cannot specify the orientation or position of the division plane. Therefore, a mechanism to signal positional information was likely just as important for the evolution of morphological complexity in the streptophytes. In this regard, cell polarity signalling could have played a pivotal role.

1.2.1 Cell polarity regulates cell differentiation and patterning

Cell polarity refers to the asymmetric distribution of subcellular components that make up a cell, which often translates into asymmetry in cell shape. The nature of cell polarity is defined by its orientation, sense (i.e. direction), and magnitude (Whitewoods & Coen, 2017). Numerous polarity proteins which define cell polarity have been identified in land plants, mostly in *Arabidopsis thaliana*, and these play important roles in cell differentiation and patterning. For example, in the stomatal lineage, BASL is polar localised to one side of the meristemoid mother cell (MMC) and is required for MMC polarisation (Dong et al., 2009). In the *A. thaliana basl* loss of function mutant, MMC can divide symmetrically, instead of asymmetrically as in wild-type (WT), and stomata can be derived from both or neither of the resulting daughter cells, unlike in WT where a stoma forms only from the smaller daughter cell. Hence BASL polarity function is required for stomatal differentiation and patterning. Polarity proteins, such as IRK, SOSEKI and ROP are implicated in specifying cell division orientation as their mis-expression, mis-regulation or loss of function results in defective cell division patterns in *A. thaliana* roots (Campos et al., 2020; Stöckle et al., 2016; Yoshida et al., 2019). ROP is also required for focussing polarised cell growth to a single site, critical for differentiation of cells such as root hairs (Carol et al., 2005; Jones et al., 2002). Finally, some polarity proteins are involved in setting up the plant body axis. For example, PIN proteins polar localised to the apical side of the basal cell of the *A. thaliana* embryo promote auxin accumulation in the apical cell, specifying apical identity (Friml et al., 2003). Hence, polarity proteins convey spatial information to regulate cell growth and division patterns important for cell differentiation and patterning.

1.2.2 Many cell polarity proteins are lineage-specific

For polarity proteins identified in *A. thaliana* to have played a role in the evolution of morphological complexity, they must have been present in ancestral streptophytes. Intriguingly, many of these polarity proteins are lineage specific. BASL is dicot-specific, IRK – potentially angiosperm-specific, and SOSEKI – land plant specific (Nir et al., 2022; Ramalho et al., 2022; van Dop et al., 2020). Similarly in animals, the PAR proteins best known for their role in *C. elegans* zygote polarisation are animal specific, indicating that many polarity signalling genes evolved independently in different lineages (Goldstein & Macara, 2007).

1.2.3 PIN may be associated with the evolution of 2D and 3D body plans

PIN proteins are conserved throughout most streptophytes and given that auxin signalling regulates diverse developmental processes in land plants, it is likely that PIN evolution contributed to body plan evolution in streptophytes (Bennett, 2015; Wang et al., 2020). However, algal and land plant PIN sequences are dissimilar (Bennett et al., 2014). Consistently, although *Klebsormidium nitens* PIN localises to the plasma membrane like canonical land plant PIN proteins, it does not exhibit polar subcellular localisation, unlike canonical land plant PIN proteins. Kn*PIN* is also unable to complement *A. thaliana pin* mutants, unlike bryophyte *PIN* genes, suggesting that PIN polarity function evolved after the divergence of the Klebsormidiales (Skokan et al., 2019; Y. Zhang et al., 2020). Intercellular polar auxin transport by PIN may have contributed to morphological innovations associated with 2D or 3D body plans but is unlikely to have facilitated earlier innovations.

1.2.4 Precise ROP origin is unknown

ROP (short for **R**HO **O**f **P**lants) proteins are conserved throughout land plants and they are reported to form a plant specific subfamily of the RHO GTPase (Boureux et al., 2007; Fowler, 2010; Zheng & Yang, 2000). RHO GTPase itself is conserved throughout most eukaryotes (Elias, 2008). RHO proteins in animals and fungi also signal cell polarity, indicating that the cell polarity function of ROP has an ancient origin (Etienne-Manneville & Hall, 2002). However, it is unclear when ROP first emerged from the ancestral RHO as past ROP evolutionary studies have focused

only on land plants (Christensen et al., 2003; Fowler, 2010). The functional distinction between ROP and ancestral RHO is also unknown. Depending on the timing of its origin, ROP may have played a role in streptophyte body plan evolution. Investigating the evolutionary origin of ROP signalling is the subject of chapters 2 and 4. In the following sections, I provide a more in-depth introduction of RHO signalling and review our current understanding of RHO function.

1.3 RHO signalling is a robust, yet flexible, mechanism which encodes subcellular spatial information

1.3.1 Discovery of RHO and its polarity function

RHO together with Ras, Rab, Ran, and Arf, form the Ras superfamily of small GTPases (Wennerberg et al., 2005). The *Rho* gene was first discovered in 1985 in the marine snail *Aplysia* (Madaule & Axel, 1985). It was name *Rho*, which stands for ***R****as* ***ho****mologous*, because the deduced protein sequence shared several homologous regions with the human H-Ras protein. The importance of RHO for cell polarity was first revealed in 1990, with the isolation of a temperature sensitive *Saccharomyces cerevisiae cdc42* mutant, which is unable to polarise the actin cytoskeleton for bud formation (i.e. unable to form a polarised outgrowth) and instead swells isotropically under the non-permissive condition (Adams et al., 1990; Johnson & Pringle, 1990). The plant *RHO* gene was first cloned in *Pisum sativum* (pea) and its cell polarity function was genetically confirmed in *A. thaliana* (Li et al., 1999; Yang & Watson, 1993). Since then, many *RHO* genes have been identified in a diverse range of eukaryotes (Elias, 2008). Consequently, the *RHO* gene family has been phylogenetically split into sub-families, the most notable ones in the opisthokonts (which includes animals and fungi) being *Rho*, *CDC42* and *Rac* (Boureux et al., 2007). To avoid confusion, I use capitalised *RHO* to refers to the *RHO* family in general, and *Rho* to refer to the *Rho* subfamily. Since the seminal work in the budding yeast demonstrating *RHO* function in cell polarity, understanding of *RHO* function has greatly advanced.

1.3.2 RHO acts as a molecular signalling switch which encodes sub-cellular spatial information

The general molecular mechanism of RHO signalling is broadly conserved within eukaryotes. As a small GTPase, RHO proteins slowly catalyse the hydrolysis of GTP to GDP (Vetter & Wittinghofer, 2001). Crucially, the GTP- and GDP-bound conformations of RHO differ, and this allows GTP-bound RHO to specifically interact with downstream effectors which promote cell polarisation (Etienne-Manneville & Hall, 2002). In this regard, RHO can be considered as a molecular signalling switch – ON/active when bound to GTP and OFF/inactive when bound to GDP. The critical difference with transcription factors (TFs), which can also in some instances be considered as an ON/OFF switch that regulates cell differentiation, is that TFs specify ON/OFF status at the cellular level, whilst RHO signalling does this at the sub-cellular level. For proper cell polarisation, it is vital that the subcellular distribution of the GDP- and GTP-bound RHO are tightly regulated. This is achieved by three main classes of RHO regulators (Fig. 1.02, Etienne-Manneville & Hall, 2002). Guanine Exchange Factor (GEF) promotes the formation of GTP-bound RHO, by catalysing the exchange of GDP for GTP, and hence activates RHO signalling. In contrast, GTPase Activating Protein (GAP) promotes the formation of GDP-bound RHO by enhancing the hydrolysis of GTP to GDP, and hence deactivates RHO signalling. Finally, the Guanine-nucleotide Dissociation Inhibitor (GDI) suppresses RHO signalling by inhibiting the dissociation of GDP from RHO. Below, I review in greater detail how RHO and its regulators establish cell polarity.

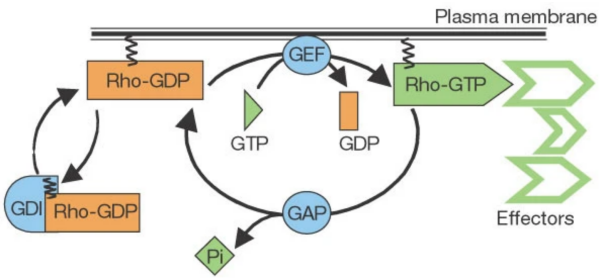

Figure 1.02 RHO signalling is regulated by GEF, GAP, and GDI (figure from Etienne-Manneville & Hall, 2002)
Guanine Exchange Factor (GEF) promotes RHO signalling by catalysing the formation of GTP-bound RHO, which can interact with downstream effectors. Guanine Activating Protein (GAP) suppresses RHO signalling by accelerating GTP hydrolysis by RHO, promoting the formation of GDP-bound RHO, which cannot interact with effectors. Guanine-nucleotide Dissociation Inhibitor (GDI) suppresses RHO signalling by actively sequestering plasma membrane bound RHO to the cytosol.

1.3.3 RHO together with its regulators establishes the cell polarity axis

The cortical site at which active RHO locally accumulates defines the polarity site and this in turn determines the cell polarity axis which orients cellular processes such as growth and division. How this asymmetric distribution of RHO is established is best understood in *S. cerevisiae* (Bi & Park, 2012; Chiou et al., 2017). Here I describe our current understanding of RHO polarity establishment in *S. cerevisiae* and plants.

Positive feedback involving GEF establishes RHO polarity

Polarity domain establishment in *S. cerevisiae* initiates with plasma membrane localised active CDC42 (i.e. GTP-bound) recruiting one of its effectors, PAK. PAK is held in a complex with CDC24 (GEF for CDC42) by the scaffolding protein Bem1 (Butty et al., 2002; Irazoqui et al., 2003; Kozubowski et al., 2008). Consequently, CDC24 is also recruited to the same cortical site. The recruited CDC24 activates more CDC42, which in turn recruits more CDC24 (Kozubowski et al., 2008). This positive feedback mechanism can amplify the initial slight asymmetric distribution of GTP-CDC42, resulting in GTP-CDC42 accumulating at a single cortical site (Woods & Lew, 2019). Therefore, positive feedback loop involving RHO and GEF contribute to the establishment of RHO polarity site.

Consistent with the requirement of both RHO and GEF for polarity establishment, Sc*cdc42* and Sc*cdc24* single mutants both grow isotropically, instead of initiating polarised outgrowth for budding (Adams et al., 1990; Hartwell et al., 1973). Similarly in *A. thaliana*, both *rop2 rop4* and *ropgef3 ropgef4* double mutants almost completely lack root hairs, indicating that ROP and RopGEF are required for establishing the polar growth axis (Denninger et al., 2019). ROP polar localisation in trichoblasts is RopGEF dependent, and RopGEF polar localisation is partially ROP dependent, which is consistent with positive feedback between ROP and RopGEF. In tip growing pollen tubes, positive feedback between ROP and RopGEF has also been suggested (Hwang et al., 2010; Luo et al., 2017).

Negative feedback involving GAP keeps RHO polarity domain in check

If the positive feedback mechanism which recruits polarity proteins continues in an uncontrolled manner, the cortical polarity domain would continue to expand and lose its focus. A negative feedback loop between CDC42 and GAP has been suggested, whereby active CDC42 recruits GAP which in turn deactivates CDC42 (Chiou et al., 2017). Since GAPs accelerate the conversion of GTP-bound CDC42 to GDP-bound CDC42, it ensures that CDC42 does not remain in the active conformation for too long as CDC42 diffuses away from the polarity site, confining the size of the polarity domain. In *A. thaliana* pollen tubes, loss of function in REN1, a GAP, results in a broader ROP polarity domain and balloon-like tubes, indicating that GAPs in plants are also required for restricting ROP polarity domain size (Hwang et al., 2008). As REN1 is believed to be delivered to the pollen tube tip via ROP mediated exocytosis, a negative feedback mechanism whereby active ROP recruits REN has been proposed.

GDI ensures selection of a single RHO polarity site

To define a cell axis, a single polarity domain must be selected to distinguish one side of the cell from the other. In WT *S. cerevisiae*, multiple CDC42 polarity sites can initially form but through positive feedback, one site outcompetes the others, resulting in the establishment of a single polarity domain (Howell et al., 2012). In the *rdi1* mutant lacking functional GDI, this competition

between polarity sites fail to take place, resulting in multiple buds (Wu et al., 2015). As GDI actively sequesters RHO from the plasma membrane, Wu et al. proposed that GDI allows the dynamic cycling of RHO between the plasma membrane and the cytosol, which aids the single dominant polarity domain to outcompete the rest through positive feedback. Similarly in *A. thaliana*, loss of function mutation in *SCN1*, which encodes a GDI, results in multiple root hair grow sites initiated on trichoblasts instead of one as in WT (Carol et al., 2005). This therefore suggests that GDI function for selecting a single polarity site is conserved between fungi and plants.

1.3.4 Intrinsic and extrinsic cues can orient RHO polarity axis but is not required for polarity establishment

Through interactions with its regulators, it is clear that RHO can specify a cortical polarity site. But how is the position of this site selected in the first place?

Intrinsic cue

In the case of budding *S. cerevisiae*, landmark proteins deposited to the cortex in the previous cell cycle determine the future RHO polarity site. For example, in diploid *S. cerevisiae*, the landmark protein BUD8 is deposited to the distal pole away from the bud scar in the daughter cell (Harkins et al., 2001). BUD8 indirectly recruits CDC24, and through the CDC24-CDC42-PAK positive feedback mechanism, the polarity site at the distal pole of the daughter cell is established (Chant & Herskowitz, 1991; Chiou et al., 2017; Kang et al., 2001).

No such landmark proteins specifying ROP polarity sites have been found in plants. There are, however, indications that a similar system exists. In trichoblasts which have not initiated tip growth, RopGEF3 polar localises to the future site of hair formation, before ROP (Denninger et al., 2019). The initial RopGEF3 polar localisation is unaffected in *rop* mutants indicating that the initial recruitment of RopGEF to the polarity site is independent of ROP. It is therefore possible that RopGEF3 is initially recruited to the polarity site by a landmark protein.

Extrinsic cue

As well as intrinsic spatial cues like landmark proteins, extrinsic cues can also guide RHO polarity site selection. Instead of budding, haploid *S. cerevisiae* can produce a polarised outgrowth known as a mating projection or shmoo, in response to perception of mating pheromone released by another haploid cell (Merlini et al., 2013). At the site of pheromone perception by cell surface receptors, the scaffolding protein Far1, bound to CDC24, is recruited (Butty et al., 1998). Through the same positive feedback mechanism as for bud site selection, a single CDC42 polarity site is established at the cortical site where there is the greatest level of pheromone perception (Merlini et al., 2013). This ensures that shmoo polarised growth is oriented towards the mate.

Similarly in plants, the ROP polarity domain, which specifies the site of pollen tube tip growth can be influenced by an extrinsic cue. The tip localised receptor PRK6 is required for reorienting pollen tube tip growth in response to LURE1 peptide secreted from the female gametophyte (Takeuchi & Higashiyama, 2016). PRK6 interacts with RopGEF proteins which activate ROP1 for tip growth. Therefore, extrinsic cues can feed into RHO mediated polarity establishment to ensure that the polarity axis is oriented appropriately with respect to the external environment.

No cue

In the absence of intrinsic positional cues (e.g. landmark signalling mutants), *S. cerevisiae* can still polarise, in a random orientation with respect to the bud scar, so long as the core RHO signalling machinery is present (Bender & Pringle, 1989). The phenomenon where the CDC42 polarity domain is established spontaneously/*de novo* from an initial state lacking polarity, can be explained by the Gierer-Meinhardt activator-substrate model, an extension of the Turing mechanism of *de novo* pattern formation (Meinhardt, 2012; Turing, 1952). In the activator-substrate model, there are two interacting substances – a slowly diffusing activator, and a rapidly diffusing substrate, both initially distributed homogenously. Applied to a single cell system, the model states that an activator which promotes further production of itself (i.e. positive feedback) at the expense of the substrate, will become polar localised when the substrate level is limited. In the case of *S.*

cerevisiae, GTP-CDC42 can be considered the activator and GDP-CDC42 the substrate. In early G1, GTP-CDC42 is distributed homogenously in the plasma membrane (Gulli et al., 2000). A stochastic local increase in GTP-CDC42 level is sufficient to trigger the local accumulation of GTP-CDC42, according to a computational model which takes into account the positive feedback interaction between CDC42 and the PAK.Bem1.CDC24 complex (Goryachev & Pokhilko, 2008). Crucially, membrane associated GTP-CDC42 diffuses much slower than cytoplasmic GDP-CDC42 (Woods & Lew, 2019). Hence the rate at which cytoplasmic GDP-CDC42 becomes incorporated and converted to GTP-CDC42 by CDC24 at the polarity site, is greater than the rate at which plasma membrane associated GTP-CDC42 diffuses out laterally, resulting in local accumulation of GTP-CDC42. A similar Turing mechanism has been proposed to self-organise the active ROP domain in trichoblasts for root hair tip growth (Payne & Grierson, 2009). Hence, positional cues merely bias where the initial stochastic local increase in GTP-RHO takes place and thereby influence RHO polarity orientation but are not required for RHO polarity establishment.

In the absence of extrinsic positional cues (i.e. pheromone present but without a gradient) or in mutants incapable of responding to the extrinsic positional cue (e.g. *far1* mutant), shmoo formation happens at the incipient bud site marked by landmark proteins (Dorer et al., 1995). This demonstrates the presence of a hierarchy in terms of positional cues. When extrinsic and intrinsic cues are both present, the extrinsic cue is favoured but in the absence of extrinsic cue, the intrinsic, default cue is followed. In the absence of both, polarity site is selected randomly, *de novo*.

To summarise, the general molecular mechanism of RHO signalling is analogous in plants and opisthokonts and RHO regulators are vital in proper RHO polarity establishment. Together with RHO, GEF promotes polarisation, and GAP and GDI stabilise the polarity domain. These core regulators allow RHO polarity domain to self-organise and establish cell polarity *de novo*, however, the RHO polarity axis can also be oriented by positional cues. It is therefore a robust, yet flexible, signalling system which encodes spatial information. As such, it is natural to hypothesise that the RHO signalling system could have been co-opted for morphological evolution in the streptophytes. Consistent with ROP being a plant specific subfamily of RHO, some GAPs and

GEFs are plant specific. The evolutionary origins of some ROP specific regulators are unknown and this is investigated in chapter 2. Next, I review the cellular processes regulated by RHO signalling.

1.4 RHO signalling was likely co-opted independently in different eukaryotic lineages to regulate cellular processes important for morphogenesis

ROP proteins have been implicated in regulating many cellular processes – such as pathogen response signalling – some of which are unrelated to its polarity function (Feiguelman et al., 2018). In this section, I focus on reviewing RHO cellular functions directly linked to morphogenesis, namely cell growth, division, and adhesion. Although plants regulate these cellular processes through distinct mechanisms from other eukaryotes, the involvement of RHO is a common theme.

1.4.1 Polarised cell growth

The fundamental mechanism of cellular morphogenesis associated with cell polarisation is the same in fungi, plants, and other eukaryotes with a cell wall. After the site(s) of polarised growth is selected, local modification of the cell wall allows the uniform/isotropic turgor pressure within the cell to promote anisotropic growth (Geitmann & Ortega, 2009). For tip focussed anisotropic growth, RHO regulation of the actin cytoskeleton has been shown to be vital. For example, in *S. cerevisiae*, CDC42 recruits the formin Bni1 to the cortical polarity site, which nucleates actin monomers to form actin cables (Evangelista et al., 1997, 2002). Myosin V transports vesicles along these actin cables, delivering cell wall remodelling enzymes to the polarity site (Schott et al., 2002). Vesicle fusion to the plasma membrane is achieved by the exocyst complex. EXO70, a subunit of the exocyst complex is also a CDC42 effector, ensuring that polar exocytosis happens at the polarity site (Wu et al., 2010). Therefore, through regulating actin nucleation and exocytosis at the polarity site, CDC42 controls bud emergence.

Actin organisation in tip growing plant cells differ slightly from that in fungi. Instead of dense actin patches, like at the growing *S. cerevisiae* shmoo apex, fine actin filaments are found at the apex of pollen tubes and root hairs (Geitmann & Emons, 2000). In *A. thaliana* pollen tubes, ROP1,

through its effector RIC4, is predicted to regulate tip growth by promoting the assembly of these fine actin filaments at the tube apex (Fu et al., 2001; Gu et al., 2005). The dominant negative *rop2* mutation inhibits root hair tip growth and this has been attributed to the loss of fine actin filaments at the root hair apex (Jones et al., 2002). In the moss *P. patens*, actin organisation and tip growth are also disrupted in *rop* mutants (Burkart et al., 2015; Yi & Goshima, 2020). Therefore, although precise actin organisation differs between fungi and plants, RHO controls tip growth through regulating the actin cytoskeleton in both groups of organisms.

Cortical microtubules, involved in regulating tip growth have also been associated with ROP. Unlike AtROP2 which localises at the root hair apex to promote tip growth, AtROP10 localises to the shank (Hirano et al., 2018). Here, it is proposed to regulate the formation of microtubule arrays, parallel to the long axis, which in turn is expected to promote xylan deposition to harden the shank secondary cell wall. Hence, ROP likely regulates tip growth by controlling both actin and microtubule cytoskeleton organisation.

ROP regulates polarised diffuse growth as well as tip growth. Diffuse cell growth is a unique growth form in plants, where growth happens across the whole cell surface instead of it being focused to a single cortical site (Braidwood et al., 2014). Diffuse growth can be polarised if cell wall stiffness is anisotropic. The defining cytoskeletal feature of diffuse growing plant cells is the parallel arrangement of cortical microtubule arrays oriented perpendicular to the cell growth axis (Hamada, 2014). Cellulose synthase travels along these microtubule arrays, locally stiffening the cell wall to restrict cell growth in the orientation parallel to the microtubule arrays (Paredez et al., 2006). ROP regulation of the cytoskeleton for diffuse growth has been studies in a range of *A. thaliana* cell types such as trichomes (Yanagisawa et al., 2018) and hypocotyl cells (Fu et al., 2009) but is best understood in pavement cells, where different ROP proteins function antagonistically to form the jigsaw puzzled shaped cells. AtROP2 and AtROP4 act redundantly at the lobe outgrowth sites to promote RIC4 mediated actin assembly required for outgrowth, and inhibit RIC1 mediated cortical microtubule organisation which would otherwise restrict outgrowth (Fig. 1.03B, Fu et al., 2005). Conversely, between the indented neck regions of the pavement cells,

AtROP6 promotes RIC1 mediated formation of parallel microtubule arrays by activating the microtubule severing enzyme Katanin, and REN excludes AtROP2 and AtROP4 from the indented regions (Fu et al., 2009; Lauster et al., 2022; D. Lin et al., 2013). Therefore, ROPs regulate polarised diffuse cell growth through controlling the organisation of both actin and microtubule cytoskeleton.

1.4.2 Cell division

Although fungal and plant cell cytokinesis is different, RHO is involved in both. Cytokinesis in *S. cerevisiae* happens through the constriction of the actin ring at the bud neck and the formation of the septum cell wall (Bi & Park, 2012). ScRho1 is required for formin-mediated actin ring assembly (Tolliday et al., 2002). It is also required for directing polar exocytosis to the bud neck, for delivering enzymes such as chitin synthase for septum formation (Wloka & Bi, 2012). In contrast to Rho1, CDC42 function is required indirectly for cytokinesis. When grown at the restrictive temperature (RT) from the G1 cell cycle stage, temperature sensitive *cdc42* mutant fails to undergo cytokines, however, when grown at the RT from metaphase, cytokinesis happens successfully, indicating that CDC42 function before mitosis is required for cell division (Tolliday et al., 2002). Polar localised CDC42 at late G1 recruits septin for the assembly of the septin ring at the pre-bud site, and this later at the end of mitosis acts as a scaffold for actin ring assembly (Iwase et al., 2006). Therefore, RHO regulation of the actin and septin cytoskeleton, before as well as during cytokinesis is required for cell division in *S. cerevisiae*.

Plants, unique amongst eukaryotes, lack septin, and most streptophyte cells divide through the centrifugal expansion of the phragmoplast, a cytoskeletal structure made of actin and microtubules (Livanos & Müller, 2019). This contrasts with the cleavage type division in fungi and animals. Additionally, in land plants and some Zygnematales, a pre-prophase band (PPB) composed predominantly of microtubules, marks the future cortical division zone of some cells (Buschmann & Zachgo, 2016). ROP signalling has been implicated in orienting cell division as loss of REN function causes misaligned PPB and phragmoplast in *A. thaliana* root cells, resulting in abnormal cell division orientations (Fig. 1.03D, Stöckle et al., 2016). REN together with the mitosis specific

kinesin, POK1, is believed to regulate microtubule organisation for specifying division orientation. Cell division defects have also been reported for *rop* mutants. Asymmetric cell division of maize *rop2/+ rop9/rop9* double mutant subsidiary cells, and *P. patens rop2 rop3 rop4* triple mutant protonema are defective (Humphries et al., 2011; Yi & Goshima, 2020). In both cases, ROP has been suggested to direct actin mediated nuclear migration to asymmetrically position the nucleus before division. Therefore, although division mechanisms in land plants are unique compared to fungi, RHO in plants are also involved in regulating cell division.

1.4.3 Cell adhesion

Cell adhesion between animal cells is mediated by transmembrane proteins, whilst in plants, this is thought to be mediated via cell wall polysaccharides, such as pectin (Atakhani et al., 2022). In animal epidermal cells, transmembrane cadherin proteins from neighbouring cells link up with one another to form adherens junctions (Alberts et al., 2015). RHO regulation of the actin cytoskeleton is required for establishing adherens junctions (Hall, 1998). The molecular mechanism for cell adhesion in plants is not as well understood as in animals, however, there is evidence that actin and RHO are also important for plant cell adhesion. Mutants defective in actin nucleation as well as ROP signalling display cell adhesion defects. For example, the *P. patens rop* RNAi mutant with reduced expression of all four *ROP* genes produce protonema which break apart into single cells under mild sonication, unlike WT protonema which remain intact (Burkart et al., 2015). Similarly, loss of function mutation in the *GGB* gene, which encodes a prenylation enzyme required for post-translational modification of ROP for its plasma membrane anchoring, causes protonema cell adhesion defects (Sorek et al., 2011; Thole et al., 2014). The GEF protein SPIKE1 is also required for cell adhesion as its loss of function in *A. thaliana* results in gaps appearing in between leaf epidermal cells (Basu et al., 2008; Qiu et al., 2002). Thus, although cell adhesion mechanisms completely differ in animals and plants, RHO function and the actin cytoskeleton are implicated in both.

To summarise, RHO signalling controls cellular morphological processes through organising the cytoskeleton. Regulation of the actin cytoskeleton is likely an ancestral RHO function which has

remained conserved since plants last shared a common ancestor with opisthokonts. However, how RHO precisely regulates cellular processes such as cell growth, division, and adhesion differ between plants and opisthokonts, suggesting that RHO signalling was recruited independently to regulate these processes (i.e. convergent evolution). This is consistent with the belief that the last common ancestor of opisthokonts and plants were unicellular eukaryotes, and that morphological complexity evolved independently among plants and opisthokonts. It is tempting to speculate that the capabilities of the ancestral RHO signalling machinery primed it for its independent co-option into a range of fundamental cellular processes. Overall, this adds weight to the hypothesis that RHO signalling was co-opted for evolution of morphological complexity in streptophytes.

1.5 It is unclear how RHO regulates morphogenesis of complex body plans in extant streptophytes

If RHO formed part of the genetic basis for the evolution of morphological complexity in streptophytes, one would expect RHO signalling in extant streptophytes to regulate the morphogenesis of complex tissue. However, there is very limited evidence of this. First, RHO function has not been characterised for any streptophyte algal species. Although genomes of many streptophyte algal spices have been sequenced recently, no genetically tractable system has been established to date, hence there is virtually no mechanistic understanding of their development, let alone how RHO signalling contributes to their morphogenesis. Most of our understanding of RHO function in streptophytes comes from genetic studies in *A. thaliana*. Although cellular level defects are evident in *A. thaliana rop* mutants, morphogenesis at the tissue level is not significantly affected even in higher order *rop* mutants (Fig. 1.03, Gendre et al., 2019; Schepetilnikov et al., 2017; Xu et al., 2010). This could be due to genetic redundancy because no *A. thaliana* mutant lacking all 11 *ROP* genes has ever been generated. A recent study has shown that a *P. patens* mutant lacking all four *ROP* genes produces clumps of spherical protonema cells, instead of filamentous branching protonema as in WT, supporting the hypothesis that RHO function is important for tissue level morphogenesis (Cheng et al., 2020). However, RHO functional studies in *P. patens* have focussed on the filamentous protonema stage, which is a relatively simple body

plan compared to the 3D leafy gametophore which develops later. It is therefore unclear how RHO function contributes to the morphogenesis of complex 3D tissues, characteristic of land plants. How RHO function regulates the morphogenesis of complex plant tissues is investigated in chapter 3.

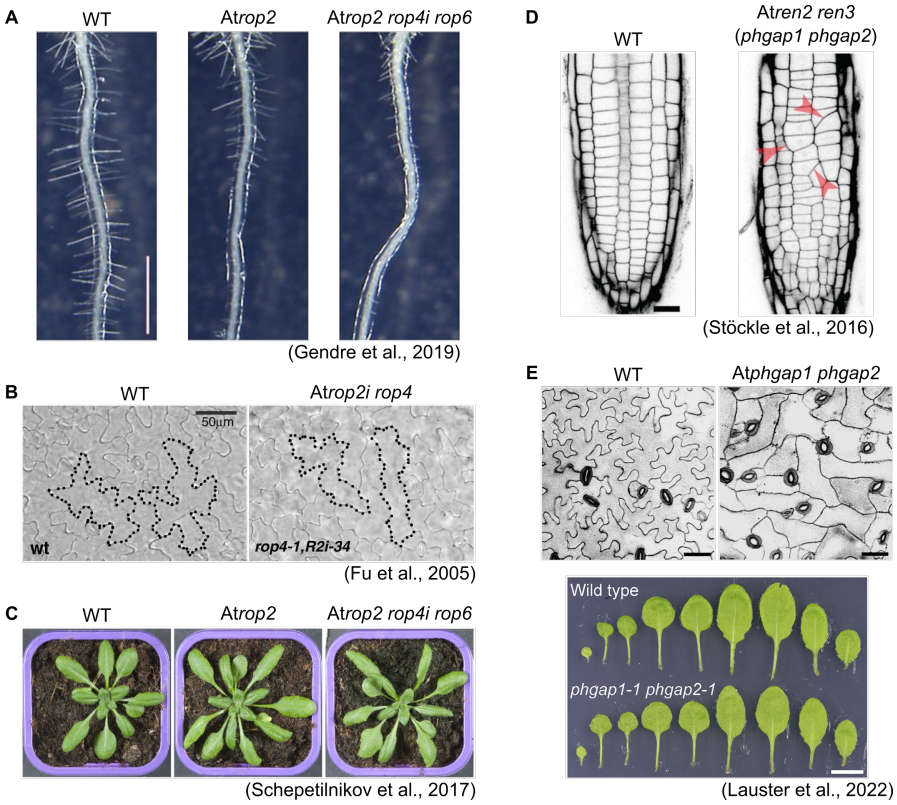

Fiugre 1.03 Cellular morphogenesis is defective in *Arabidopsis thaliana rop* and *ren* loss of function mutants, however, tissue level morphogenesis is not severely impaired
At*rop* mutants (A-C) and At*ren* mutants (D and E).
(A) Compared to WT, root hairs are slightly shorter in At*rop2* single mutant and much shorter in At*rop2 rop4i rop6* triple mutant (*rop2* and *rop6*: T-DNA knockout mutant alleles; *rop4*: RNAi knockdown allele). No noticible defects in overall primary root development (Gendre et al., 2019).
(B) Pavement cell lobe outgrowth is defective in At*rop2i rop4* double mutant (*rop2*: RNAi knodown; *rop4*: T-DNA knockout) (Fu et al., 2005).
(C) No notible defects in overall shoot morphology of single and higher order *rop* mutants. Same mutant alleles as in A (Schepetilnikov et al., 2017).
(D) Abnormal cell division orientation in At*ren2 ren3* double mutant root (both T-DNA mutant alleles) (Stöckle et al., 2016).
(E) Pavement cell morphology is defective in At*ren2 ren3* double mutant, due to loss of growth suppression at the indented neck regions. However, overall cotyledon and leaf morphologies are not severely impaired (Lauster et al., 2022).

1.6 Summary and thesis plan

Since the emergence of the first streptophytes 630–890 mya (Morris et al., 2018), morphological complexity gradually increased in the lineage which gave rise to the land plants. The genetic basis for body plan evolution in the streptophytes is poorly understood, especially for the early streptophytes. Given that increased capacity to regulate cell growth and division patterns was likely critical, it is plausible that cell polarity signalling was co-opted for morphological evolution in the streptophytes. In particular, the plant specific form of RHO signalling, ROP signalling, could have played a part. RHO signalling is a robust and versatile molecular signalling mechanism which encodes subcellular spatial information. It regulates cell growth, division, and adhesion in both plants and opisthokonts, albeit through varying mechanisms, suggesting independent co-option of RHO signalling in different eukaryotic lineages for regulating fundamental cellular morphological processes. How ROP signalling evolved from the ancestral RHO signalling is unknown. Furthermore, although ROP functions at the molecular and cellular levels are well characterised, how it contributes to the morphogenesis of complex tissues is unclear.

To investigate the role of ROP signalling evolution and function in the morphological evolution of streptophytes, I investigate in this thesis:

- The evolution of ROP signalling genes (chapter 2)
- The role of the *ROP* gene in the morphogenesis of complex tissues (chapter 3)
- The ancestral ROP signalling function in morphogenesis (chapter 4)

Chapter 2: ROP signalling genes became established early in the streptophyte lineage

2.1 Abstract

RHO signalling is an ancient mechanism essential for cell polarity signalling in eukaryotes. Since its origin in early eukaryotes, RHO signalling has evolved independently in different lineages. Consequently, RHO signalling in plants is distinct from that in other eukaryotes like animals and fungi and have therefore been termed RHO Of Plant (ROP) signalling. It is unknown how or when features specifically associated with ROP signalling evolved. Here, I report phylogenetic and sequence analyses for ROP proteins and ROP-specific regulator proteins from a diverse range of Archaeplastida species, to determine how the transition from ancestral RHO to modern ROP took place. I demonstrate that the *ROP* gene was established early in the streptophyte lineage, sometime after the divergence of the *Mesostigma*/*Chlorokybus* lineage and before the divergence of the Klebsormidiales. I also show that this event coincided with the evolution of two ROP specific regulators, RopGAP and REN. As all the other know core ROP regulators have a more ancient origin, this period early in the streptophyte lineage represents when ROP signalling became established.

2.2 Introduction

RHO GTPase proteins, encoded by *RHO* genes, are conserved amongst eukaryotes, and play a fundamental role in signalling cell polarity (Etienne-Manneville & Hall, 2002). The presence of *RHO* genes throughout most of the eukaryotic tree of life and its absence in prokaryotes indicate that the *RHO* gene originated early in the eukaryotic lineage (Boureux et al., 2007; Dong et al., 2007; Elias, 2008). Since this ancient origin, RHO signalling has evolved independently in different eukaryotic lineages. Hence RHO proteins in plants and their distant eukaryotic relatives, such as animals and fungi, differ in several ways. Due to these differences, RHO in plants are termed ROP, for RHO Of Plant (or RHO-related proteins from Plant) (Zheng & Yang, 2000).

ROP is unique from RHO in animals and fungi. Previous phylogenetic analyses of *RHO* genes in eukaryotes have consistently shown that *ROP* genes constitute a monophyletic clade (Boureux et al., 2007; Brembu et al., 2006; Winge et al., 2000; Zheng & Yang, 2000). This contrasts with *RHO*

genes of animals and fungi, which together constitute multiple distinct clades, which each represent *RHO* subfamilies such as *Rac* and *CDC42*. Consistent with ROP proteins being phylogenetically distinct from animal and fungal RHO proteins, there are unique sequence motifs conserved specifically among ROP proteins (Berken & Wittinghofer, 2008). In addition, some of the proteins which spatially regulate ROP activity, necessary for proper cell polarity signalling, are unique to plants. These include RopGEF (also known as PRONE-GEF), which activates ROP, and RopGAP and REN-GAP, which deactivate ROP (Berken et al., 2005; Hwang et al., 2008; Wu et al., 2000). Both RopGEF and RopGAP have been shown to act efficiently on ROP but not on human Rho proteins *in vitro*, confirming that these are ROP specific regulators (Fricke & Berken, 2009; Wu et al., 2000). However, the origin of these ROP-specific regulators, and of ROP itself, is poorly understood. Therefore, although there are multiple pieces of evidence highlighting how RHO signalling in plants differs from that in animals and fungi, it is unclear how and when this ancestral signalling mechanism emerged in plants and what impact this had on plant evolution.

Past phylogenetic analyses on *ROP* genes have provided insight into the evolutionary relationship of *ROP* genes in different land plant species. With an emphasis on angiosperm species, they have been particularly useful for understanding the course of *ROP* gene evolution in angiosperms (Christensen et al., 2003; Fowler, 2010). For example, these studies indicate the presence of at least four *ROP* genes in the last common ancestor of angiosperms, and that the *ROP* gene family subsequently continued to expand independently in dicots and monocots. The presence of *ROP* homologues in the moss *Physcomitrium patens* also suggested that *ROP* is at least as ancient as land plants. However, they were precluded from making further evolutionary inferences about the origin of *ROP*, due to the lack of sequence information from a range of plant taxa, most notably the streptophyte algae. Therefore, although previous phylogenetic studies illustrated the relatively recent expansion patterns of the *ROP* gene family, they were insufficient for investigating the origin of the *ROP* gene.

Since the publication of the last comprehensive *ROP* phylogenetic analysis more than a decade ago (Fowler, 2010), the number of plant species with their genome and or transcriptome sequenced

have increased enormously. Crucially, genomic/transcriptomic information for a much broader range of plant species, not limited to land plants but spanning many of the major lineages within the Archaeplastida, is now available (Leebens-Mack et al., 2019). It is therefore possible to phylogenetically examine the evolutionary history of the *ROP* gene family with much greater taxonomic breadth than before, providing an opportunity to investigate the origin of ROP signalling.

To investigate the evolutionary origin of ROP signalling, I have conducted phylogenetic and sequence analyses of ROP and ROP-specific regulators, utilising the recently published genomes and transcriptomes of a diverse range of Archaeplastida species. I demonstrate that ROP has remained highly conserved from early in the streptophyte lineage and that this was accompanied by the emergence of two ROP specific regulators. Thus, the establishment of ROP signalling far predates the origin of land plants and coincides with the proposed timing for the origin of multicellular body plan in streptophytes. This potentially signifies a role for ROP signalling in the evolution of plant body plan complexity.

2.3 Materials and Methods

2.3.1 Sequence identification and validation

To identify RHO homologues in Archaeplastida species with published genome assemblies, the *M. polymorpha* ROP amino acid sequence was used as the query sequence in tBLASTn and BLASTp searches in genome/CDS and protein databases, respectively, detailed in Table 2.01. For species distantly related to *M. polymorpha*, RHO homologues from closer relatives were also used as query sequences. Where possible, gene models (in terms of intron-exon boundaries) predicted in CDS and protein databases were checked against transcriptome databases (through BLAST or examining transcript reads mapped to the genome in genome browsers) and incorrect gene models were manually corrected. Through comparison with homologous genes, the annotated translation start site was also corrected for several *RHO* genes.

For species with unannotated genomes (e.g. *Chlorokybus atmophyticus*), tBLASTn searches were performed on both genome and transcriptome databases to accurately predict the number of *RHO* homologues and the gene model for each. To identify RHO homologues in species with only published transcriptome assemblies, tBLASTn searches were performed in transcriptome databases, detailed in Table 2.01 and Table 2.02. When genome, CDS, protein, or transcriptome databases of interest were not available on online BLAST servers, the datasets were downloaded for a local BLAST search on BioEdit (Hall, 1999).

Instead of relying on an arbitrary BLAST E-value threshold, each hit was examined manually to assess homology. As well as manually inspecting sequences for the presence of conserved domains (annotated in Fig. 2.02), the presence of the RHO domain was evaluated using the PROSITE and SMART protein domain databases (de Castro et al., 2006; Letunic & Bork, 2018).

RhoGAP homologues were identified using the same approach outlined above, but only for species in bold in Table 2.01, and by using the whole or just the RhoGAP domain sequence of RhoGAP proteins primarily from *M. polymorpha* as queries in BLAST searches.

Genes potentially encoding a RhoGAP domain and a Formin homology-2 domain were identified in a few species, but these were excluded from the analysis due to the low RhoGAP domain score predicted by PROSITE. Similarly, RhoGAP proteins identified and included in Fig. 2.06C but with a PROSITE RhoGAP domain score < 18 were excluded from the phylogenetic analysis in Fig. 2.07, as phylogenetic positions of these highly divergent proteins could not be determined with confidence and inclusion appeared to cause long branch attraction artifacts.

2.3.2 Sequence alignment and trimming

Multiple sequence alignments of amino acids and coding sequences were generated using MAFFT version 7, employing the L-INS-i iterative refinement method (Katoh & Standley, 2013). The resulting alignments were manually refined in BioEdit. The coding sequence alignment was compared to the amino acid sequence alignment to ensure matching codon alignment. Alignments

were manually trimmed in BioEdit to retain only homologous regions (essentially the G-domain and the RhoGAP domain for RHO and RhoGAP, respectively).

2.3.3 Phylogenetic reconstruction

To build the phylogenetic trees in Fig. 2.05, Fig. 2.07, and Fig. 2.09A, maximum-likelihood analyses were performed on the PhyML 3.0 online server (Guindon et al., 2010). The most appropriate amino acid or DNA substitution model was selected by the Smart Model Selection tool using the Bayesian Information Criterion (Lefort et al., 2017). To statistically evaluate branch support, the Shimodaira-Hasegawa-like approximate likelihood-ratio test (SH-like aLRT) was used.

To build the phylogenetic tree in Fig. 2.09B, maximum-likelihood analysis was performed on the IQ-TREE web server (Trifinopoulos et al., 2016). The best-fit codon substitution model was selected by ModelFinder (Kalyaanamoorthy et al., 2017). To statistically evaluate branch support, ultrafast bootstrap approximation (UFBoot) was performed (Minh et al., 2013).

The resulting phylogenetic trees were visualised and edited in iTOL v6 (Letunic & Bork, 2007) and further annotated in Inkscape.

2.3.4 Protein motif analysis

Multiple sequence alignments were inspected in BioEdit to test conservation of various protein motifs. LOGO diagrams for the SYRGA motif and the Rho insert (Fig. 2.04A) were generated using WebLogo 3 (Crooks et al., 2004).

Species	Genome/Proteome databases	Reference	BLAST server	Transcriptome
Saccharomyces cerevisiae	S288C reference R64-2-1	Engel et al., 2014	www.yeastgenome.org	-
Cyanidioschyzon merolae	ASM9120v1	Nozaki et al., 2007	plants.ensembl.org	NCBI (PRJNA362819)
Porphyridium purpureum	P.purpureum v2	Lee et al., 2019	porphyra.rutgers.edu	1KP (db.cngb.org/onekp)
Chondrus crispus	ASM35022v2	Collén et al., 2013	plants.ensembl.org	1KP
Cyanophora paradoxa	ASM443141v1	Price et al., 2019	phycocosm.jgi.doe.gov	NCBI (PRJNA634446)
Chloropicon primus	ASM785969v1	Lemieux et al., 2019	NCBI	-
Chlorella variabilis NC64A	C.variabilis v1.0	Blanc et al., 2010	NCBI	-
Coccomyxa subellipsoidea	C.subellipsoidea C-169 v2.0	Blanc et al., 2012	phytozome.jgi.doe.gov	1KP
Ulva mutabilis	Ulvmu_genome/Ulvmu_PROT_LATEST	De Clerck et al., 2018	bioinformatics.psb.ugent.be/orcae	-
Chlamydomonas reinhardtii	C. reinhardtii v5.6	Merchant et al., 2007	phytozome.jgi.doe.gov	-
Volvox carteri	V. carteri v2.1	Prochnik et al., 2010	phytozome.jgi.doe.gov	-
Micromonas sp. RCC299	Micromonas sp RCC299 v3.0	Worden et al., 2009	phytozome.jgi.doe.gov	-
Micromonas pusilla	M.pusilla CCMP1545 v3.0	Worden et al., 2009	phytozome.jgi.doe.gov	van Baren et al., 2016
Bathycoccus prasinos	Bathy_genome/PROT_FINAL_RELEASE	Moreau et al., 2012	bioinformatics.psb.ugent.be/orcae	1KP
Ostreococcus lucimarinus	O.lucimarinus v2.0	Palenik et al., 2007	phytozome.jgi.doe.gov	-
Ostreococcus tauri	O.tauri_genome_v2.2/OsttaV2_PEP_LAST	Blanc-Mathieu et al., 2014	bioinformatics.psb.ugent.be/orcae	-
Mesostigma viride NIES296	ASM974604v1; MeVI296_assembly3	Liang et al., 2020 Sato, unpublished	NCBI	-
Mesostigma viride NIES995	-	-	-	Ju et al., 2015 Cooper & Delwiche, 2016
Mesostigma viride CCAC1140	ASM910319v1	Wang et al., 2020	NCBI	1KP
Chlorokybus atmophyticus	ASM910322v1	Wang et al., 2020	NCBI	1KP
Entransia fimbriata	-	-	-	1KP
Klebsormidium nitens	K.nitens NIES-2285 v1.1	Hori et al., 2014	www.plantmorphogenesis.bio.titech.ac.jp/~algae_genome_project/klebsormidium	Cooper & Delwiche, 2016
Chara braunii	chara_genome/Chbra.pep.20180417.orcae	Nishiyama et al., 2018	bioinformatics.psb.ugent.be/orcae	Bonnot et al., 2019
Chaetosphaeridium globosum	-	-	-	1KP
Coleochaete irregularis	-	-	-	1KP
Coleochaete scutata	-	-	-	1KP
Spirogyra sp.	-	-	-	1KP
Mesotaenium endlicherianum	ASM960273v1	Cheng et al., 2019	NCBI (BLASTP on marchantia.info)	1KP

Roya obtusa	-	-	-	1KP
Penium margaritaceum	scaffold/master gene protein sequence	Jiao et al., 2020	bioinfo.bti.cornell.edu/Penium	1KP
Nothoceros vincentianus	-	-	-	1KP
Anthoceros agrestis	AagrOXF	Li et al., 2020	hornworts.uzh.ch/en/Blast	1KP
Anthoceros angustus	ASM1090916v1	Zhang et al., 2020	NCBI (downloaded protein datbase for local BLASTP in BioEdit)	NCBI (PRJNA543724)
Ricciocarpos natans	-	-	-	1KP
Marchantia inflexa	M_inflexa_v1.1	Marks et al., 2019	NCBI	-
Marchantia polymorpha	MpTak1v5.1	Montgomery et al., 2020	marchantia.info	marchantia.info JBrowse & 1KP
Bazzania trilobata	-	-	-	1KP
Metzgeria crassipilis	-	-	-	1KP
Takakia lepidozioides	-	-	-	1KP
Sphagnum fallax	S.fallax v1.1	Sphagnum fallax v1.1, DOE-JGI	phytozome.jgi.doe.gov	-
Anomodon attenuatus	-	-	-	1KP
Physcomitrium patens	P.patens v3.3	Lang et al., 2018	phytozome.jgi.doe.gov	-
Lycopodium annotinum	-	-	-	1KP
Isoetes sp.	-	-	-	1KP
Selaginella moellendorffii	S. moellendorffii v1.0	Banks et al., 2011	phytozome.jgi.doe.gov	1KP (*S. stauntoniana* ZZOL) You et al., 2017
Salvinia cucullata	Salvinia cucullata v1.1	Li et al., 2018	www.fernbase.org	Ferbnase JBrowse
Azolla filiculoides	Azolla filiculoides v1.1	Li et al., 2018	www.fernbase.org	de Vries et al., 2016
Ginkgo biloba	Ginkgo_biloba.HiC	Guan et al., 2019	No server. Download databases and ran local BLAST in BioEdit.	1KP
Picea abies	P. abies v1.0	Nystedt et al., 2013	congenie.org/?r=archive	congeie.org (Trinity & 454)
Amborella trichopoda	A. trichopoda v1.0	Amborella Genome Project, 2013	phytozome.jgi.doe.gov	1KP
Oryza sativa	Release 7	Kawahara et al., 2013	rice.uga.edu	NCBI (refseq_rna)
Zea mays	B73 RefGen_V4	Jiao et al., 2017	phytozome.jgi.doe.gov	-
Solanum lycopersicum	S. lycopersicum ITAG2.4	The Tomato Genome Consortium, 2012	phytozome.jgi.doe.gov	NCBI (PRJNA583029)
Arabidopsis thaliana	TAIR10	Lamesch et al., 2012	phytozome.jgi.doe.gov	-

Table 2.01 Sequence source for the 52 species examined in this study

Both RHO and RhoGAP homologues were searched from species in bold, whilst only RHO homologues were searched from the rest

Taxon	Species	Name abbreviation	1KP sample code	Number of *ROP* genes
Klebsormidiales	*Interfilum paradoxum*	Ipa	FPCO	1
Zygnematales	*Spirotaenia sp.*	Spsp	TPHT	1
	Mesotaenium braunii	Mbr	WSJO	2
	Cylindrocystis brebissonii	Cbre	RPGL	1
	Mougeotia sp.	Msp	ZRMT	1
	Netrium digitus	Ndi	FFGR	1
Hornworts	*Leiosporoceros dussii*	Ldu	ANON	2
	Paraphymatoceros hallii	Pha	FAJB	2
	Phaeoceros carolinianus	Pca	WEEQ	2
	Megaceros tosanus	Mto	UCRN	2
Liverworts	*Lunularia cruciata*	Lcr	TXVB	1
	Pellia neesiana	Pne	JHFI	1
	Pallavicinia lyellii	Ply	YFGP	1
	Porella pinnata	Ppi	UUHD	1
Mosses	*Atrichum angustatum*	Aang	ZTHV	1
	Polytrichum commune	Pco	SZYG	1
	Leucobryum albidum	Lal	VMXJ	1
	Funaria sp.	Fsp	XWHK	2
Lycophytes	*Huperzia lucidula*	Hlu	GKAG	5 (3)*
	Isoetes tegetiformans	Ite	PKOX	2
	Selaginella selaginoides	Sse	KUXM	2
	Selaginella kraussiana	Skr	ZFGK	2
	Selaginella apoda	Sap	LGDQ	2
Monilophytes	*Equisetum hymale*	Ehy	JVSZ	10 (8)**
	Osmunda sp.	Osp	UOMY	4

Table 2.02 The 25 additional streptophyte species from which *ROP* homologues were identified to reconstruct *ROP* gene phylogeny in Figure 2.09B

*Five *ROP* transcripts were identified in the *Huperzia lucidula* transcriptome, however, transcript sequences were incomplete for two, hence only the three complete sequences were used for phylogenetic analysis.

**Ten *ROP* transcripts were identified in the *Equisetum hymale* transcriptome, however, transcript sequences were incomplete for two, hence only the eight complete sequences were used for phylogenetic analysis.

2.4 Results

2.4.1 RHO genes are present in all the major streptophyte lineages

To investigate the evolutionary origin of RHO Of Plant (ROP) signalling, I initially examined how widely conserved RHO proteins are among plants. To this end, I searched for *RHO* genes in the genome and/or transcriptome of 51 Archaeplastida species, from a diverse range of taxa – 5 angiosperms, 2 gymnosperms, 2 ferns, 3 lycophytes, 4 mosses, 5 liverworts, 3 hornworts, 4 Zygnematales, 3 Coleochaetales, 1 Charale, 2 Klebsormidiales, 1 *Chlorokybus*, 1 *Mesostigma*, 6 core chlorophytes, 5 prasinophytes, 1 glaucophyte, and 3 rhodophytes (Fig. 2.01). *RHO* genes were identified with the tBLASTn and BLASTp algorisms, using the *Marchantia polymorpha* ROP amino acid sequence as the query sequence. For species with both published genome and transcriptome, BLAST searches were performed on both to ensure identification of all *RHO* genes and to determine correct gene models (intron splice sites). The number of *RHO* genes could be confidently determined for all but four species with sequenced genomes (*Picea abies*, 6-7; *Ginkgo biloba*, 7-9; *Penium margaritaceum*, 2-5; *Cyanidioschyzon merolae*, 1-2). For 14 species, only transcriptomes were available and therefore it is formally possible that unexpressed *RHO* genes were missed by my search. However, based on comparison with closely related species with published genomes, it is likely that the number of *RHO* genes identified accurately reflects the number of *RHO* genes encoded in the genomes of the 14 species.

In total, 120 *RHO* genes were identified from the 51 Archaeplastida species. For 23 *RHO* genes, gene models annotated on genome databases had to be manually corrected using published transcriptomes. Of the 120 genes, 119 were confirmed to encode the RHO GTPase domain by both the PROSITE and SMART protein domain databases. The single *RHO* gene from the rhodophyte *Porphyridium purpureum* was predicted to encode the RAB GTPase domain by PROSITE, and the RHO GTPase domain by SMART. As this gene encodes a Rho insert, the defining feature of RHO, I classified the *Porphyridium* gene as a *RHO* gene. Overall, I am confident with the number of *RHO* genes identified for each species (except for the four species mentioned above, *P. abies*; *G.*

biloba; *P. margaritaceum*; *C. merolae*), the sequence of each *RHO* gene and that they all belong to the *RHO* gene family.

Out of the 51 Archaeplastida species surveyed, *RHO* genes were identified in all rhodophytes, glaucophytes, and Viridiplantae (the green plants), excluding the core chlorophytes (Fig. 2.01). The presence of the *RHO* gene in the prasinophytes, the sister group of the core chlorophytes, suggests the *RHO* gene was secondarily lost in the last common ancestor of core chlorophytes. *RHO* genes were identified in all 12 species belonging to the five major streptophyte algal lineages. *RHO* genes were also identified in all 24 land plant species, belonging to the major bryophyte and vascular plant lineages. Therefore, *RHO* genes are present in all the major streptophyte lineages. This raises the question of when ROP specific features which distinguishes RHO signalling in plants from other eukaryotes were acquired.

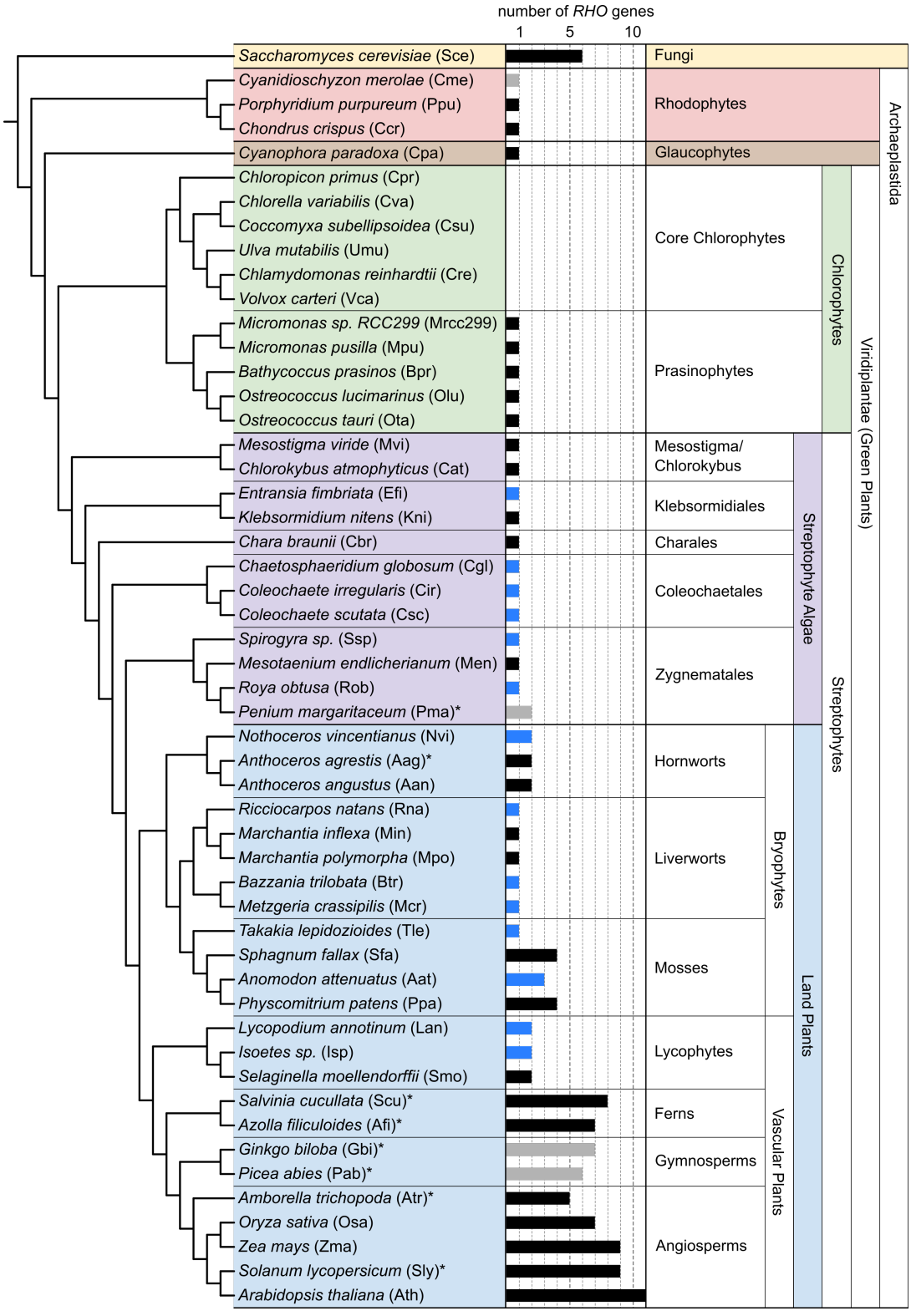

Figure 2.01 *RHO* genes are present throughout streptophytes

Species tree of Archaeplastida (plus *Saccharomyces cerevisiae*) combined with a bar graph displaying the number of *RHO* genes identified in each of the 52 species. Abbreviated species names used in following figures are in parentheses. For species marked with an asterisk, gene model annotation for at least one *RHO* gene had to be corrected. Bar graph colour coded as follows: black – *RHO* genes identified primarily from genome; grey – *RHO* genes identified primarily from genome, but where gene number could not be determined with high confidence;

blue – *RHO* genes identified solely from transcriptome. Species tree was based on Harris et al., 2020; Leebens-Mack et al., 2019; Lemieux et al., 2019; Puttick et al., 2018.

2.4.2 Two ROP-defining features have been conserved at least since the divergence of Klebsormidiales

To determine which of the 120 RHO proteins from 51 Archaeplastida species are ROP proteins, I aligned (Fig. 2.02) and examined these amino acid sequences for the presence of previously defined ROP specific features. The two major features which distinguish ROP from other RHO proteins are the SYRGA motif and the Rho insert that is 12 amino acids long (12-AA).

The SYRGA motif, within the switch II region (Fig. 2.02), is exposed on the surface of ROP proteins and suggested to act as an interaction site for ROP-specific regulators (Berken & Wittinghofer, 2008; Fricke & Berken, 2009). The serine residue is highly conserved throughout RHO GTPases and is a phosphorylation site in Human Rac1 (Kwon et al., 2000). Phosphomimetic mutation of this serine in *Medicago sativa* and *Arabidopsis thaliana* ROP proteins alters their binding affinities to ROP-specific regulators and effectors, suggesting that this is also a conserved regulatory phosphorylation site in ROP (Fodor-Dunai et al., 2011). Previous analysis demonstrated that the SYRGA motif is conserved in 149/150 ROP proteins from 36 land plant species (Fowler, 2010). Although the SY amino acid pair are conserved throughout eukaryotes, the RGA part is unique to plants, leading to the hypothesis that the SYRGA motif represents a ROP-specific kinase recognition motif (Berken, 2006; Fowler, 2010; Zheng & Yang, 2000).

RHO proteins from the rhodophyte, glaucophyte, and chlorophyte species surveyed all lack the SYRGA motif (Fig. 2.03). In all nine RHO proteins from these three taxa, the RG amino acid pair is not conserved (Fig. 2.04). Instead of glycine at the fourth position, rhodophyte and glaucophyte RHO proteins have either a polar or charged amino acid, like typical animal and fungal RHO proteins (Amin et al., 2016; Eliáš & Klimeš, 2012). This suggests that SYRGA motif emerged sometime after the divergence of the chlorophytes and the streptophytes.

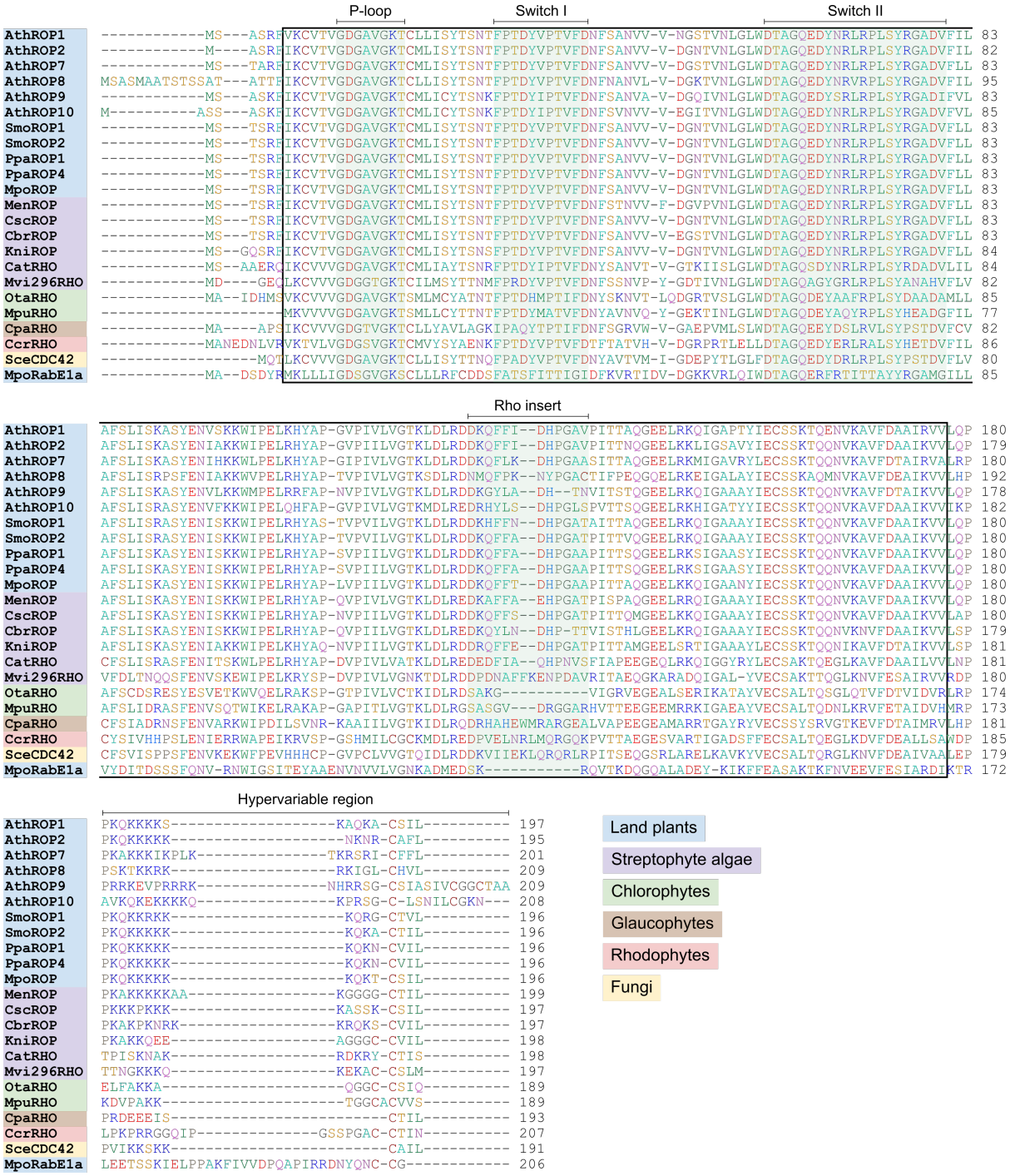

Figure 2.02 RHO protein sequence alignment for motif and phylogenetic analyses
Multiple sequence alignment of Archeplastida RHO proteins, *S. cerevisiae* CDC42, and *M. polymoprha* RabE1a. Due to space limitation, only 21 Archaeplastida RHO sequences are shown. The black box encloses the G-domain broadly conserved across small GTPases (including Rab), and represents the trimmed region used for the phylogenetic analysis in Figure 2.05. Species names are highlighted in different colours according to taxa. See Figure 2.01 for species name abbreviations.

Figure 2.03 Two ROP-defining features are conserved exclusively in streptophytes
Species tree of Archaeplastida (plus *S. cerevisiae*) combined with bar graphs displaying the number of RHO proteins with (black) and without (red) the SYRGA motif (left), or the 12 amino acids long Rho insert (right). Species name colour coded as in Figures 2.01.

Amongst the streptophytes, *Chlorokybus atmophyticus* and *Mesostigma viride* are the only species to lack SYRGA motif containing RHO proteins (Fig. 2.03). Instead of the glycine (small uncharged) at position 4, there is an aspartic acid (negatively charged) in *C. atmophyticus* and an asparagine (polar) in *M. viride* (Fig. 2.04). In addition, the *M. viride* RHO protein lacks the arginine in position 3. The absence of the RG amino acid pair was confirmed in two further *M. viride* accessions (Fig. 2.04). In contrast, the SYRGA motif is conserved in RHO proteins from the ten other streptophyte algal species, which are more closely related to land plants than to *C. atmophyticus* and *M. viride* (Fig. 2.03). The SYRGA motif is conserved in 95 out of 98 RHO homologues in 24 land plant species. The three RHO proteins which lack the conserved motif belong to three species, all of which encode at least five additional *RHO* genes encoding the SYRGA motif. Therefore, the SYRGA motif has remained highly conserved in the streptophyte lineage, at least since the time land plants last shared a common ancestor with Klebsormidiales.

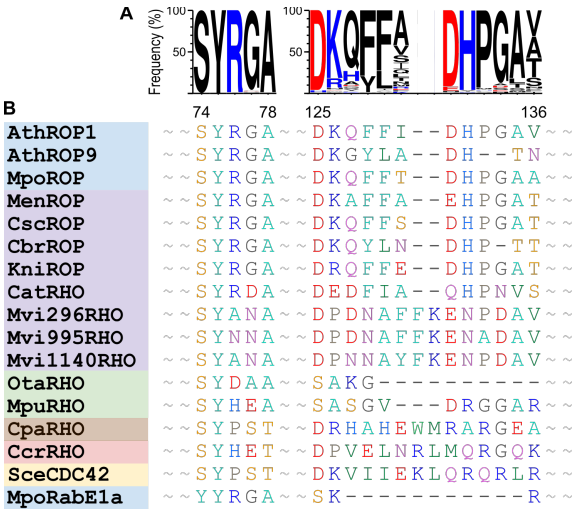

Figure 2.04 The sequences of the two ROP-defining features are conserved in most streptophytes but not in *Chlorokybus atmophyticus* and *Mesostigma viride*
(A) Logo diagram showing sequence conservation of the SYRGA motif and the Rho insert between 111 RHO proteins from 36 streptophyte species. Numbers below represent amino acid positions in *A. thaliana* ROP1.
(B) Multiple sequence alignment of the regions corresponding to the SYRGA motif and Rho insert sequences of 15 Archaeplastida RHO proteins, *S. cerevisiae* CDC42, and the *M. polymorpha* RabE1a. Although *C. atmophyticus* RHO has a 12-AA Rho insert, some residues conserved throughout most streptophytes (shown in A) are not conserved. See Figure 2.01 for species name abbreviations and colour coding.

I next examined the second ROP-defining feature, the 12-AA Rho insert. The Rho insert is the hallmark of RHO type GTPases, which distinguishes it from other small GTPases. Like the SYRGA motif, it forms a surface exposed region, implicated in interactions with RHO regulators and effectors (Schaefer et al., 2014). The Rho insert length varies but is typically 14-AA in length in animal and fungal RHO GTPases. In contrast, the Rho insert of ROP proteins are shorter, almost always 12-AA in length (Berken & Wittinghofer, 2008). The significance of the shorter length is not fully understood, however there is some evidence that this is required to mediate interaction with ROP specific regulators (Fricke & Berken, 2009).

RHO proteins from the rhodophyte, glaucophyte, and chlorophyte species surveyed all have a Rho insert with a length other than 12-AA (Fig. 2.03). The Rho insert is 14-AA in length in the rhodophyte and glaucophyte RHO proteins, like CDC42, Rho1, and Rho5 of *Saccharomyces cerevisiae* (Fig. 2.04). Within the chlorophytes, there is a wide range of Rho insert lengths; 4-AA in *Ostreococcus*, 11-AA in *Micromonas* and 39-AA in *Bathycoccus*. As neither of the two ROP-defining features are conserved in rhodophytes, glaucophytes, and chlorophytes, RHO proteins in these taxa should be classified as non-ROP RHO proteins.

Among the 111 RHO protein sequences from the 36 streptophyte species, only three have a Rho insert with a length of other than 12-AA; one each from *A. thaliana* (10-AA), *Chara braunii* (11-AA) and *M. viride* (14-AA) (Fig. 2.03). The shorter Rho insert in AthROP9 is likely due to a relatively recent loss of 2 amino acids as its closet homologues from the eudicot *Solanum lycopersicum* (SlyROP7 and SlyROP8) have a 12-AA Rho insert. This was further supported by a tBLASTn search with the AthROP9 amino acid sequence against the transcriptomes of 257 rosid species on the 1KP database, which revealed only a few species, all belonging to the Brassicales class, to have a AthROP9 homologue with a 10-AA Rho insert, indicating that the loss of the 2 amino acids took place after the divergence of the Brassicales and the Malvales. The shorter Rho insert in *C. braunii* is also likely due to a secondary loss as RHO proteins from Klebsormidiales and Coleochaetales all have a 12-AA Rho insert and their sequences are highly conserved (Fig. 2.04). The Rho insert is 14-AA in length in all three *M. viride* isolates. Moreover, some residues

conserved among most streptophyte Rho insert sequences are missing in the *M. viride* Rho insert. Interestingly, although the *C. atmophyticus* RHO has a 12-AA Rho insert, some of these potentially ROP specific Rho insert residues are also not conserved in the *C. atmophyticus* RHO. Therefore, the 12-AA Rho insert has remained conserved at least since the time land plants last shared a common ancestor with Klebsormidiales.

To summarise, the two ROP-defining features, the SYRGA motif and the 12-AA Rho insert, are both uniquely conserved among streptophytes, and likely became fixed/established after the divergence of the *Mesostigma*/*Chlorokybus* lineage and before the divergence of the Klebsormidiales lineage. Therefore, I propose that all streptophyte RHO, excluding those from *Chlorokybus* and *Mesostigma*, are ROP.

2.4.3 ROP protein has remained highly conserved at least since the divergence of Klebsormidiales

To investigate the evolution and origin of ROP, a phylogenetic analysis of Archaeplastida RHO proteins was conducted. An amino acid sequence alignment of 122 Archaeplastida RHO proteins (plus SceCDC42 and MpoRabE1a), trimmed to exclude the hypervariable C-terminal region and to retain the conserved G-domain sequence was used to build maximum-likelihood trees (Fig. 2.02). Trees were re-rooted with either the *S. cerevisiae* CDC42 or the *M. polymorpha* RabE1a. As expected, RHO proteins from glaucophyte and rhodophytes branch from deep nodes, leaving a clade of Viridiplantae RHO proteins (Fig. 2.05). Within this Viridiplantae clade, there is a clade which consists of all streptophyte RHO proteins excluding those from *C. atmophyticus* and *M. viride*. This clade, which I have termed the ROP clade, is statistically well supported in both trees rooted with either SceCDC42 or MpoRabE1 (aLRT-SH-like branch support of 91 and 97, respectively). In the SceCDC42 re-rooted tree, the chlorophyte RHO proteins form a clade that is sister to the ROP clade, whilst in the MpoRabE1a re-rooted tree, *C. atmophyticus* and *M. viride* RHO proteins are sister to the ROP clade. This uncertainty regarding the sister group to the ROP clade highlights how diverged *C. atmophyticus* and *M. viride* RHO proteins are from ROP. This is also reflected in the relatively long branch lengths for *C. atmophyticus* and *M. viride* RHO

proteins. In contrast, branches within the ROP clade are relatively very short, indicating that the ROP amino acid sequence has remained highly conserved from the last common ancestor of Klebsormidiales and land plants. Therefore, these data suggest that sometime after the divergence of the *Chlorokybus*/*Mesostigma* lineage, and before the divergence of the Klebsormidiales, some change prompted a marked increase in selective advantage for ROP sequence conservation, resulting in the establishment of ROP.

Figure 2.05 ROP protein sequence has remained highly conserved at least since the divergence of the Klebsormidiales (on following page)
Maximum-likelihood trees of 122 Archaeplastida RHO proteins (including three from three separate *M. viride* isolates) plus (A) *S. cerevisiae* CDC42 or (B) *M. polymorpha* RabE1a for re-rooting. Phylogeny inferred from multiple sequence alignment trimmed to the G-domain (see Figure 2.02) with the (A) LG+G+I or (B) LG+G substitution models. The aLRT support values for the major nodes are annotated. Nodes with an aLRT support value of <10 were collapsed. The ROP clade which consists of all streptophyte RHO, excluding those from *C. atmophyticus* and *M. viride*, is highlighted in beige and its aLRT support value marked in bold. Branch colour: green and red represent high and low aLRT support values, respectively. See Figure 2.01 for species name abbreviations and colour coding.

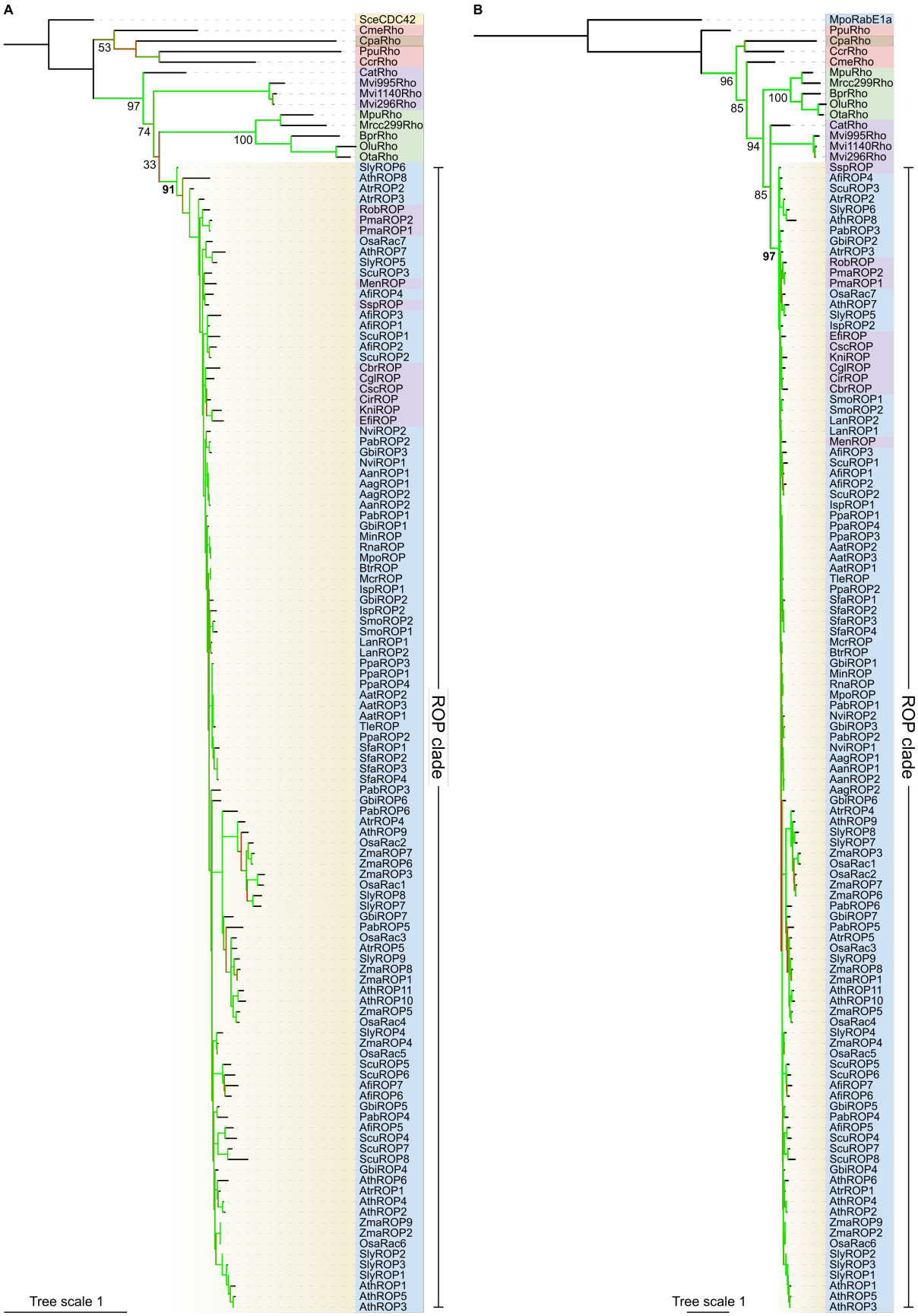
A
SceCDC42
CmeRho
CpaRho
PpuRho
CcrRho
CatRho
Mvi995Rho
Mvi1140Rho
Mvi296Rho
MpuRho
Mrcc299Rho
BprRho
OluRho
OtaRho
SlyROP6
AthROP8
AtrROP2
AtrROP3
RobROP
PmaROP2
PmaROP1
OsaRac7
AthROP7
SlyROP5
ScuROP3
MenROP
AfiROP4
SspROP
AfiROP3
AfiROP1
ScuROP1
AfiROP2
ScuROP2
CbrROP
CglROP
CscROP
CirROP
KniROP
EfiROP
NviROP2
PabROP2
GbiROP3
NviROP1
AanROP1
AagROP1
AagROP2
AanROP2
PabROP1
GbiROP1
MinROP
RnaROP
MpoROP
BtrROP
McrROP
IspROP1
GbiROP2
IspROP2
SmoROP2
SmoROP1
LanROP1
LanROP2
PpaROP3
PpaROP1
PpaROP4
AatROP2
AatROP3
AatROP1
TleROP
PpaROP2
SfaROP1
SfaROP2
SfaROP3
SfaROP4
PabROP3
GbiROP6
PabROP6
AtrROP4
AthROP9
OsaRac2
ZmaROP7
ZmaROP6
ZmaROP3
OsaRac1
SlyROP8
SlyROP7
GbiROP7
PabROP5
OsaRac3
AtrROP5
SlyROP9
ZmaROP8
ZmaROP1
AthROP11
AthROP10
ZmaROP5
OsaRac4
SlyROP4
ZmaROP4
OsaRac5
ScuROP5
ScuROP6
AfiROP7
AfiROP6
GbiROP5
PabROP4
AfiROP5
ScuROP4
ScuROP7
ScuROP8
GbiROP4
AthROP6
AtrROP1
AthROP4
AthROP2
ZmaROP9
ZmaROP2
OsaRac6
SlyROP2
SlyROP3
SlyROP1
AthROP1
AthROP5
AthROP3
ROP clade
Tree scale 1
B
MpoRabE1a
PpuRho
CpaRho
CcrRho
CmeRho
MpuRho
Mrcc299Rho
BprRho
OluRho
OtaRho
CatRho
Mvi995Rho
Mvi1140Rho
Mvi296Rho
SspROP
AfiROP4
ScuROP3
AtrROP2
SlyROP6
AthROP8
PabROP3
GbiROP2
AtrROP3
RobROP
PmaROP2
PmaROP1
OsaRac7
AthROP7
SlyROP5
IspROP2
EfiROP
CscROP
KniROP
CglROP
CirROP
CbrROP
SmoROP1
SmoROP2
LanROP2
LanROP1
MenROP
AfiROP3
ScuROP1
AfiROP1
AfiROP2
ScuROP2
IspROP1
PpaROP1
PpaROP4
PpaROP3
AatROP2
AatROP3
AatROP1
TleROP
PpaROP2
SfaROP1
SfaROP2
SfaROP3
SfaROP4
McrROP
BtrROP
GbiROP1
MinROP
RnaROP
MpoROP
PabROP1
NviROP2
GbiROP3
PabROP2
NviROP1
AagROP1
AanROP1
AanROP2
AagROP2
GbiROP6
AtrROP4
AthROP9
SlyROP8
SlyROP7
ZmaROP3
OsaRac1
OsaRac2
ZmaROP7
ZmaROP6
PabROP6
GbiROP7
PabROP5
AtrROP5
OsaRac3
SlyROP9
ZmaROP8
ZmaROP1
AthROP11
AthROP10
ZmaROP5
OsaRac4
SlyROP4
ZmaROP4
OsaRac5
ScuROP5
ScuROP6
AfiROP7
AfiROP6
GbiROP5
PabROP4
AfiROP5
ScuROP4
ScuROP7
ScuROP8
GbiROP4
AthROP6
AtrROP1
AthROP4
AthROP2
ZmaROP9
ZmaROP2
OsaRac6
SlyROP2
SlyROP3
SlyROP1
AthROP1
AthROP5
AthROP3
ROP clade
Tree scale 1

2.4.4 The emergence of two ROP specific regulators, RopGAP and REN, coincided with the establishment of ROP

My finding that ROP protein sequence has remained highly conserved since the time land plants last shared a common ancestor with the Klebsormidiales, led me to hypothesise that ROP-specific regulators may have emerged at around the same time. The selective advantage for retaining residues necessary for interacting with new regulators could have restricted further ROP sequence divergence. To test this hypothesis, I investigated the evolutionary origin of ROP specific regulators.

Amongst the known ROP regulators, one class of RhoGEF, RopGEF (PRONE-GEF), and two classes of RhoGAP, RopGAP and REN, have been reported previously to be ROP-specific (Berken et al., 2005; Hwang et al., 2008; Wu et al., 2000). RopGEF was initially described as being plant specific based on the lack of homologues in the opisthokonts. However, since its initial discovery, genes encoding RopGEF homologues have been identified in the genomes of several rhodophytes (but none outside the Archaeplastida), suggesting that the origin of RopGEF preceded that of green plants (Elias, 2008). In contrast to the RopGEF, the origins of RopGAP and REN remain elusive as no comprehensive survey of RopGAP and REN encoding genes have been conducted to date.

To determine the evolutionary origins of RopGAP and REN, a systematic survey for RhoGAP encoding genes was conducted in the genome/transcriptome of 24 diverse Archaeplastida species. RhoGAP proteins are defined by the presence of the conserved RhoGAP domain. Sequence outside of this domain is less conserved and different types of RhoGAP proteins have different auxiliary motifs and domains (Amin et al., 2016). Therefore, as well as using the full-length amino acid sequences of MpoRopGAP and MpoREN, their RhoGAP domain sequences alone were used as queries in tBLASTn searches. Genes identified were validated to encode RhoGAP proteins by checking for the presence of the RhoGAP domain using the PROSITE protein domain database. These were then further classified, as *RopGAP* if they also encoded a CRIB motif, or as *REN* if they additionally encoded a pleckstrin homology (PH)-domain, and as "other *RhoGAP*", if neither of these additional features were present (Fig. 2.06).

RopGAP and *REN* genes are both present in all seven land plant species surveyed (Fig. 2.06C). Amongst streptophyte algae, *RopGAP* and *REN* genes are both present in *Mesotaenium endlicherianum*, *Coleochaete irregularis*, and *Klebsormidium nitens*, while *C. braunii* only has *REN*, presumably due to the secondary loss of *RopGAP*. *RopGAP* and *REN* genes are both absent in *C. atmophyticus* and *M. viride*, as well as in chlorophytes, glaucophytes, and rhodophytes. These data suggest that RopGAP and REN first emerged sometime after the divergence of the *Chlorokybus*/*Mesostigma* lineage and before the divergence of the Klebsormidiales.

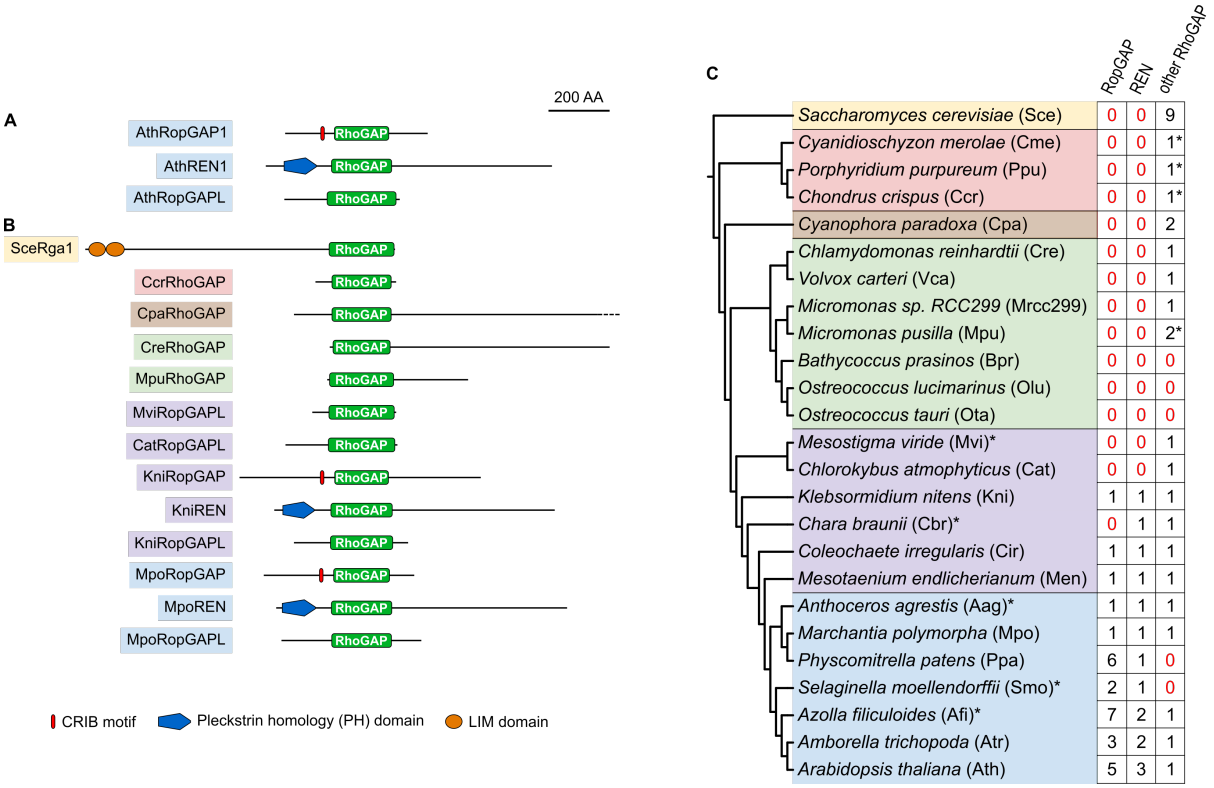

Figure 2.06 ROP specific regulators, RopGAP and REN, are streptophyte specific
Domain architecture of RhoGAP proteins in (A) *A. thaliana* and (B) other Archaeplastida species plus (*S. cerevisiae*). (C) Species tree of Archaeplastida (plus *S. cerevisiae*) combined with table displaying the number of different *RhoGAP* genes identified in each species. For species marked with an asterisk, gene model annotation for at least one *RhoGAP* gene had to be corrected. For *M. viride*, which has an unannotated genome, genome and transcriptome sequences had to be combined to determine the full-length protein sequence. Four putative *RhoGAP* genes identified encode a RhoGAP domain only with low confidence based on the PROSITE protein domain database (numbers marked with asterisk). These four were excluded from the phylogenetic analysis in Figure 2.07. Species name colour coded as in Figures 2.01.

To further investigate the evolutionary origins of RopGAP and REN, a phylogenetic analysis of RhoGAP proteins was conducted using the sequences identified from surveying 24 Archaeplastida genomes/transcriptomes. A maximum-likelihood tree was built using the alignment of 60 Archaeplastida RhoGAP amino acid sequences (+ the SceRhoGAP Rgd1 as outgroup) trimmed to only include the conserved RhoGAP domain. Both RopGAP and REN clearly form their own well supported monophyletic groups (Fig. 2.07). The sister relationship between the RopGAP and REN clades indicates that these two protein classes emerged through a gene duplication event. Since the RopGAP/REN clade is streptophyte specific, and because all the major streptophyte lineages, excluding the *Chlorokybus*/*Mesostigma* lineage, are represented in the RopGAP/REN clade, it is likely that the gene duplication event that gave rise to the RopGAP and REN protein classes occurred sometime after the divergence of the *Chlorokybus/Mesostigma* lineage and before the divergence of the Klebsormidiales. Therefore, RopGAP and REN likely emerged at approximately the same stage as ROP, early in the streptophyte lineage.

2.4.5 RopGAPL originated earlier than previously speculated, and its catalytic GAP activity was lost after the emergence of RopGAP and REN

In the survey for RhoGAP proteins across Archaeplastida, I identified proteins which are neither RopGAP nor REN, based on the absence of the CRIB motif and the PH-domain (Fig. 2.06C). Although RopGAP and REN are the only RhoGAP proteins functionally characterised in plants, there is evidence that other RhoGAP domain containing proteins exist in plants; for example RopGAP-like (RopGAPL) in *A. thaliana* (Eklund et al., 2010). Unlike RopGAP and REN, RopGAPL lacks additional recognisable domains (Fig. 2.06A), and it was speculated to have a more recent origin than RopGAP and REN because of its absence in *Selaginella moellendorffi* and *P. patens* (Fowler, 2010). However, its presence in other bryophytes or in streptophyte algae was not examined and the evolutionary relationship of the different plant RhoGAP proteins has not been investigated previously.

The phylogenetic analysis of Archaeplastida RhoGAP proteins revealed that all streptophyte RhoGAP proteins that are neither RopGAP nor REN, constitute their own well supported

monophyletic group (Fig. 207). The *A. thaliana* RopGAPL is a member of this clade, indicating that other members of this clade are RopGAPL homologues. This clade consists of RhoGAP proteins from bryophytes and streptophyte algae, demonstrating that RopGAPL originated earlier than previously speculated. The presence of *M. viride* and *C. atmophyticus* RhoGAP in this clade suggests that RopGAPL may in fact be more ancient than REN and RopGAP.

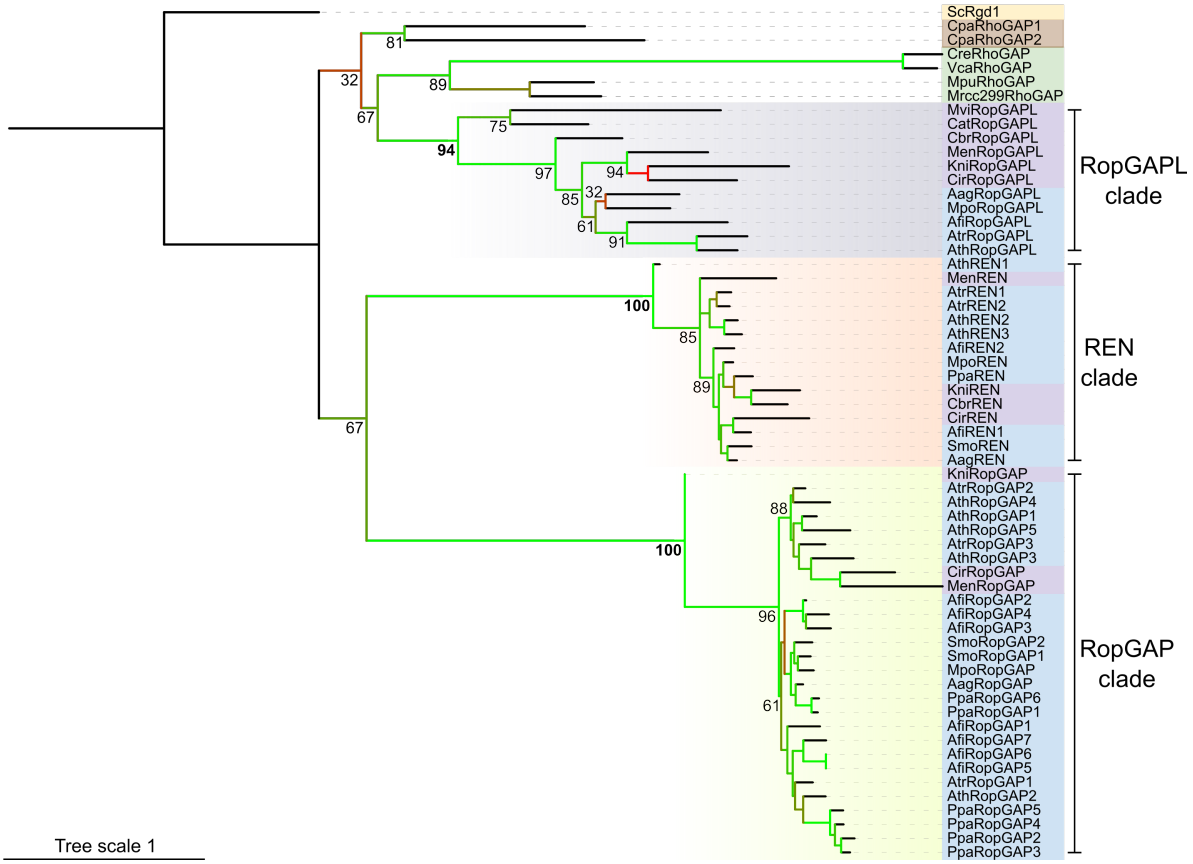

Figure 2.07 RopGAP and REN likely emerged through a gene duplication event early in the streptophyte lineage

Maximum-likelihood tree of 60 Archaeplastida RhoGAP proteins plus *S. cerevisiae* Rgd1. Phylogeny inferred from trimmed multiple sequence alignment of the RhoGAP domain of these proteins with the LG+G substitution model. The aLRT support values for the nodes of interest are annotated. Nodes with an aLRT support value of <10 were collapsed. The RopGAP, the REN, and the RopGAPL clades are highlighted and their aLRT support values marked in bold. Branch colour: green and red represent high and low aLRT support values, respectively. See Figure 2.01 for species name abbreviations and colour coding.

To gain further insight into the evolution of RhoGAP proteins early in the streptophyte lineage, I inspected the RhoGAP amino acid sequences. GAP proteins, not only for RHO but for other GTPases have a highly conserved arginine residue, termed the "arginine finger", essential for GAP catalytic activity (Scheffzek et al., 1998). It was previously reported that unlike RopGAP and REN, RopGAPL in *A. thaliana* lacks this conserved arginine in the RhoGAP domain, and hence was suggested to modulate ROP activity differently from conventional RhoGAP proteins (Eklund et al., 2010). To establish the extent of conservation of this critical arginine, I examined the RhoGAP sequence alignment. The arginine finger is conserved in all RopGAP and REN proteins (Fig. 2.08). Consistent with previous reports, the catalytic arginine is not conserved in RopGAPL from land plants and from *M. endlicherianum*, *C. irregularis*, and *C. braunii*. However, intriguingly, RopGAPL from *K. nitens*, *C. atmophyticus*, and *M. viride* all have the conserved arginine residue, suggesting that these function as conventional RhoGAP proteins. Therefore, the catalytic arginine was lost after the emergence of RopGAP and REN. I propose that the emergence of RopGAP and REN diminished the selection pressure on RopGAPL to retain the invariant arginine and potentially facilitated neofunctionalization of RopGAPL as an additional ROP regulator.

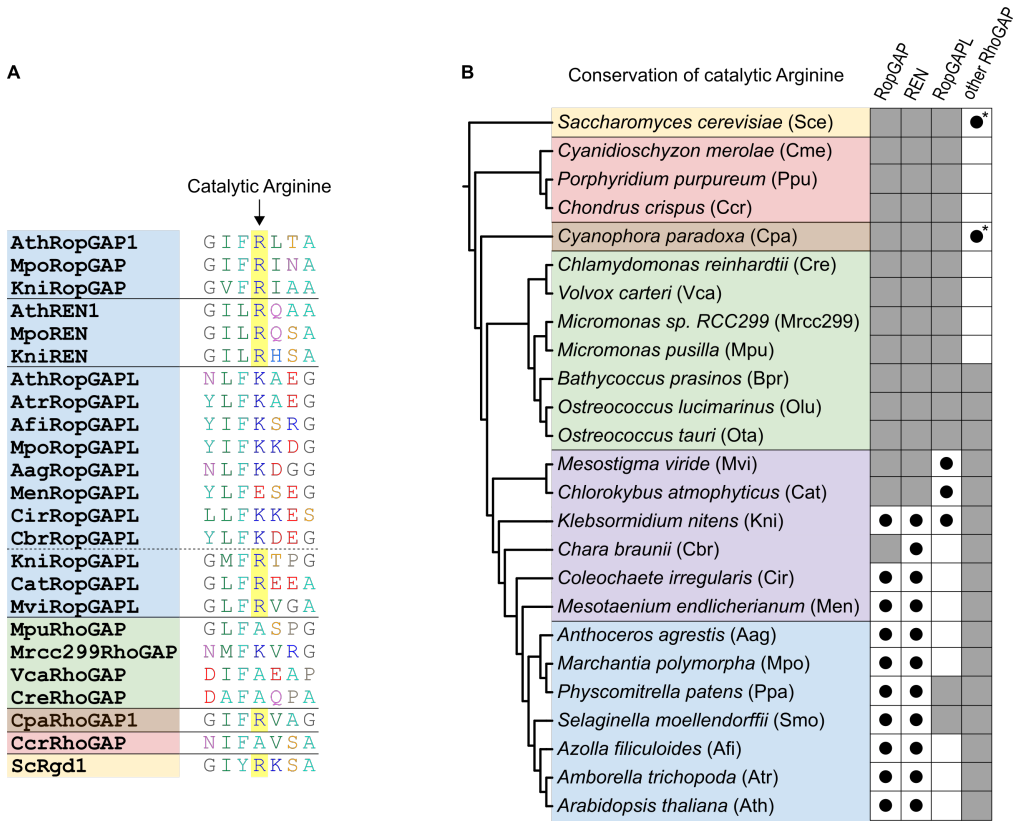

Figure 2.08 Arginine finger essential for GAP catalytic activity was lost in RopGAPL, after the divergence of Klebsormidiales

(A) Multiple sequence alignment of part of the RhoGAP domain with the catalytic arginine (R). In contrast to the conservation of the catalytic R in all RopGAP and REN, the catalytic R is only conserved in RopGAPL in the streptophyte algal lineages most distantly related to land plants. (B) Species tree of Archaeplastida (plus *S. cerevisiae*) combined with table marking the presence of the catalytic R in different types of RhoGAP proteins. Asterisk (●*) indicates the lack of the catalytic R in one RhoGAP homologue within a particular category (species, RhoGAP type). Absence of asterisk (●) indicates conservation of the catalytic R in all members of a given category. Species name colour coded as in Figure 2.01.

2.4.6 A single *ROP* gene was likely present in the last common ancestor of land plants and Zygnematales

The *ROP* gene is restricted to a single copy in most streptophyte algal species, whilst most land plant species encode multiple *ROP* genes in their genome (Fig. 2.01, 2.05). How the *ROP* gene family expanded in angiosperms has been previously described (Christensen et al., 2003; Fowler, 2010). However, how this expansion started in the streptophytes remains unclear. If a single *ROP* gene was present in the algal ancestors of land plants, and the presence of multiple *ROP* genes in many extant land plant species is due to gene duplication events which started after the emergence of the first land plants, all land plant *ROP* genes should be more closely related to one another than to any streptophyte algal *ROP* genes. In other words, a phylogenetic analysis of streptophyte *ROP* genes should resolve a monophyletic land plant group, if a single *ROP* gene was present in the last algal ancestor of land plants. To understand how the *ROP* gene family expanded, I generated a maximum-likelihood tree from the coding sequence (CDS) alignment of 109 *ROP* genes, as the trees generated from the RHO amino acid sequence alignment are inadequate for resolving evolutionary relationships within the ROP clade, due to the high degree of sequence conservation (Fig. 2.05).

The maximum-likelihood tree generated from the coding sequence alignment of 109 *ROP* genes resolves a clade comprising *ROP* genes from Zygnematales and land plants, when re-rooted with the Klebsormidiales *ROP* genes (Fig. 2.09A). However, the Zygenmatales *ROP* genes are scattered within this clade, and do not constitute a monophyletic group. Furthermore, the phylogenetic relationships depicted for some land plant *ROP* genes deviate from the taxonomic relationships of land plants. This incongruence between the *ROP* gene tree and the species tree could be explained by the presence of multiple *ROP* genes in the last common ancestor of Zygnematales and land plants and many independent duplications and losses of the *ROP* gene ever since. However, incongruence between the gene tree and the species tree could also arise if an inaccurate gene tree is reconstructed due to insufficient information within the multiple sequence alignment (Rasmussen & Kellis, 2007). In an attempt to improve the reconstruction of the *ROP* gene

phylogeny, a second maximum-likelihood tree was built with greater species sampling (Table 2.02 – 47 additional *ROP* genes identified from a further 25 species), more conservative alignment trimming (alignment length increased from 585bp to 600bp), and utilising a codon substitution model instead of a DNA substitution model (Fig. 2.09B). Within this updated maximum-likelihood tree, re-rooted with the Klebsormidiales *ROP* genes, the land plant clade (UFBoot = 88) and the Zygnematales clade (UFBoot = 85) were resolved to have a sister relationship (UFBoot = 94). Moreover, the phylogenetic relationships between this Zygnematales-land plant clade and the other streptophyte algal *ROP* genes follow taxonomic relationships. Therefore, the topology of the second tree is consistent with the hypothesis that *ROP* remained as a single copy gene at least until the time land plants last shared a common ancestor with the Zygnematales.

Unlike the relationships between the streptophyte algal *ROPs* outside of the land plant clade, the relationships within the land plant clade still do not clearly follow taxonomic relationships in the updated tree (Fig. 2.09B). At the deepest node, the land plant clade diverges to form a small sub-clade comprising *ROP* genes from some Selaginellales, ferns, and angiosperms, and a large sub-clade comprising *ROP* genes from all surveyed land plants species, excluding some Selaginellales. Within the large sub-clade, bryophyte *ROP* genes are paraphyletic. If an accurate representation of *ROP* phylogeny, these topologies would indicate the presence of multiple *ROP* genes in the last common ancestor of land plants and extensive independent losses in different lineages. However, based on the relatively low support values for some of the deep nodes within the land plant clade and the unstable placement of some groups within this clade, which are sensitive to changes in species composition and substitution model (illustrated by differences between the two trees in Fig. 2.09) as well as slight changes in sequence alignment, it is not possible to make robust inferences on *ROP* gene duplication patterns in early land plants. Nevertheless, some sub-clades were resolved with high support in both trees. *ROP* genes from hornworts (UFBoot = 100), mosses (UFBoot = 100), and liverworts (UFBoot = 96) are respectively monophyletic, indicating that the *ROP* genes in bryophytes radiated independently after the divergence of the three lineages. A few well supported monilophyte and seed plant clades also stand out, demonstrating *ROP* radiation in

the monilophytes and confirming the *ROP* radiation pattern previously reported within the angiosperms (Christensen et al., 2003). These well supported clades highlight that the diversity of *ROP* genes in land plants was shaped, at least in part, by lineage specific gene duplication events.

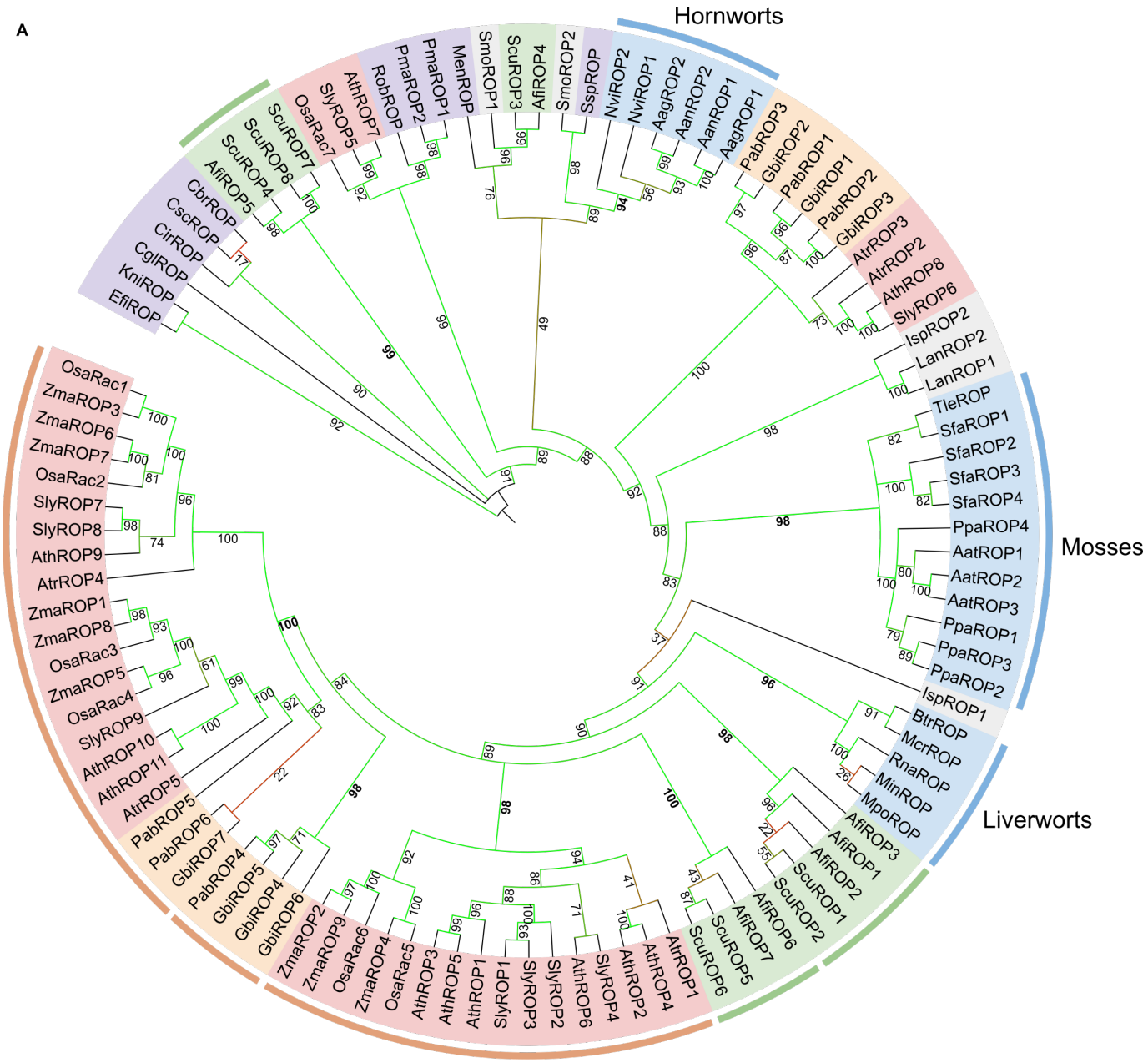

Figure 2.09 The last common ancestor of land plants and Zygnematales likely encoded a single *ROP* gene

Maximum-likelihood trees of (A) 109 *ROP* genes from 34 streptophyte species, and (B) 156 *ROP* genes from 59 streptophyte species, re-rooted with the *ROP* genes from Klebsormidiales. (A) GTR+G+I DNA substitution model used. The aLRT support value for every node is annotated. Nodes with an aLRT support value of <10 were collapsed. Figure continued on next page.

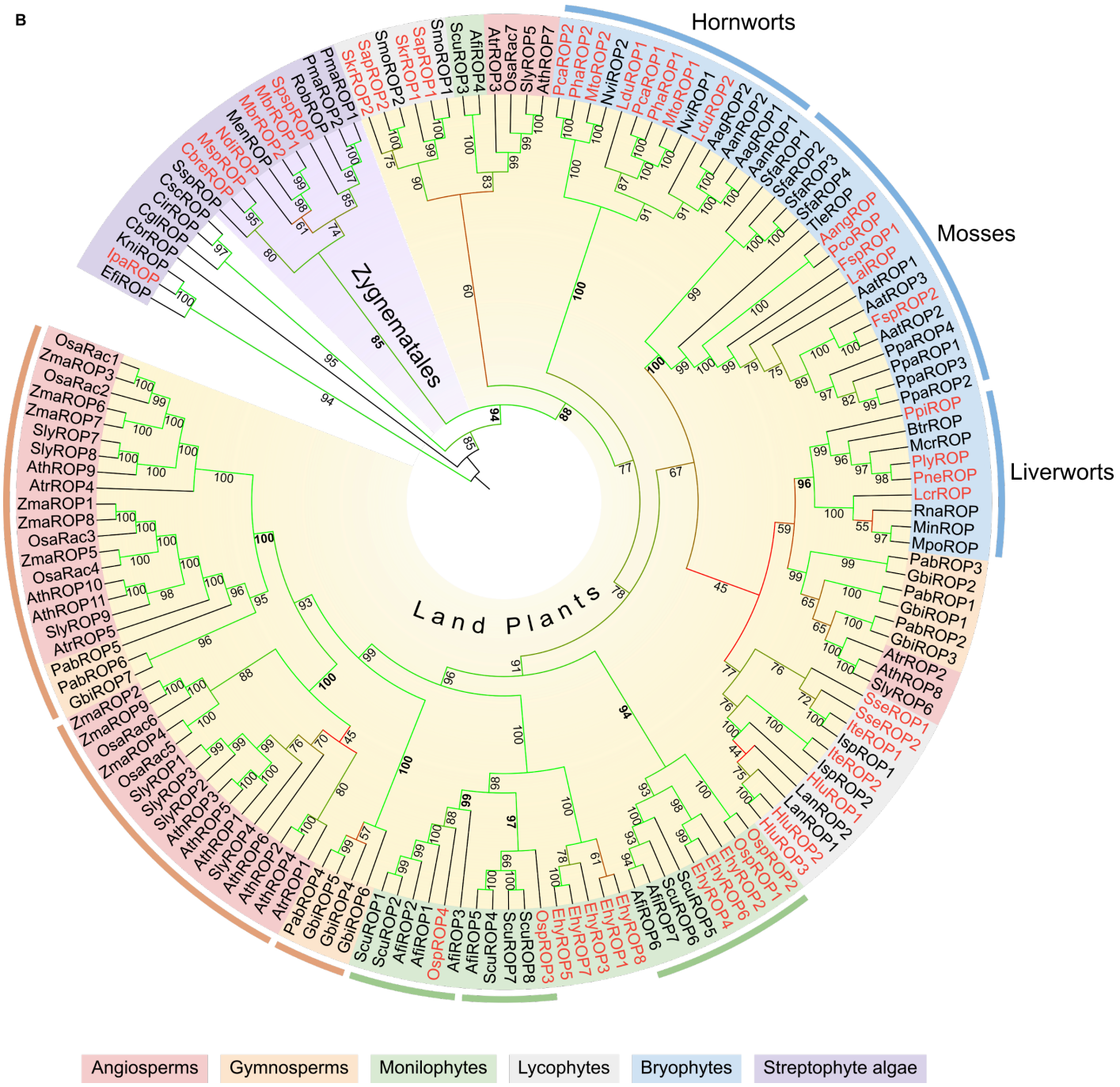

(B) MGK+F3X4+G4 codon substitution model used. The ultrafast bootstrap approximation (UFBoot) support value for every node is annotated. The 47 new genes included for this tree are written in red.

Clades comprising more than three genes which were resolved with high confidence (support value >90) in both (A) and (B) are marked with an arc. Branch colour: green and red represent high and low support values, respectively. See Figure 2.01 and Table 2.02 for species name abbreviations.

2.5 Discussion

2.5.1 ROP signalling was established early in the streptophyte lineage

In this chapter, I demonstrated that ROP likely evolved from an ancestral RHO protein early in the streptophyte lineage. The ROP amino acid sequence has remained highly conserved since the time land plants last shared a common ancestor with the Klebsormidiales (Fig. 2.05). Two ROP-defining features are conserved exclusively in streptophytes and the absence of these features in members of the earliest diverging streptophyte lineage, *Mesostigma* and *Chlorokybus*, suggests that ROP became established sometime after the divergence of this lineage and before the divergence of the Klebsormidiales (Fig. 2.03, 2.04). Furthermore, I showed evidence that during this transition period, the ROP specific regulators RopGAP and REN emerged (Fig. 2.06, 2.07). As all the other known core regulators of ROP signalling (SPIK1, RopGEF, RhoGDI) have a more ancient origin (Elias, 2008; Garcia-Mata et al., 2011; Meller et al., 2005), this period early in the streptophyte lineage represents when ROP signalling became fully established.

Based on the high degree of ROP amino acid sequence conservation within all streptophytes excluding *M. viride* and *C. atmophyticus*, it is evident that the ROP protein became fixed or established sometime after the divergence of the *Mesostigma*/*Chlorokybus* lineage. However, it is possible that the ROP-defining features first emerged at an earlier timepoint and were subsequently lost in the *Mesostigma*/*Chlorokybus* lineage. This possibility should not be neglected as there are clear evidence of losses, as well as gains, during RHO evolution in plants, most notably in the chlorophytes (Fig. 2.01, 2.06). Nonetheless, from an evolutionary adaptive standpoint, the timepoint at which a molecular trait became fixed/established is arguably more important than when it first emerged, as the timing of establishment likely represents the first time a molecular trait conferred a significant selective advantage. This is therefore consistent with the hypothesis that the establishment of ROP signalling influenced the course of early streptophyte evolution. The timing of ROP signalling establishment coincides with one of the proposed major transitions in plant body plan complexity – the transition from a unicellular to a multicellular filamentous form

(Umen, 2014). Given its importance in regulating cellular morphogenesis in extant land plants, it is plausible that the establishment of ROP signalling contributed to the evolution of morphological complexity in the streptophytes.

2.5.2 Timing of ROP establishment coincided with RopGAP and REN emergence

The emergence of RopGAP and REN proteins and the establishment of the ROP protein happened at around the same period. This is unlikely to be a coincidence because interacting proteins are known to co-evolve to maintain functional interactions (De Juan et al., 2013). Following the emergence of RopGAP and REN, the selection pressure to retain the ability to interact with these novel regulators likely restricted further divergence of ROP amino acid sequence. The emergence of RopGAP and REN, which are thought to spatially regulate ROP signalling through distinct mechanisms in extant land plants (Hwang et al., 2008; Klahre & Kost, 2006), would have provided the early streptophytes with greater spatiotemporal control over polarity signalling. Furthermore, the addition of novel components could have expanded the range of cellular processes regulated by RHO signalling. Amongst metazoan species, the repertoire of RHO regulator genes and the number of cell types are correlated, leading some to speculate that the expansion of RHO regulators was a major contributor to cellular signalling complexity (Fort & Blangy, 2017). The emergence of RopGAP and REN undoubtably offered ancestral streptophytes with selective advantages and therefore it is likely that the emergence of RopGAP and REN is responsible for the establishment of ROP in the last common ancestor of land plants and Klebsormidiales.

2.5.3 Emergence of RopGAP and REN may have contributed to the loss of GAP catalytic activity in RopGAPL

Based on the phylogenetic relationship of RopGAP, REN, and RopGAPL, it is likely that RopGAPL already existed when RopGAP and REN emerged through a gene duplication event (Fig. 2.07). This is contrary to past suggestions that RopGAPL had a more recent origin than RopGAP and REN (Eklund et al., 2010; Fowler, 2010). The ancestral RopGAP gained a CRIB motif whilst the ancestral REN acquired a PH-domain (Fig. 2.06). The PH-domain as well as 32 other types of domains have been identified within the 66 human RhoGAP proteins, indicating that

the addition of auxiliary domains was a strategy employed in both animals and plants to expand the repertoire of RHO regulators (Amin et al., 2016). The conservation of the catalytic arginine in RopGAPL of *M. viride*, *C. atmophyticus*, and *K. nitens*, but not in RopGAPL belonging to the rest of the streptophytes is consistent with the hypothesis that the emergence of RopGAP and REN resulted in the loss of GAP catalytic activity of RopGAPL (Fig. 2.08). As well as the loss of the catalytic arginine, the loss of the whole *RopGAPL* gene in multiple lineages (mosses and lycophytes) suggests that RopGAPL became functional less important after the emergence of RopGAP and REN. However, it is also conceivable that RopGAPL evolved to become a novel ROP regulator. The invariant arginine is required for GAP catalytic activity but is not required for ROP interaction (Hwang et al., 2010; Klahre & Kost, 2006) and there are examples of human RhoGAP proteins without the catalytic arginine which still influence RHO signalling (Marchesi et al., 2014). Therefore, the emergence of RopGAP and REN likely influenced RopGAPL evolution.

2.5.4 The *ROP* gene family expanded and diversified in land plants

The *ROP* gene in the last common ancestor of land plants and Klebsormidiales was almost certainly present as a single copy gene (Fig. 2.09). Subsequently, the *ROP* gene duplicated in many land plant lineages. This is likely linked, at least in part, to whole genome duplication events which have occurred in most land plant lineages, after the divergence of bryophytes and vascular plants (Clark & Donoghue, 2018; Leebens-Mack et al., 2019). Consistently, *ROP* genes have duplicated independently in bryophytes and vascular plants (Fig. 2.09). The sequence of duplicated *ROP* genes in some lineages like mosses have remained highly conserved, whilst they have clearly diverged in others like angiosperms. Distinct, even antagonistic, functions have been reported for different *A. thaliana* ROP proteins, highlighting that *ROP* gene family expansion facilitated neofunctionalization. For example, in pavement cells, AthROP2 and AthROP4 promote lobe outgrowth whilst AthROP6 restricts outgrowth at the neck region, contributing to formation of the jigsaw puzzle shaped cells (Fu et al., 2005, 2009). And in root hair cells, AthROP2 localises to the apex to promote tip growth, whilst AthROP10 localises to the shank to regulate cell wall deposition for shank hardening (Hirano et al., 2018; Jones et al., 2002). Therefore, *ROP* gene

duplications in land plants effectively relieved the tight selection pressure which until then had restricted sequence divergence of the single *ROP* gene. This in turn promoted neofunctionalization. Hence *ROP* gene family expansion had a profound impact on shaping ROP signalling evolution in land plants, especially in seed plants.

2.5.5 Liverwort *ROP* genes likely closely resemble the ancestral *ROP* gene

The expansion of *ROP* genes and evidence for their neofunctionalization in some land plants lineages raise the question – which *ROP* genes in extant land plants most closely resemble the ancestral *ROP* gene in terms of sequence and function? Previous *ROP* phylogenetic analyses were heavily skewed in terms of taxon sampling as they included many angiosperm species but only ever included a single bryophyte species, *P. patens* (Christensen et al., 2003; Fowler, 2010). These analyses yielded tree topologies which suggested that Ath*ROP7* and Ath*ROP8* were more closely related to the *P. patens ROP* genes than to other *A. thaliana ROP* genes, leading some to suggest that these resemble the ancestral *ROP* gene (Fowler, 2010). Consistent with previous tree topologies, Ath*ROP7* and Ath*ROP8* do not cluster with other *A. thaliana ROP* genes in my trees (Fig. 2.09). However, in my analysis with greater taxon sampling, there is no evidence that bryophyte *ROP* genes are more closely related to Ath*ROP7* than to the other *A. thaliana ROP* genes and only weak evidence that they are closely related to Ath*ROP8*. Instead, Ath*ROP7* and Ath*ROP8* likely represent *ROP* genes that underwent extensive sequence divergence for which their position within the *ROP* gene tree cannot be determined reliably. Consistent with this, the two clades which comprise *AthROP7* and *AthROP8* are positioned in different parts of the two trees in Fig. 2.09. The grouping of Ath*ROP7* with *ROP* genes from Zygnematales in Fig. 2.09A is almost certainly inaccurate, especially as increased species sampling helped resolve a Zygnematales clade in Fig. 2.09B. Thus, contrary to previous suggestions, neither Ath*ROP7* nor Ath*ROP8* likely resemble the ancestral *ROP* gene.

Liverworts are the only major land plant lineage in which all surveyed species encode a single *ROP* gene. The presence of a single *ROP* gene resembles the ancestral state as the *ROP* gene likely remained as a single copy gene at least until the time land plants last shared a common ancestor

with the Zygnematales (Fig. 2.09B). As the liverwort *ROP* genes constitute a monophyletic group, a single *ROP* gene was also likely present in the last common ancestor of liverworts. However, it is unclear if a single *ROP* gene was present in the last common ancestor of bryophytes. This is because although moss and hornwort *ROP* genes form respective monophyletic groups with high confidence, the precise relationship between the three bryophyte clades could not be resolved with high confidence (as illustrated by the different topologies of the trees in Fig. 2.09 and the relatively low support values for the relevant nodes). This poor resolution is likely due to the lack of informative sites in the multiple sequence alignment, which can happen when the aligned genes are short and highly conserved (Kapli et al., 2020; Rasmussen & Kellis, 2007). Consequently, it remains unclear if the *ROP* gene duplicated and became secondarily lost during the period spanning from the time liverworts last shared a common ancestor with Zygnematales to the time liverworts first emerged. Nevertheless, there is clear evidence that the tight selection pressure restricting *ROP* sequence and hence functional divergence was maintained in the lineage which gave rise to the liverworts. The *M. polymorpha* ROP protein shares 93% identity with the *Coleochaete scutata* ROP protein, in contrast to AthROP8 which only shares 70% sequence identity with the streptophyte algal ROP. With only a single *ROP* gene which has likely undergone little divergence from the ancestral *ROP* gene, *M. polymorpha* is therefore a uniquely attractive system to study ancestral ROP function.

To summarise, through phylogenetic analyses employing diverse taxon sampling, I have shown that ROP became established early in the streptophyte lineage. This was accompanied by the emergence of ROP specific regulators. The *ROP* gene has remained highly conserved ever since, but has expanded and diversified into a multi-gene family in many land plant lineages. In the following chapter, I investigate the ancestral function of the *ROP* gene using the liverwort *M. polymorpha*.

Chapter 3: The *Marchantia polymorpha ROP* gene regulates tissue level morphogenesis

3.1 Abstract

Cell polarity, broadly defined as the asymmetric distribution of subcellular components, influences how a cell grows and divides. RHO GTPase proteins are central regulators of cell polarity conserved throughout eukaryotes. Previous genetic studies have highlighted the importance of RHO Of Plant (ROP) proteins for cellular morphogenesis. However, relatively little is known about how their cellular functions influence plant tissue morphogenesis. This is probably because of genetic redundancy in model organisms which encode multiple *ROP* genes. Here, I have taken a reverse genetic approach to functionally characterise the single *ROP* gene in the liverwort *Marchantia polymorpha*. I demonstrate that Mp*ROP* is required for the morphogenesis of complex epidermal tissues. I show that MpROP protein influences tissue morphogenesis through controlling polarised cell growth, cell division, and possibly cell adhesion. As these cellular ROP functions are conserved between bryophytes and vascular plants, I propose that the regulation of epidermal tissue morphogenesis is an ancestral ROP function.

3.2 Introduction

Multicellular organisms can consist of elaborate three-dimensional tissues. To generate complex yet highly organised and reproducible structures, it is vital that specialised cells form in the appropriate spatiotemporal context. The regulation of cell division and growth patterns is important to achieve proper tissue morphogenesis, especially in plants where the position of a cell relative to neighbouring cells usually remain fixed, unlike in animals where cells can migrate.

Cell polarity is one factor which influences cell growth and division orientations (Muroyama & Bergmann, 2019). One class of regulators which control cell polarity in plants are the ROP proteins. RHO Of Plant (ROP) is a plant specific member of the RHO family of small GTPases, which are conserved throughout most eukaryotes (Nagawa et al., 2010). RHO GTPases function in signalling cell polarity, which primarily influences the organisation of the cytoskeleton (Etienne-Manneville & Hall, 2002). In plants, ROP function is required for polarised cell growth. For example, the tip growth of root hairs and pollen tubes (Jones et al., 2002; Li et al., 1999; Lin &

Yang, 1997), as well as anisotropic diffuse growth of pavement cells (Fu et al., 2005, 2009). They have also been implicated in orienting asymmetric cell divisions, for example for *Zea mays* subsidiary cell differentiation (Humphries et al., 2011) and *Physcomitrium patens* protonema branching (Yi & Goshima, 2020). Spatial regulation of ROP activity is necessary for proper cell polarisation. Loss of function in ROP regulators can impair root hair tip growth and pavement cell morphogenesis (Carol et al., 2005; Lauster et al., 2022). As a key regulator of cell polarity in plants, which influences cell growth and division orientations, it is therefore natural to hypothesise that ROP also contributes to plant morphogenesis.

Although ROP function in cellular morphogenesis is well characterised, its role in tissue morphogenesis remains unclear. This is because loss of function *rop* mutants in *Arabidopsis thaliana*, the species in which ROP function has been most extensively studied, lack severe tissue level defects. Even in higher order *rop* mutants, which have clear defects in both pavement cell and root hair morphogenesis, the overall shoot and root morphologies are comparable to that of wild-type (Gendre et al., 2019; Ren et al., 2016; Schepetilnikov et al., 2017; Xu et al., 2010). Ectopic overexpression of the dominant negative or constitutively active forms of AtROP2 results in a range of tissue defects (Fu et al., 2002; Li et al., 2001). However, these are not loss of function mutants, and because the aberrant forms of AtROP2 are expressed to much higher levels and in cells where the native At*ROP2* gene is not usually expressed, it is very difficult to infer ROP function in tissue morphogenesis from such studies. Recently, the *P. patens rop1 2 3 4* quadruple mutant has been shown to be defective in protonema development, suggesting ROP function in tissue patterning (Cheng et al., 2020). However, the *P. patens* protonema is a relatively simple filamentous structure which grows only in two dimensions. Therefore, an understanding of how ROP function contributes to the formation of complex three-dimensional tissue is still lacking.

The liverwort *Marchantia polymorpha* could be an ideal system to genetically study ROP function in tissue morphogenesis. Unlike other land plants, liverworts are unique in encoding only a single *ROP* gene in their genomes (chapter 2). The lack of severe tissue defects in *A. thaliana* loss of function *rop* mutants is likely due to functional redundancy between some of the 11 At*ROP* genes.

M. polymorpha therefore provides a unique opportunity to take a reverse genetic approach to study *ROP* function in the absence of genetic redundancy. Furthermore, *M. polymorpha* belongs to the complex thalloid lineage of liverworts and is thus characterised by the presence of intricate three-dimensional structures like the air chamber (Shimamura, 2016; Villarreal A. et al., 2016). It is thus an appropriate system to genetically study how ROP shapes complex plant tissues.

To investigate ROP function in plant tissue morphogenesis, here I report the functional characterisation of the single *ROP* gene in *M. polymorpha*. Through examining the phenotypes of Mp*rop* complete and partial loss of function mutants, I discovered that Mp*ROP* is required for tissue morphogenesis. In combination with studying the cellular defects of Mp*rop* mutants, investigation of Venus-MpROP subcellular localisation demonstrated that MpROP contributes to tissue morphogenesis through controlling polarised cell growth, formative cell divisions, and possibly cell adhesion. As these cellular ROP functions are conserved among land plants, my findings suggest that the regulation of tissue morphogenesis is an ancestral ROP function.

3.3 Materials and Methods

3.3.1 Plant material and growth conditions

Transgenes were introduced into sporelings generated from a cross between the Takaragaike-1 (Tak-1, male) and Takaragaike-2 (Tak-2, female) wild-type accessions of *Marchantia polymorpha*. For phenotypic comparisons with T_1 mutant plants, wild-type siblings of the T_1 mutants were used as wild-type (see Fig. 3.01B for detail). The Mp*ren* mutant was generated and kindly provided by Honkanen et al., 2016. Unless stated otherwise, plants were grown on sterile plates containing modified Johnson's medium 6mM KNO_3, 500µM $MgSO_4.7H_2O$, 4mM $Ca(NO_3)_2.4H_2O$, 25µM KCl, 12.5µM H_3BO_3, 1µM $MnSO_4.4H_2O$, 1µM $ZnSO_4.7H_2O$, 0.25µM $CuSO_4.5H_2O$, 0.25µM $(NH_4)_6Mo_7O_{24}.4H_2O$, 25µM $FeSO_4.7H_2O$, 25.5µM FeNaEDTA, 400µM $(NH_4)_2SO_4$, 600µM $NH_4H_2PO_4$, 555µM myo-Inositol, 0.5g/L MES hydrate, 1% sucrose, pH adjusted to 5.6) or ½-strength B5 Gamborg's medium (1.5g/L B5 Gamborg's, 0.5g/L MES hydrate, 1% sucrose, pH

adjusted to 5.5), solidified with 1% plant agar. Plants on agar plates were grown at 23°C under continuous white light (50–60µmol m^{-2} s^{-1}).

For crossing, 2–3 weeks old gemmalings grown under the above condition, were transplanted onto soil (1:3 mixture of fine vermiculite and John Innes No.2 or Neuhaus N3 compost) in SacO2 Microbox containers. Plants on soil were grown at 20°C under white light (50–60µmol m^{-2} s^{-1}) supplemented with far-red light (30–40µmol m^{-2} s^{-1}), in long day conditions (16 hours light, 8 hours dark).

3.3.2 Plasmid construction

CRISPR/Cas9 constructs for Mp*ROP* mutagenesis:

Within the Mp*ROP* (Mp7g17540) genomic sequence, three target sites, which satisfy the sequence criteria (5' $GN_{19}NGG$ 3'), were selected. BLAST search was performed against the *M. polymorpha* genome using the three target sequences as query, to confirm that these sequences are specific to Mp*ROP*. For each target site, a forward (CTCG N_{19}) and a reverse (AAAC rev.comp.N_{19}) oligonucleotide was designed (Appendix table 1). To generate entry clones with a single gRNA sequence, the annealed oligonucleotides were ligated with *Bsa*I digested pMpGE_En03 (Sugano et al., 2018). To generate CRISPR expression constructs, LR reaction was performed between the entry clones containing specific sgRNA sequences and the pMpGE010 destination vector which contains the $_{pro}$Mp*EF1α:Cas9* cassette (Sugano et al., 2018).

$_{pro}$Mp*ROP*:*NLS-Venus* and $_{pro}$Mp*ROP*:*Venus*-Mp*ROP*:

The Mp*ROP* promoter (4900bp region upstream of Mp*ROP* start codon), and gene (3069bp, from start codon to end of 3' UTR) sequences were amplified from the genomic DNA of Tak-1. Sanger sequencing confirmed that Mp*ROP* sequences are identical in Tak-1 and Tak-2. The Venus-YFP coding sequence with and without upstream nuclear localisation signal, and the NOS terminator sequence were amplified from constructs kindly provided by Dr Anna Thamm (Honkanen et al., 2018). Phusion High-Fidelity DNA Polymerase (Thermo) or CloneAmp HiFi PCR Premix (Takara) was used to PCR amplify all the above sequences with primers listed in Appendix table 1.

Both the transcriptional and translational Mp*ROP* reporter constructs were generated using In-Fusion cloning (Toyobo) to introduce the above amplified sequences into the multiple cloning site of pCAMBIA1300. See Appendix figure 1 for details.

3.3.3 Plant transformation

Sporeling transformation based on method developed by Ishizaki et al., 2008, and adapted by Honkanen et al., 2016.

Intact wild-type (Tak-1 x Tak-2) sporangia were harvested in 1.5ml Eppendorf tubes, which were then sealed with micropore tape and left to dry in a SacO2 Microbox container, 1/5 filled with silica gel. After two weeks of drying, Eppendorf tubes containing sporangia were closed and transferred to the -80°C freezer for storage until transformation. To sterilise, thawed sporangia were crushed in 0.1 % (w/v) sodium dichloroisocyanurate (Sigma) solution and left for 2 minutes. The spore suspension was then spun down at 15,000g for 2 minutes to pellet the spores. The supernatant was removed, and spores were resuspended in sterile water. The spore suspension was added to sterile 125ml Erlenmeyer flasks containing 25ml M51C medium (Honkanen et al., 2016; Ono et al., 1979), to achieve a spore concentration of roughly 1 sporangium per flask. Spores in sealed sterile flasks were cultured for 7 days at 23°C under continuous white light (50–60µmol m^{-2} s^{-1}) with constant agitation (130 rpm).

GV3101 *Agrobacterium tumefaciens* transformed with the desired expression construct was cultured from a single colony in 5ml of M51C at 28°C in the dark with constant agitation (180rpm). After 2 days incubation, 2ml of the culture was spun down (3,000g, 10 minutes) and the pellet resuspended in 10ml of M51C containing 100µM acetosyringone. After a further 6 hours of incubation, 1ml of the induced *Agrobacterium* culture was added to the 7-day old sporeling culture, together with acetosyringone (final concentration of 100µM), and left to co-cultivate for 2 days at 23°C under continuous white light (50–60µmol m^{-2} s^{-1}) with constant agitation (130 rpm).

The liquid co-culture was passed through a 40µM nylon cell strainer (Corning) and captured sporelings were washed with sterile water. Sporelings were then plated on modified Johnson's agar plates containing 150µg/ml cefotaxime and 10µg/ml hygromycin for selection.

3.3.4 Genotyping CRISPR mutants

To check for CRISPR/Cas-9 induced mutations, Phire Plant Direct PCR kit (Thermo Scientific) was used with primers listed in Appendix table 1 to amplify parts of the Mp*ROP* genomic sequence, directly from thallus tissue of transformants. Gel purified PCR products were sent for Sanger sequencing with primers listed in Appendix table 1.

To check Mp*ROP* transcript sequence of Mp*rop* mutants, total RNA was extracted from 12-day old gemmalings using RNeasy Plant Mini Kit (Qiagen) with DNase-I digestion. From 1µg of total RNA, cDNA was synthesized in a 20µl reaction with ProtoScript II Reverse Transcriptase (NEB) and oligo(DT) (Sigma) in the presence of Murine RNase inhibitor (NEB), following NEB protocol (#M0368). cDNA diluted 10 times in nuclease-free water was used as template to amplify Mp*ROP* coding sequence, with Phire Plant Direct PCR kit (Thermo Scientific) and primers listed in Appendix table 1. Gel purified PCR products were sent for Sanger sequencing with primers listed in Appendix table 1.

To select *Cas9*-free T_1 Mp*rop* mutants and wild-type siblings, fresh sporangia produced after crossing T_0 Mp*rop* mutants to wild-type (Tak-1 or Tak-2) were sterilised in 1 % (w/v) sodium dichloroisocyanurate (Sigma) solution for 3 minutes, before washing three times in sterile water. Sporangia were burst in sterile water to release spores, and these were plated on modified Johnson's agar plates without antibiotics. After three weeks, hygromycin sensitivity, which indicates the lack of the *Cas9* transgene, was tested by taking two thallus clippings from each selected T_1 plant and replica plating on Johnson's agar plates with and without hygromycin. The inheritance of the parental Mp*rop* or Mp*ROP* alleles were assessed by Sanger sequencing for hygromycin sensitive T_1 plants with Mp*rop* or wild-type phenotypes, respectively. For those where

the inheritance of the parental allele was confirmed, replica plating on plates with and without hygromycin was repeated to verify the lack of the *Cas9* transgene.

3.3.5 Rhizoid imaging and length measurement

To prepare plates for the rhizoid growth assay, 50ml of autoclaved molten ½-strength B5 Gamborg's medium containing 0.8% Phytagel was poured in each square petri dish (120x120x17mm). When the dish is propped up vertically, to have a horizontal Phytagel surface on which gemmae can be placed, Phytagel occupying the top 30mm of the dish was cut out neatly, to leave a phytagel surface approximately 5mm in width (corresponds to the thickness of the poured Phytagel), which is perpendicular to the dish surface. Four to five gemmae were plated along this narrow surface and sealed dishes were left vertically under standard growth conditions. Seven and ten days after plating, rhizoids of individuals gemmalings were imaged using the Leica M165 FC stereomicroscope, equipped with the Leica DFC310 FX camera. Maximum rhizoid length, defined as the vertical distance from the phytagel surface, on which the thallus sits, to the tip of the rhizoid which has grown the furthest away from the phytagel surface, was measured for each gemmaling in Fiji.

3.3.6 Phenotypic characterization of mutant tissue using stereomicroscopy

Wild-type and mutant tissues were imaged with the Leica M165 FC stereomicroscope, equipped with the Leica DFC310 FX camera.

3.3.7 Tissue fixation and clearing

The fixative, 4% (w/v) paraformaldehyde in 1x PBS, supplemented with 0.1% (v/v) Brij® L23, was freshly prepared as described by Ursache et al., 2018. Gemmae and meristematic notches (dissected from 6-day old gemmalings) were suspended in the fixative in Eppendorf tubes and fixed under vacuum (2x 30-minute vacuum treatment). After removing the fixative, samples were washed in 1x PBS twice. Samples in Eppendorf tubes were then suspended in the clearing solution, ClearSeeα, and vacuum (1x 30-minute) was applied to promote infiltration (Kurihara et al., 2021).

Samples were left in ClearSeeα at room temperature in the dark for at least a week (replacing ClearSeeα with fresh ClearSeeα every 1–2 days) before imaging.

3.3.8 Cell wall staining of live and fixed specimens

Live gemmae were stained in 10μg/ml propidium iodide (PI) for 10 minutes. To image very immature gemmae still attached to the base of the gemma cup, transversely dissected gemma cups were stained. PI was washed off with water before confocal imaging.

Fixed specimens were stained in 0.2% (v/v) SCRI Renaissance2200 (SR2200) in ClearSeeα at room temperature in the dark, overnight. SR2200 was replaced with ClearSeeα a few hours before imaging.

3.3.9 Epifluorescence microscopy

Venus epifluorescence images were acquired on the Leica MZ16FA stereomicroscope equipped with Leica EL6000 mercury lamp and Leica DFC300 FX camera, through the YFP filter (excitation: 500–520nm; emission: 540–580nm).

3.3.10 Confocal microscopy

Confocal live imaging was performed on an upright Zeiss LSM780 equipped with GaAsP detectors. All PI stained gemmae expressing $_{pro}$Mp*ROP:NLS-Venus* were imaged with a x20/0.8 NA air objective. Overall images of gemmae expressing $_{pro}$Mp*ROP:Venus*-Mp*ROP* and $_{pro}$Mp*UBE2:mScarletI*-At*LTI6b* were also acquired with a x20/0.8 NA air objective. Higher magnification 16-bit images for fluorescence quantification in gemma epidermal cells and rhizoids were acquired with a x40/1.1 NA water objective. The following excitation laser wavelength and emission capture bandwidth were used: Venus (ex 514nm, em 518–544nm), mScarletI (ex 561nm, em 571–624nm), PI (ex 561nm, em 580–624nm). Sequential scanning was used to avoid bleed through. All specimens were placed in a chamber setup described by Kirchhelle & Moore, 2017 for live imaging. Rhizoid were imaged after growing 0-day old gemmae in the chamber for 24 hours under standard growth conditions.

Confocal imaging of fixed specimens cleared in ClearSeeα was performed on an inverted Zeiss LSM880 equipped with GaAsP detectors. All images were acquired with a 40x/NA 1.2 objective, using silicon immersion oil, which closely matches the refractive index of ClearSeeα. The tile scan function was used to image large specimens and the resulting images were stitched using the online stitching tool in ZEN Black. The following excitation laser wavelength and emission capture bandwidth were used: SR2200 (ex 405nm, em 420–500nm, based on Tofanelli et al., 2019), Venus (ex 514nm, em 518–560nm). Sequential scanning was used to avoid bleed through when imaging both SR2200 and Venus fluorescence. For quantifying surface curvature in MorphoGraphX, 16-bit images were obtained with voxel size of 0.35x0.35x0.35µm. All fixed and cleared specimens were mounted in ClearSeeα in a Gene Frame (Thermo Scientific) attached to a standard microscope slide.

3.3.11 Fluorescence intensity quantification

To compare Venus-MpROP and mScarlaetI-AtLTI6b localisation patterns, Venus and mScarletI fluorescence intensities along a plasma membrane region of interest were measured in Fiji. After background subtraction from the sum projection image (sum of 5 consecutive slices), the segmented line tool (line width adjusted to cover the whole width of the plasma membrane, spline fit) was used to manually trace a line over the plasma membrane. Profile plots of the normalised signal intensities of Venus and mScarletI along the traced line were generated. For rhizoid (Fig. 3.03B), signal intensities were normalised so that the mean signal intensities of Venus and mScarletI are equal. For gemma epidermal cells, (Fig. 3.06 E & F), signal intensities were normalised so that the maximum signal intensities of Venus and mScarletI are equal.

3.3.12 Morphometric analysis in Fiji

Height, width, and depth of fixed gemmae imaged on the confocal were measured in Fiji. To measure height and width, first, a maximum z-projection image of a gemma was rotated along the XY plane to orient the gemma stalk to the base of the image. Then the area selection tool was used to draw the smallest rectangle encompassing the whole gemma. The height and width of this rectangle was taken as the height and width of the gemma. To measure gemma depth, the

orthogonal view function was used to manually find the XZ plane with the thickest gemma cross section. Within this XZ plane image, the line tool was used to draw a vertical line along the thickest part of the gemma, connecting the epidermal surfaces of the upper and lower sides of the gemma. The length of this line was taken as the gemma depth. The number of cell layers making up this thickest part of the gemma was taken as the maximum cell layer number for the gemma.

3.3.13 Quantification of gemma epidermal surface curvature

The MorphoGraphX manual (de Reuille et al., 2015) and methods by Kirchhelle et al., 2016 were used as guides to carry out the below analysis. TIF stacks were loaded into MorphoGraphX for 2.5D segmentation of gemma epidermal cells. To extract the surface topology of the whole tissue, the image was first filtered using Gaussian blur (radius 0.3µm), then the Edge Detect function (threshold: 7000) was performed. Holes in the resulting mask were filled. A mesh was created using the Marching Cubes Surface algorism with a cube size of 2µm. After smoothing and subdividing the mesh, the SR2200 cell wall signal was projected on to the mesh. To segment the gemma epidermal cells, cells were manually seeded based on the projected cell wall signal, then Watershed segmentation was performed. After correcting segmentation errors and refining the segmentation, average surface curvature for a neighbourhood with a radius of 20µm was computed for each cell. The radius of 20µm was determined empirically to give an appropriate approximation of the average cell surface curvature for most gemma epidermal cells but not for very small cells. Hence statistical analysis was restricted to cells with an area greater than 150µm^2.

3.3.14 Statistical analysis

Data plotted on graphs and statistically analysed in R.

3.4 Results

3.4.1 Twenty-one independent Mp*rop* mutant alleles were generated using CRISPR/Cas9

To study *ROP* gene function in *M. polymorpha*, I set out to generate loss of function Mp*rop* mutants using CRISPR/Cas9 mediated mutagenesis. As the *M. polymorpha* genome encodes only a single *ROP* gene, a complete loss of Mp*ROP* function in the haploid gametophyte may cause lethality, like recessive lethal *cdc42* alleles of the *Saccharomyces cerevisiae* (Kozminski et al., 2000). However, there are also numerous Sc*cdc42* alleles which display conditional or partial loss of function, and these have been instrumental in understanding *CDC42* function (Adams et al., 1990; Kozminski et al., 2000). With the aim to generate multiple independent Mp*rop* mutant alleles, some with partial loss of Mp*ROP* function, I designed three CRISPR single guide RNAs (sgRNAs) to independently target three different regions of the Mp*ROP* coding sequence (Fig. 3.01A). The first sgRNA targets a highly conserved region in exon 2, which encodes the switch I domain, essential for RHO function (Feiguelman et al., 2018). The second sgRNA targets a region which encodes the Rho insert. The Rho insert is the hallmark of RHO proteins which distinguishes this class from other small GTPases (Schaefer et al., 2014). The Rho insert sequence varies between different RHO proteins and thus may be less sensitive to minor mutations compared to more conserved regions of the protein. The third sgRNA targets just upstream of a region which encodes the C-terminal hypervariable region, required for active RHO protein to anchor to the plasma membrane where it signals cell polarity (Sorek et al., 2011). Thus, through targeting different parts of the Mp*ROP* gene, which have different functional significance, I attempted to generate a range of Mp*rop* loss of function mutants.

Table 3.01 Twenty-one independent Mp*rop* mutants were generated using CRISPR/Cas-9

Three sgRNAs were designed to independently target three regions of the Mp*ROP* coding sequence. Sites targeted by each sgRNA are marked in Figure 3.01. Mutant alleles in bold and marked with an asterisk are described in greater detail in Figure 3.01.

Guide RNA	Allele	Mutation induced	Genetic consequence	Expected consequence on protein
sgRNA1	*1_1-19*	T116 deletion	1bp deletion	Truncation after 46AA
	1_1-25	GTT (117-119) deletion	3bp deletion	Loss of 1 AA (Phe40)
	1_2-25	TGTTCG (116-121) deletion	6bp deletion	Loss of 2 AA (Val39 Phe40)
	1_3-8*	T insertion before T116	1bp insertion	Truncation after 41AA
	1_3-13	CCGTGT (113-118) deletion	6bp deletion	Loss of 2 AA (TVF → I at AA38)
	1_3-17	ATAATGTATGTAAATA insertion before T116	16bp insertion	Truncation after 46AA
	1_4-15	TG (116-117) deletion	2bp deletion	Truncation after 40AA
sgRNA2	*2_2-11*	GC (403-404) deletion	2bp deletion	Truncation after 142AA
	2_2-16	GCTGCTCCTATCAC (403-416) deletion & TG → CT (420-421)	14bp deletion + 2bp substitution	Truncation after 138AA
	2_3-13*	107bp insertion in place of G403	New splice donor site	Loss of 2AA (AAPITTA → SYHNC)
	2_4-3	G insertion before G403	1bp insertion	Truncation after 143AA
	2_4-7	TCACTGACCACA insertion in place of G403	11bp insertion	Truncation after 149AA
	2_5-7	TCCTATCACAA insertion in place of G403	10bp insertion	Truncation after 146AA
sgRNA3	*3_3-4*	TCGACGCTGCCATAAAGG (509-526) deletion	18bp deletion	Loss of 6 AA (DAAIKV)
	3_3-5	AGG (524-526) --> GCAGTTT	4bp insertion	Frame shift, addition of 4AA
	3_3-17	CCATAAAG (518-525) deletion	8bp deletion	Frame shift, no net extra AA
	3_4-1*	AT insertion after A524	2bp insertion	Frame shift, addition of 7AA
	3_4-3	CTGCCATAAAGGTCG (515-529) → GATCAATCAATCAATCATAATTGATCACAGGAT	18bp insertion	Truncation after 177AA, before HVR
	3_4-7	G526 deletion	1bp deletion	Frame shift, addition of 6 AA
	3_4-15	A524 deletion	1bp deletion	Frame shift, addition of 6AA
	3_4-18	A insertion before A524	1bp insertion	Frame shift, addition of 3AA

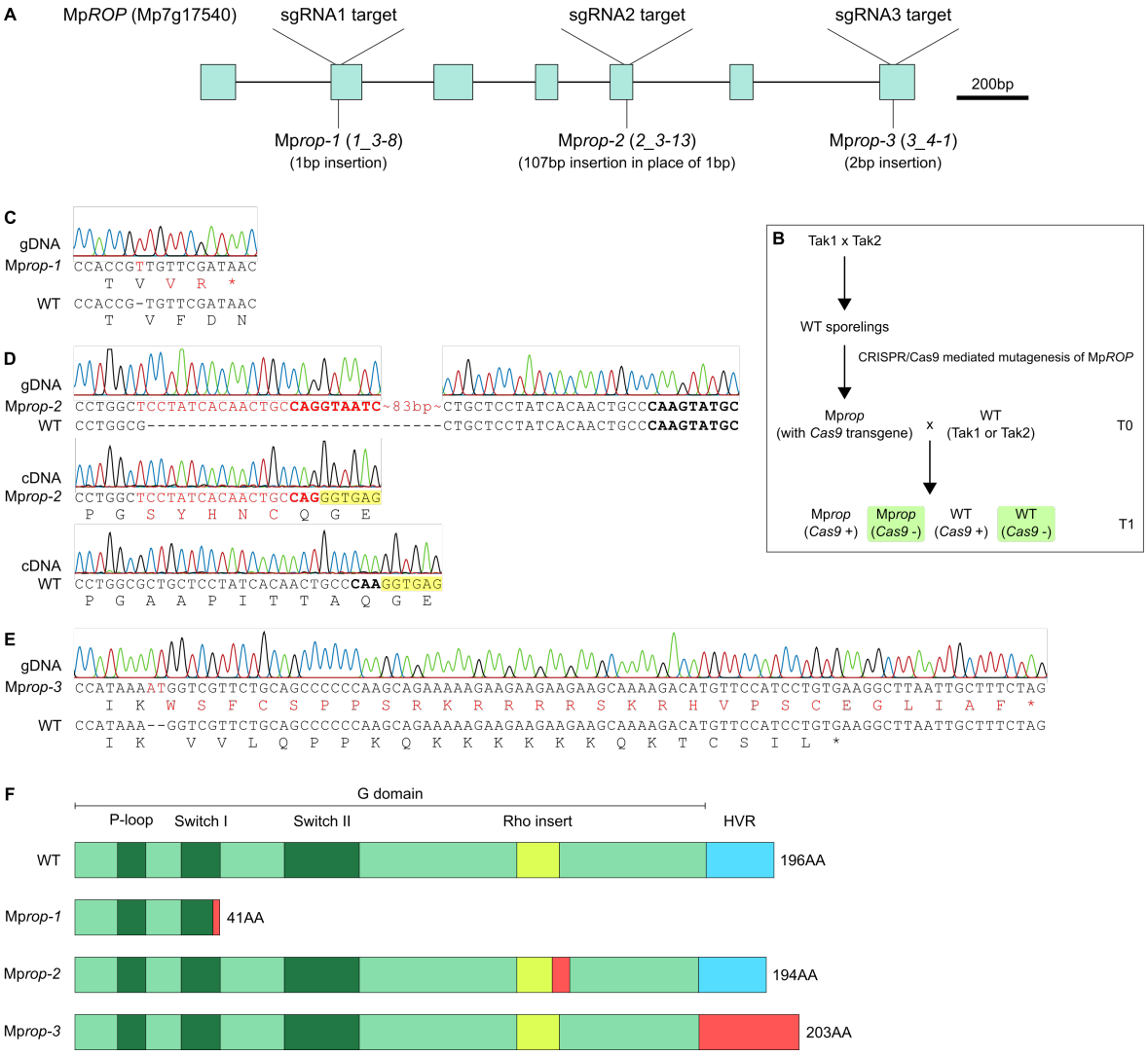

Figure 3.01 Mp*rop-1* and Mp*rop-3* are putative complete loss of function mutants and Mp*rop-2* is a putative partial loss of function mutant

(A) Gene structure (from the start to the stop codon) of Mp*ROP*, annotated with target sites of sgRNAs used for CRISPR/Cas9 mediated mutagenesis. Mutation sites in Mp*rop-1*, Mp*rop-2*, and Mp*rop-3* are also marked. Turquoise boxes represent exons and lines represent introns.

(B) *Cas9*-free Mp*rop-1*, Mp*rop-2*, Mp*rop-3*, and wild-type siblings (as controls) were isolated by crossing T_0 Mp*rop* mutants to wild-type.

(C-E) Genotyping through Sanger sequencing revealed specific mutations in the Mp*ROP* gene in Mp*rop-1,* Mp*rop-2*, and Mp*rop-3* alleles. Inserted nucleotides in the Mp*rop* alleles are in red. Predicted changes in amino acid sequence caused by the mutation are also in red.

(D) A large insertion was found in the Mp*ROP* locus from Mp*rop-2* genomic DNA. The insert contains a sequence which closely matches the splice donor consensus sequence. This and the native splice donor sequence for intron 5 are in bold. Sanger sequencing of Mp*ROP* cDNA from Mp*rop-2* confirmed the sequence within the insert as the new splice donor site for intron 5. Nucleotides highlighted in yellow belong to exon 6.

(F) MpROP protein domain architecture and predicted consequences of mutations in Mp*rop-1*, Mp*rop-2*, and Mp*rop-3* on the MpROP protein. Domains and motifs of interest are annotated. Domains with highly conserved sequences among RHO proteins are in dark green. HVR stands for

Hypervariable Region. Amino acid sequence predicted to be altered in Mp*rop* mutants are in red. Annotations for P-loop and Rho insert is based on Berken, 2006, and Switch I and Switch II are based on Kosami et al., 2014. G domain was determined using https://prosite.expasy.org/ and the region immediately following this was annotated as the HVR.

Twenty-one independent Mp*rop* mutant lines were identified following *Agrobacterium* mediated transformation of wild-type (WT) *M. polymorpha* sporelings with the three CRISPR constructs (Table 3.01). Twenty of these have consistent severe morphological defects, whilst one (*2_3-13*) has minor defects. Before in-depth phenotypic characterisation, I attempted to obtain stable *Cas9*-free Mp*rop* mutants by crossing *Cas9* encoding Mp*rop* mutants (T_0 generation) to WT and selecting progeny which had inherited the mutant Mp*rop* gene but not the *Cas9* transgene (in the T_1 generation) (Fig. 3.01B). This is to eliminate the risk of Cas9 inducing further mutations and to ensure that mutant phenotypes I observe are caused by the mutation in the Mp*ROP* gene and not due to gene disruption caused by the T-DNA insertion. Three out of 21 T_0 Mp*rop* alleles (*1_3-8*, *2_3-13*, and *3_4-1*) were successfully crossed with WT and produced T_1 *Cas9*-free Mp*rop* progeny. From here on, these three, *1_3-8*, *2_3-13*, and *3_4-1* mutant lines are referred to as Mp*rop-1*, Mp*rop-2*, and Mp*rop-3*, respectively.

3.4.2 Mp*rop-1* and Mp*rop-3* are putative complete loss of function mutants and Mp*rop-2* is a putative partial loss of function mutant

To determine if Mp*rop-1*, Mp*rop-2,* or Mp*rop-3* could be synthesising a partially functional MpROP protein, I interpreted the mutations in the three Mp*rop* alleles to predict the consequences of each on the MpROP protein sequence.

Mp*rop-1* has a single base pair (bp) insertion in exon 2, which is predicted to cause a frame shift, changing the last two amino acids of the highly conserved switch I domain. This is immediately followed by a truncation due to a premature stop codon (Fig. 3.01C, F). A protein 41 amino acids (AAs) in length, compared to the full length MpROP with 196 AAs, is unlikely to retain any ROP function and hence it is highly likely that Mp*rop-1* is a complete loss of function mutant.

Mp*rop-2* has a 107bp insertion in place of 1bp in exon 5 (Fig. 3.01D). Mp*rop-2* is the only mutant allele out of 21 with relatively minor morphological defects. To understand how such a large insertion causes relatively mild morphological defects, I examined the inserted sequence. Fifteen-bp into the insert, I identified a sequence which closely matches the splice donor consensus sequence, which marks the end of an exon (Fig. 3.01D). To test if this is the new splice donor site for intron 5, I sequenced the Mp*rop* transcript from Mp*rop-2*. This confirmed that the sequence in the insert is recognised as the new splice doner site, as 18bp of the insert was directly followed by exon 6 (Fig. 3.01D). As the remaining 89bp of the insert is spliced out as part of intron 5, and because the large insertion happened 24bp upstream of the native splice donor site, the overall consequence on the MpROP protein sequence is predicted to be a net loss of just 2 amino acids, and a change in 5 amino acids in a region which is known to vary between different ROP proteins (Fig. 3.01F). This is consistent with the less severe morphological defects and indicates that Mp*rop-2* is likely a partial loss of function mutant.

Mp*rop-3* has a 2bp insertion in the final exon, which is predicted to completely alter the sequence of the final 21 AAs of the MpROP protein and add a further 7 AAs before truncation at a new stop codon (Fig. 3.01E, F). As well as the loss of the hypervariable region for plasma membrane anchoring, the mutation will result in the loss of several highly conserved residues. Based on this and the fact that it displays the same severe morphological defects as Mp*rop-1*, Mp*rop-3* is likely a complete loss of function mutant.

To summarise, Mp*rop-1* and Mp*rop-3* are likely complete loss of function mutants and Mp*rop-2* is likely a partial loss of function mutant. The phenotypic characterisation of Mp*rop* mutants I report below were conducted on *Cas9*-free T_1 Mp*rop-1*, Mp*rop-2*, and Mp*rop-3* mutants. As the male (Tak1) and female (Tak2) WT accessions of *M. polymorpha* are not isogenic, I compared T_1 Mp*rop* mutants to *Cas9*-free WT siblings of T_1 Mp*rop-1* and Mp*rop-2*.

3.4.3 Transcriptional and translational reporter lines were generated to determine the pattern of Mp*ROP* gene expression and MpROP protein subcellular localisation

To determine Mp*ROP* gene expression and MpROP protein sub-cellular localisation patterns, I generated transcriptional and translational reporter lines (Fig. 3.02A). The transcriptional reporter line expresses nuclear localised Venus YFP under the transcriptional control of the Mp*ROP* promoter ($_{pro}$Mp*ROP:NLS-Venus*). The translational reporter line expresses MpROP N-terminally fused to Venus YFP, under the transcriptional control of the Mp*ROP* promoter ($_{pro}$Mp*ROP:Venus*-Mp*ROP*). The fluorophore was fused to the N-terminus of MpROP as the C-terminus is required for plasma membrane localisation and hence C-terminally tagging ROP can cause the fusion protein to display aberrant localisation patterns (Molendijk et al., 2001; Yi & Goshima, 2020). To reliably assess if Venus-MpROP sub-cellular localisation is polar, a plasma membrane reporter ($_{pro}$Mp*UBE2:mScarletI*-At*LTI6b*, Sauret-Güeto et al., 2020) was introduced into the MpROP translational reporter line (Fig. 3.02B). The Mp*ROP* transcriptional and translational reporter lines I generated allowed me to investigate the spatiotemporal function of MpROP during *M. polymorpha* development. My findings from studying these lines are described below.

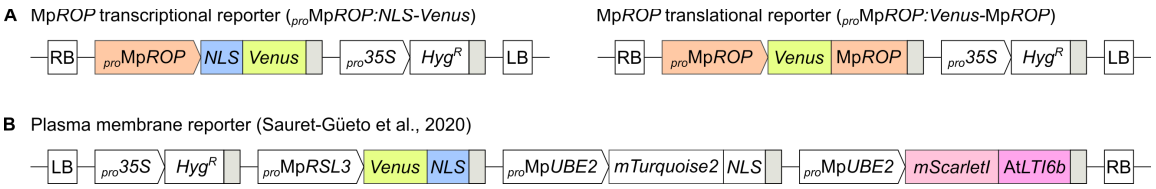

Figure 3.02 Mp*ROP* transcriptional and translational reporters were generated to study Mp*ROP* gene expression and MpROP protein subcellular localisation patterns
(A) Schematic representation of the Mp*ROP* transcriptional and translational reporter constructs, showing only region flanked by left and right borders. Grey boxes indicate terminator sequences. See materials and methods for details on vector construction.
(B) The Mp*ROP* translational reporter line was crossed to a plasma membrane reporter line (provided by the Haseloff lab, Sauret-Güeto et al., 2020) to assess polar localisation of MpROP. Schematic of the construct used to generate the plasma membrane reporter line is shown. Regions of interest are highlighted. Note, as well as encoding the plasma membrane reporter (mScarletI-AtLTI6b), the construct encodes two additional fluorophores (Venus-NLS and mTurqoise2-NLS), however mTqurqoise2 fluorescence was not imaged in this study. Schematics in A and B are not to scale.

3.4.4 Venus-MpROP protein localises at the apex of tip growing cells

To first establish if *ROP* function in signalling cell polarity is conserved in *M. polymorpha*, I tested for Mp*ROP* function in rhizoid tip growth. In contrast to the plasma membrane marker mScarletI-AtLTI6b, which localises relatively uniformly to the rhizoid plasma membrane with a slightly higher enrichment in the shank of the rhizoid, Venus-MpROP is enriched in the plasma membrane at the apex of the growing rhizoid cell (Fig. 3.03). This is consistent with the subcellular localisation of ROP proteins which promote the tip growth of pollen tubes and root hairs in angiosperms, shown through both immunolocalization of native ROP proteins and localization of fluorophore tagged ROP proteins (Jones et al., 2002; Lin et al., 1996; Molendijk et al., 2001). Therefore, this suggests that ROP function in promoting tip growth is conserved in *M. polymorpha*.

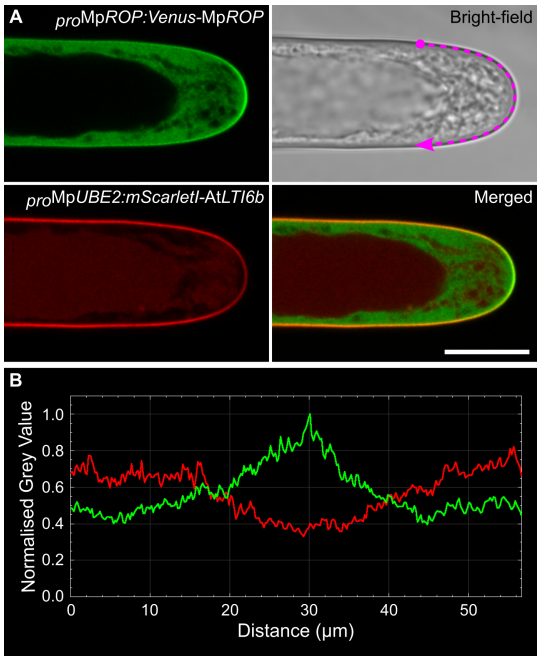

Figure 3.03 Venus-MpROP localised at the apex of tip growing rhizoid cells
(A) Confocal images of the growing end of a rhizoid cell expressing $_{pro}$Mp*ROP:Venus*-Mp*ROP* and $_{pro}$Mp*UBE2:mScarletI*-At*LTI6b* (plasma membrane reporter). Venus fluorescence is shown in green and mScarletI fluorescence in red. Dotted magenta line overlaid on the bright-field image marks the plasma membrane region along which fluorescence signal intensities from Venus-MpROP and mScarlet-AtLTI6b were compared. All images are Z-projections (sum slices) of five consecutive slices around the rhizoid medial plane. Scale bar, 20µm.
(B) Normalised fluorescence intensities of Venus-MpROP (green) and mScarlet-AtLTI6b (red) along the plasma membrane region marked with the magenta line overlaid in the bright field image in A. Measurement starts from point marked with magenta circle (distance = 0µm) and ends at point marked by the arrowhead (distance = 57µm).

3.4.5 Mp*ROP* is required for rhizoid tip growth

To test if Mp*ROP* is required for tip growth, I examined the phenotypes of Mp*rop* mutant rhizoids. The complete loss of function mutants, Mp*rop-1* and Mp*rop-3*, form very short rhizoids whilst the partial loss of function mutant, Mp*rop2*, forms rhizoids which are slightly shorter than WT, demonstrating that MpROP promotes rhizoid tip growth (Fig. 3.04A-D, K). Mp*rop-1* and Mp*rop-3* rhizoids are also curled compared to the straight WT rhizoids, indicating MpROP is also important for orienting tip growth (Fig. 3.04F, G, I). Moreover, a loss of function mutation in Mp*REN* (Honkanen et al., 2016), a negative regulator of ROP signalling, causes the development of wavy rhizoids, further indicating that proper control of ROP signalling is required for focussing tip growth in one orientation (Fig. 3.04 E, J). Overall, the tip localised subcellular localisation of MpROP protein (Fig. 3.03) and the tip growth defects of Mp*rop* mutants confirm that *ROP* function in signalling cell polarity is conserved in *M. polymorpha*.

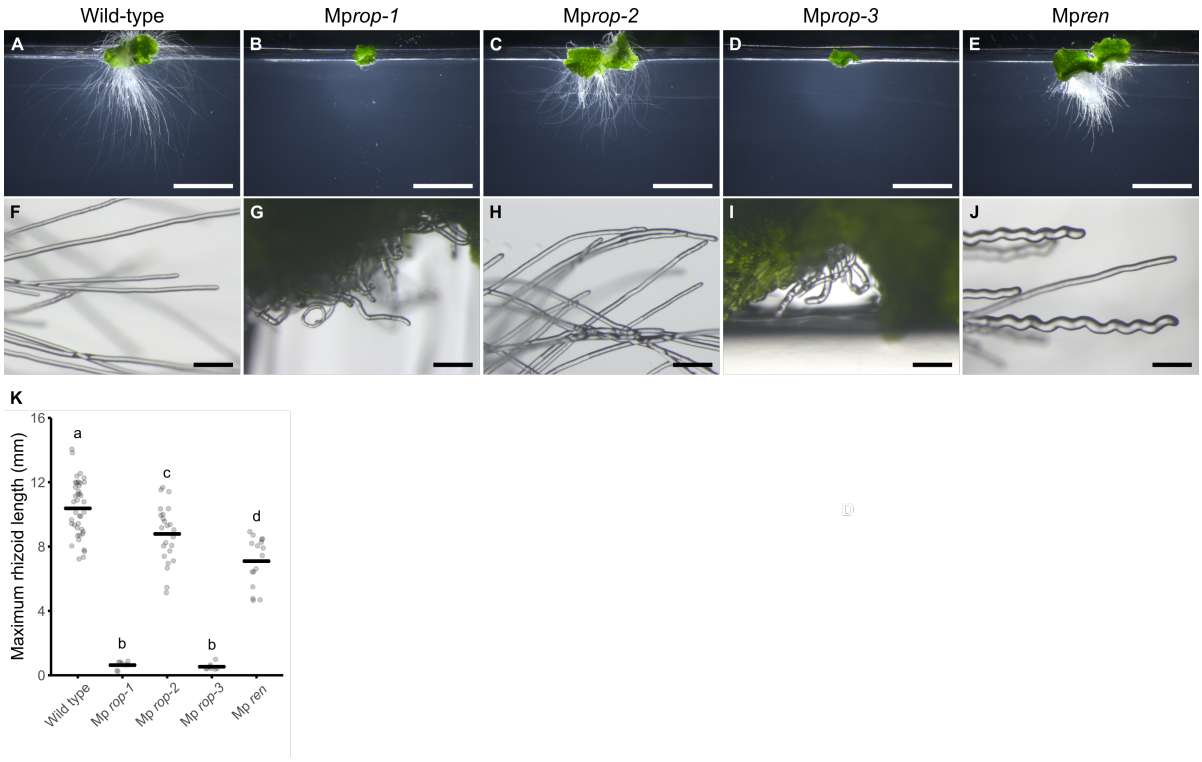

Figure 3.04 MpROP promotes and orients rhizoid tip growth

(A-E) Representative examples of wild-type, Mp*rop* mutants, and Mp*ren* mutant grown vertically on phytagel plates for 10 days from gemma. Scale bar, 5mm.

(F-J) Representative rhizoid images of 7-day old gemmalings. Wild-type and Mp*rop-2* rhizoids are relatively straight. Mp*rop-1* and Mp*rop-3* rhizoids are very short and slightly curled. Mp*ren* rhizoids are wavy. Scale bar, 200µm.

(K) Rhizoids are significantly shorter in Mp*rop-1*, Mp*rop-2*, Mp*rop-3*, and Mp*ren* compared to in wild-type. Maximum rhizoid length was measured for 10-day-old gemmalings grown vertically on phytagel plates. Maximum rhizoid length was defined as the distance from the phytagel surface, on which the thallus sits, to the tip of the rhizoid which has grown the furthest away from the phytagel surface. On the graph, each grey circle represents the maximum rhizoid length of a different plant, and the black horizontal bar represents the mean maximum rhizoid length of all the plants sampled within one genotype. Different letters indicate groups with significantly different means, based on one-way ANOVA followed by Tukey's HSD test ($p < 0.05$). The wild-type (n=40) sample consisted of four lines, two siblings of T_1 Mp*rop-1*, and two siblings of T_1 Mp*rop-2*. Samples for Mp*rop-1* (n=8), Mp*rop-2* (n=24), Mp*rop-3* (n=8) and Mp*ren* (n=16) each comprised two T_1 lines.

3.4.6 Mp*ROP* is expressed ubiquitously throughout the vegetative tissue epidermis

To explore whether Mp*ROP* could be involved in regulating tissue morphogenesis, I first examined the $_{pro}$Mp*ROP*:*NLS-Venus* expression pattern in the vegetative tissues of *M. polymorpha* using epifluorescence and confocal imaging. In the mature vegetative tissue, the thallus, $_{pro}$Mp*ROP*:*NLS-Venus* is expressed ubiquitously throughout the dorsal epidermis (Fig. 3.05A). The dorsal thallus epidermis is composed of air chambers which initiate development within the meristematic notch. To determine at what stage of air chamber development Mp*ROP* expression initiates, I examined $_{pro}$Mp*ROP*:*NLS-Venus* expression within the meristematic notch. $_{pro}$Mp*ROP*:*NLS-Venus* is expressed ubiquitously in cells around the notch, including the cells which give rise to the air chambers (Fig. 3.05C, D). These data indicates that Mp*ROP* is expressed throughout air chamber development and suggests Mp*ROP* function is required for thallus development and during air chamber morphogenesis.

Gemmae are organs that develop from single epidermal cells at the base of gemma cups that form on the dorsal thallus. The $_{pro}$Mp*ROP:NLS-Venus* reporter is expressed ubiquitously in epidermal cells at all stages of gemma development from early to late (Fig. 3.05E). I concluded that Mp*ROP* is expressed during gemma development and hypothesised that Mp*ROP* is required for gemma morphogenesis.

Overall, the expression of Mp*ROP* throughout the thallus and gemma epidermis, from an early developmental stage, suggests Mp*ROP* is required for thallus and gemma morphogenesis.

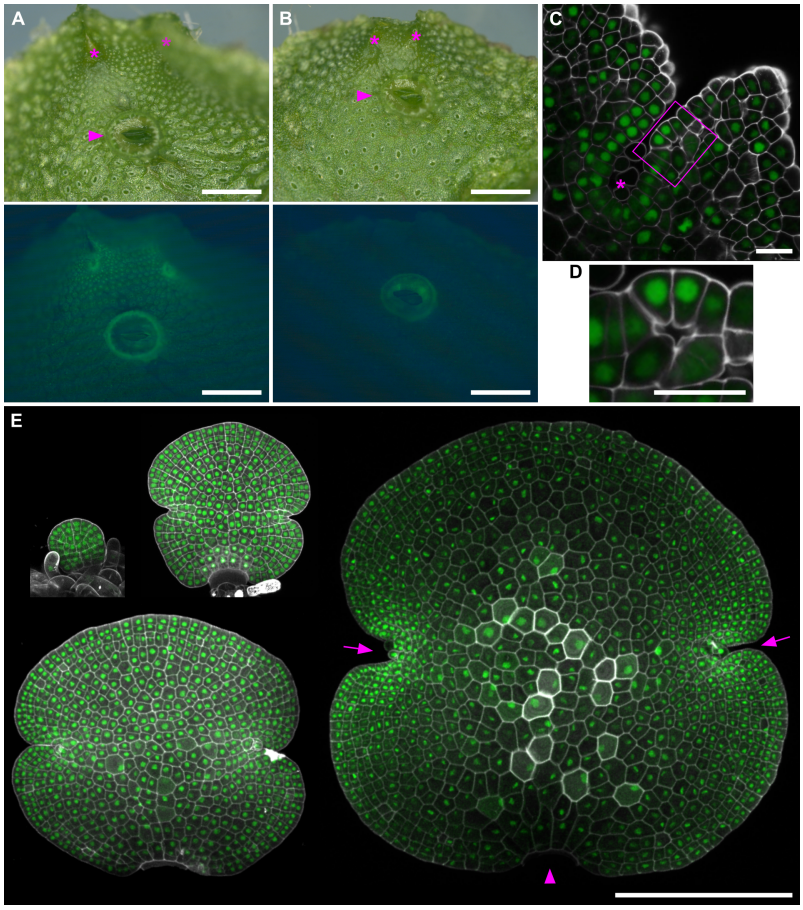

Figure 3.05 $_{pro}$Mp*ROP:NLS-Venus* is expressed ubiquitously throughout the thallus and gemma epidermis

Dorsal thallus epidermis of (A) $_{pro}$Mp*ROP:NLS-Venus* and (B) wild-type (Tak1) imaged using a fluorescent stereomicroscope. Top row shows bright field images, with the meristematic notches marked with asterisks and gemma cups marked with arrowheads. Bottom row shows fluorescence images acquired through a YFP filter. Fluorescence from wild-type gemma cup is autofluorescence and hence fluorescence from gemma cup of the Mp*ROP* transcriptional reporter is also partially autofluorescence. Scale bar, 1mm.

(C) The meristematic notch region of the $_{pro}$Mp*ROP:NLS-Venus* line fixed, cleared, and stained with a cell wall dye (SR2200) before confocal imaging. Venus fluorescence is in green, and SR2200 fluorescence in grey. Asterisk marks the meristematic notch, and the box marks an immature air chamber. Cross section image was prepared in MorphoGraphX. Scale bar, 20µm

(D) Higher magnification image of the immature air chamber marked in C. Scale bar, 20µm

(E) Gemmae at different developmental stages (from top left to bottom right in acceding order of maturity) expressing $_{pro}$Mp*ROP:NLS-Venus*. Gemma cell wall was stained with propidium iodide (PI) before confocal imaging. Venus fluorescence in green, PI fluorescence in grey. Arrows mark the meristematic notches, and the arrowhead marks the stalk attachment site for the fully mature gemma. Scale bar, 200µm.

3.4.7 Venus-MpROP subcellular localisation pattern during gemma development suggests MpROP regulates cell growth and division orientation

To test the hypothesis that MpROP functions during gemma morphogenesis, I determined the subcellular localisation of Venus-MpROP during the development of gemma epidermal cells. If MpROP plays a role in gemma morphogenesis, I hypothesised that this would be through the regulation of cell growth or division orientation, the major determinants of plant tissue morphology. Although extreme forms of polarised cell growth, like tip growth, are not observed during gemma development, gemma epidermal cells likely undergo polarised diffuse growth. I therefore sought polar localisation of Venus-MpROP indicative of MpROP function in polarised diffuse growth or cell division.

In immature developing gemmae at the base of the gemma cup, the Venus-MpROP is polar localised in some epidermal cells at the gemma margin (Fig. 3.06 A, C, E). Compared to the plasma membrane marker mScarletI-AtLTI6b, Venus-MpROP was enriched in the externally facing plasma membrane domain, perpendicular to the flattened organ surface, consistent with the hypothesis that MpROP promotes anisotropic diffuse growth of gemma epidermal cells. In an equivalent marginal region of a more mature gemma, this polarisation of Venus-MpROP was not observed, and instead Venus-MpROP was uniformly localised to the plasma membrane, relative to mScarletI-AtLTI6b (Fig. 3.06 B, D, F). Thus, these observations suggest that MpROP regulates polarised diffuse growth at an early stage of gemma morphogenesis.

At more advanced stages of gemma development, where meristematic notches have formed but rhizoid initials have not yet differentiated, Venus-MpROP was detected at the new cell plate of dividing cells near the meristem (Fig. 3.07 A, C, D). Venus-MpROP is enriched in the new cell plate during its formation, unlike the plasma membrane marker mScarletI-AtLTI6b, which is detected only after the new cell plate has formed. This suggests that MpROP could be active during cell division. In fully mature gemmae, which have completed gemma morphogenesis and are effectively dormant, Venus-MpROP also localises predominantly to the plasma membrane, however, no polar subcellular localisation was detected (Fig. 3.07 E-H). Overall, these data

demonstrate that Venus-MpROP is located at the sites of cell growth and at the cell plate of dividing cells. These data are consistent with the hypothesis that MpROP regulates cell growth and division orientation during gemma development.

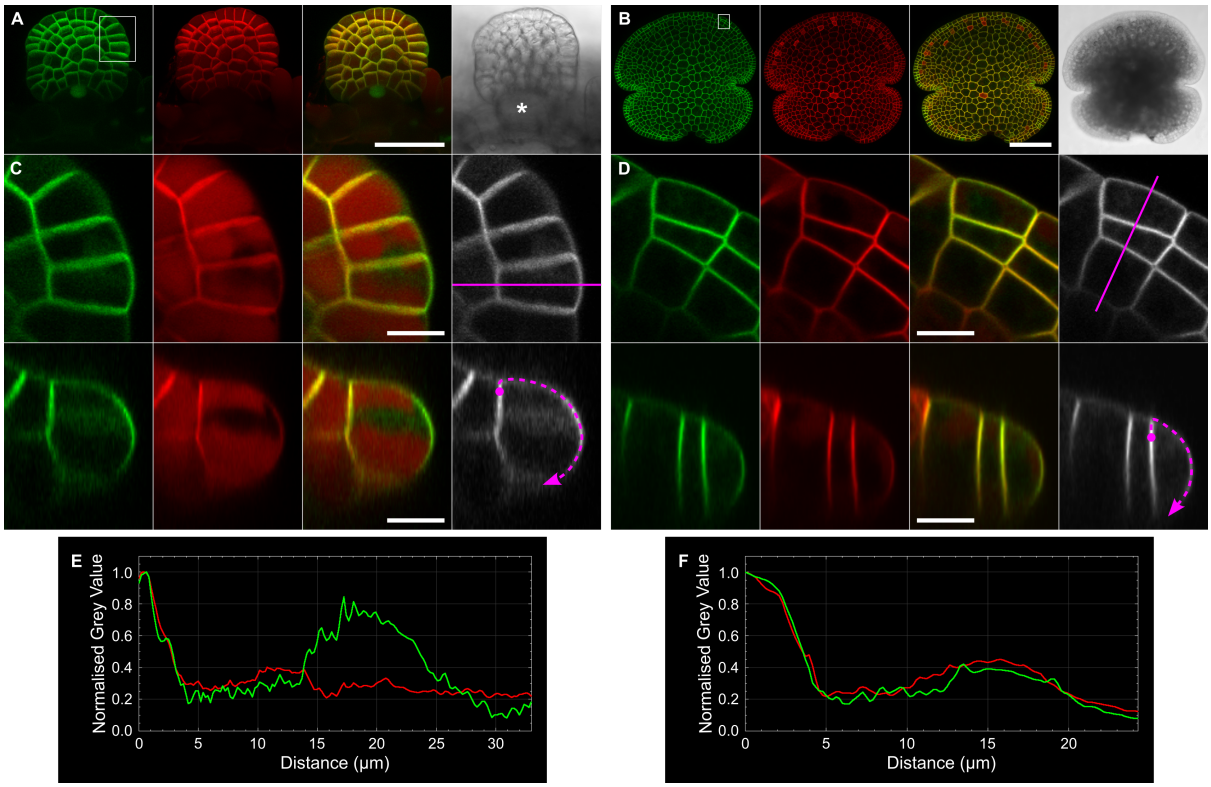

Figure 3.06 Polar subcellular localisation of Venus-MpROP in epidermal cells of developing immature gemmae

(A) Immature gemma developing at the base of a gemma cup, and (B) a maturing (yet not fully mature) gemma – expressing $_{pro}$Mp*ROP:Venus*-Mp*ROP*, $_{pro}$Mp*UBE2:mScarletI*-At*LTI6b*, and $_{pro}$Mp*RSL3:Venus-NLS*. From left to right, images of Venus fluoresce, mScarletI fluorescence, merged, and bright-field. Asterisk marks stalk connecting the gemma to the cup.
Marginal epidermal cells of (C) immature gemma (region marked by white box in A), and of (D) maturing gemma (region marked by white box in B). Optical cross section (bottom row) reveals Venus-MpROP polarised to the outer face of one of the marginal epidermal cells in the immature gemma but not in the maturing gemma. The solid magenta line overlaid on the Venus fluorescence images (in grey) indicates the optical cross section plane, and the dashed magenta line indicates the plasma membrane region along which fluorescence signal intensities from Venus-MpROP and mScarlet-AtLTI6b are compared in E and F.
(E, F) Normalised fluorescence intensities of Venus-MpROP (green) and mScarlet-AtLTI6b (red) along the plasma membrane region marked with the dashed magenta line in C and D. Measurement starts from point marked with magenta circle (distance = 0µm) and ends at point marked by the arrowhead (distance = 33µm for E, 24µm for F). Scale bars, 40µm (A), 100µm (B), and 10µm (C and D). Fluorescent images in A and B are maximum Z-projection images whilst those in C and D are sum projection of five consecutive images.

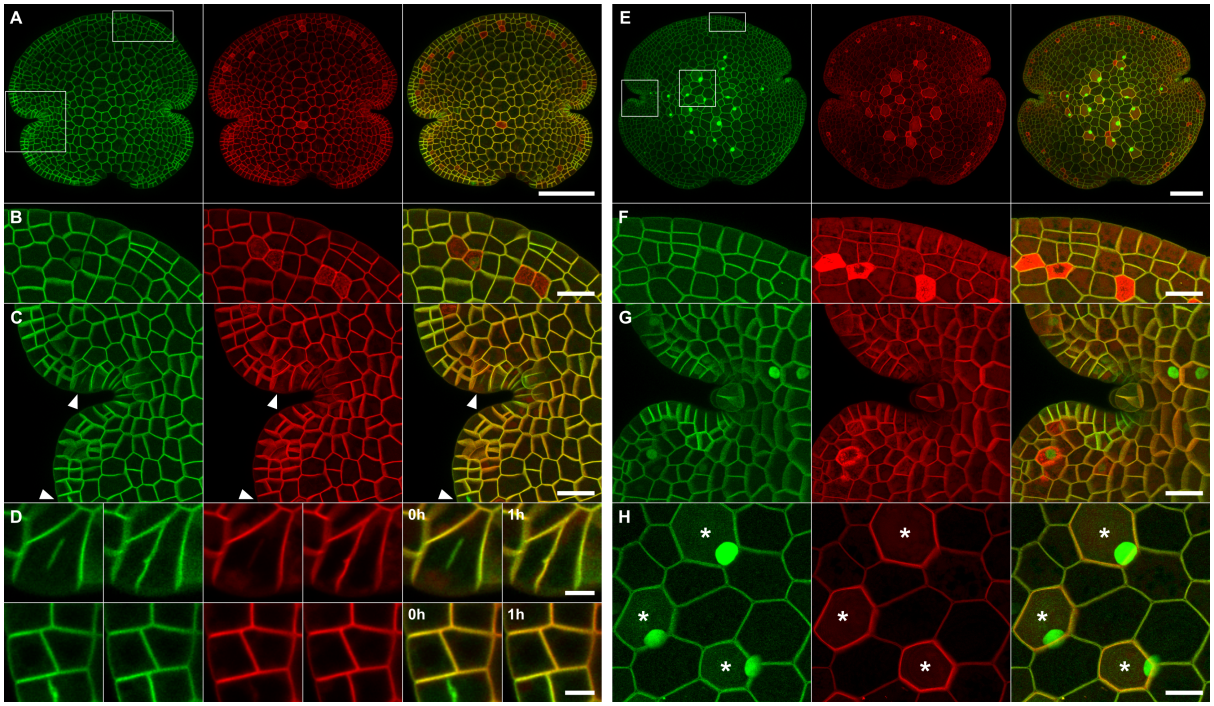

Figure 3.07 Venus-MpROP localises to the new cell plate formed by dividing epidermal cells in maturing gemmae

Maturing gemma (A-D) and fully mature gemma (E-H) expressing $_{pro}$Mp*ROP:Venus*-Mp*ROP*, $_{pro}$Mp*UBE2:mScarletI*-At*LTI6b*, and $_{pro}$Mp*RSL3:Venus-NLS*. Venus fluorescence in green and mScarletI fluorescence in red. For each gemma, merged image of Venus and mScarletI fluorescence shown in the right column. White boxes in A and E mark regions shown in B-C and F-H respectively.

(C, D). In the maturing gemma, Venus-MpROP localises to the new cell plate before the plasma membrane marker mScarletI-AtLTI6b (arrowheads in C). Higher magnification images of two dividing epidermal cells, and how they appear after 1 hour, are shown in D.

As well as difference in gemma size, the expression of $_{pro}$Mp*RSL3-Venus-NLS* in rhizoid initials (marked with asterisks in H) distinguishes fully mature gemma from maturing gemma.

Cortical polar Venus-MpROP localisation was not detected in epidermal cells at gemma margin (B, F), within the notch (C, G) or in the centre (D). Scale bars, 100µm (A, E); 20µm (B, C, F, H) and 5µm (D). Images are all maximum Z-projection images except for those in D, which are sum projection of five consecutive images around the medial plane of the new cell plate.

3.4.8 Mp*ROP* is required for gemma morphogenesis

To determine if Mp*ROP* is required for gemma morphogenesis, the phenotypes of mature gemmae in Mp*rop* mutants were described. Compared to WT gemmae which are characterised by their disk-like structure with two lateral apical notches, gemmae of the complete loss of function mutants, Mp*rop-1* and Mp*rop*-3, are globular and lack recognisable notches (Fig. 3.08A). Furthermore, Mp*rop-1* and Mp*rop-3* produce fewer gemmae compared to WT, with some mutant gemma cups being empty (Fig. 3.08B). This indicates that Mp*ROP* is required for the initiation or completion of gemma development, as well as morphogenesis. Gemma shape of the partial loss of function mutant, Mp*rop-2*, is also defective compared to WT. The two meristematic notches are present, and the general disc-like structure is similar to WT, however, the Mp*rop-2* gemma margin is irregular compared to the uniformly curved gemma margin of WT (Fig. 3.08A). This is consistent with the hypothesis that Mp*ROP* regulates polarised diffuse growth of gemma marginal cells. The gemma phenotype of Mp*ren* is also defective, further demonstrating the involvement of ROP signalling in gemma morphogenesis (Fig. 3.08A). These data overall clearly demonstrate that Mp*ROP* is required for gemma morphogenesis.

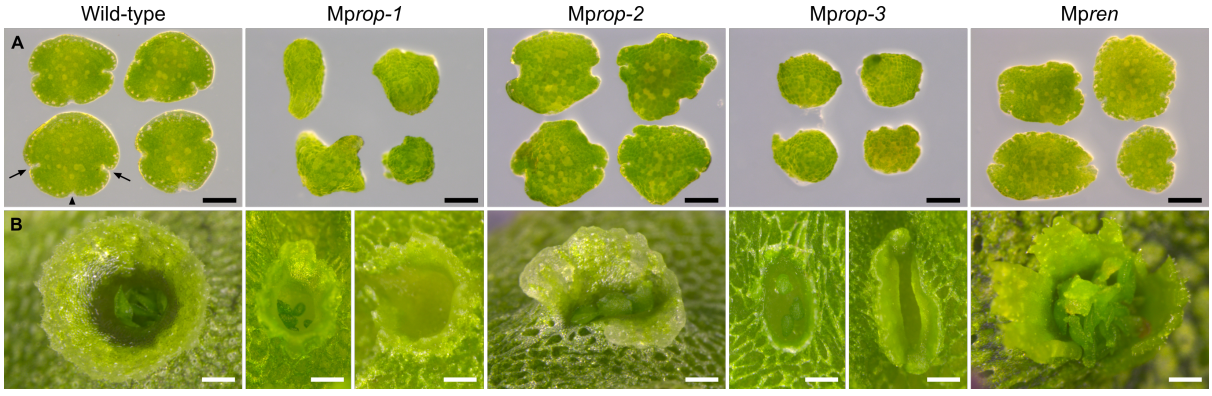

Figure 3.08 Mp*ROP* is required for gemma morphogenesis
Stereomicroscope images of (A) 0-day old gemmae, and (B) gemma cups of wild-type, Mp*rop-1*, Mp*rop-2*, Mp*rop-3*, and Mp*ren*.
(A) Meristematic notches and stalk attachment site are indicated for a wild-type gemma by arrows and arrowhead, respectively. Mp*rop-1* and Mp*rop-3* gemmae are globular and lack recognisable meristematic notches. Mp*rop-2* and Mp*ren* gemmae are misshapen but recognisable meristematic notches are present. Scale bar, 200µm.
(B) Mp*rop-1* and Mp*rop-3* gemma cups contain very few or no gemmae. Scale bar, 500µm.

To define how MpROP functions during gemma morphogenesis, morphometric analyses were performed for WT, Mp*rop-1*, and Mp*rop-2* gemmae. Mp*rop-1* gemmae are significantly smaller than WT gemmae; gemma height and width of Mp*rop-1* are less than WT (Fig. 3.09 A, B). However, Mp*rop-1* gemmae are significantly thicker than WT gemmae (Fig. 3.09 A, C). This increased gemma thickness could be due to an increase in cell layer number or cell depth compared to WT. To test which of these are responsible for increased gemma thickness in Mp*rop-1*, cell layer number and average cell depth (gemma thickness/cell layer number) were quantified. There are more cell layers in Mp*rop-1* gemmae than in WT gemmae (Fig. 3.09D). However, the Mp*rop*-1 average cell depth is also larger than WT (Fig. 3.09E). Therefore, an increase in both cell layer number and cell depth contributes to thicker gemmae in Mp*rop-1*. These parameters were indistinguishable between Mp*rop-2* and WT through the morphometric analyses, indicating that the partial loss of function mutant broadly retains the ability to control gemma morphogenesis. Based on the morphometric comparison of WT and Mp*rop-1* gemma phenotypes, I predict MpROP coordinates tissue morphogenesis by regulating both cell growth and division orientation.

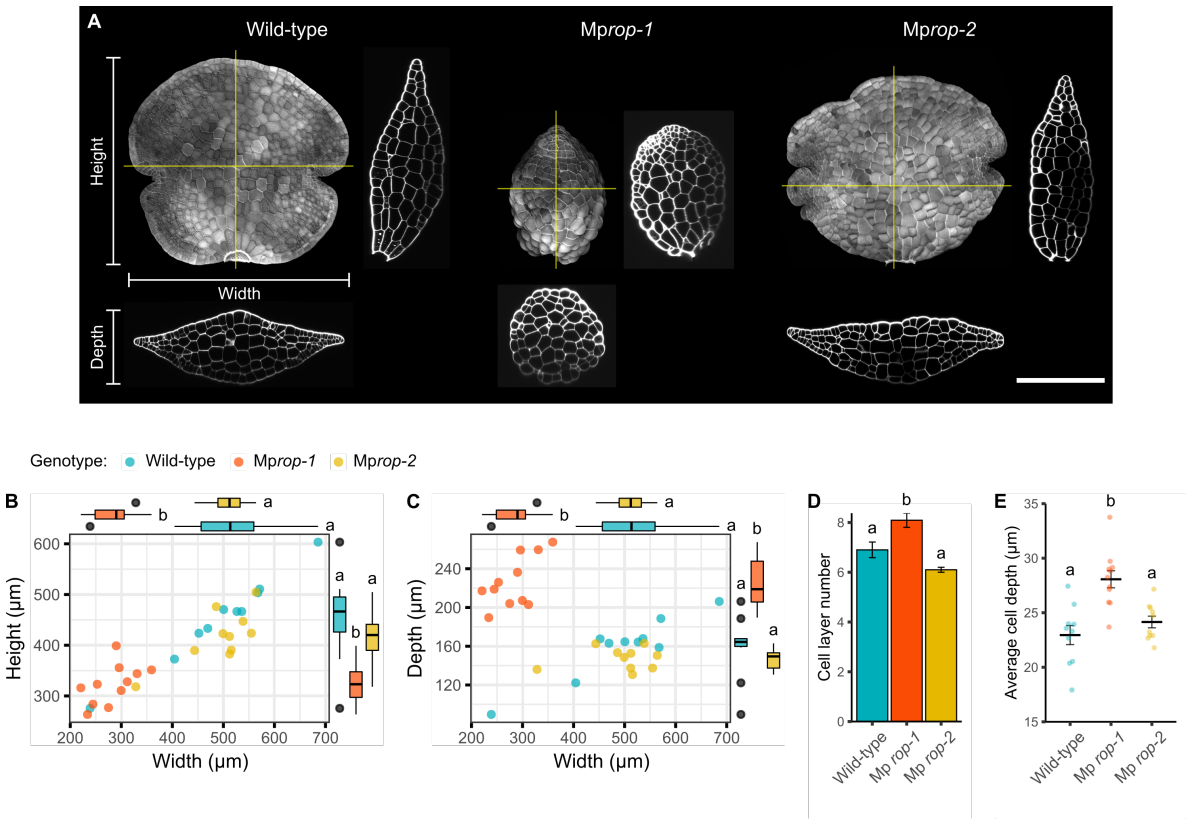

Figure 3.09 Three-dimensional shape of gemma is disrupted in Mp*rop-1*

(A) Maximum Z-projection image and a pair of orthogonal optical cross section images for wild-type, Mp*rop-1*, and Mp*rop-2* gemmae, which were fixed, cleared, and stained with the cell wall dye SR2200. Yellow lines indicate orthogonal cross section planes. Scale bar, 200µm.

(B) Mp*rop-1* gemmae are smaller than wild-type and Mp*rop-2* gemmae in terms of width and height. Each dot in the scatter plot represents height and width of an individual gemma. Box plot above represents distribution of gemma width and box plot to the right represents distribution of gemma height.

(C) Mp*rop-1* gemmae are thicker in depth than wild-type and Mp*rop-2* gemmae. Each dot in the scatter plot represents depth and width of an individual gemma. Box plot above represents distribution of gemma width and box plot to the right represents distribution of gemma depth.

(D) Mp*rop-1* gemmae consist of more cell layers on average than wild-type and Mp*rop-2* gemmae. By inspecting optical cross section images, the number of cell layers making up the thickest part of each gemma was counted. Bars represent mean and error bars represent standard error of the mean.

(E) Mp*rop-1* gemma cells are thicker on average than wild-type and Mp*rop-2* gemma cells. Average cell depth for each gemma was calculated by dividing gemma depth with the number of cell layers at the thickest part of a gemma. Main horizontal black bars represent mean and error bars represent standard error of the mean. Each dot represents average cell depth for an individual gemma.

Different lower-case letters (in B-E) indicate groups with significantly different means, based on one-way ANOVA followed by Tukey's HSD test ($p < 0.05$). n = 10 for wild-type and Mp*rop-2*, n = 11 for Mp*rop-1*.

3.4.9 MpROP controls gemma morphogenesis by regulating anisotropic diffuse growth

To test the hypothesis that MpROP controls tissue morphogenesis by regulating cell growth orientation, I defined the role of MpROP in shaping gemma epidermal cells. The gemma epidermal surface of Mp*rop-1* mutant is uneven compared to WT, and the mutant epidermal cells swell out of the epidermal surface (Fig. 3.09A). To compare the extent of cell growth at the epidermal surface in WT and Mp*rop-1*, I quantified the surface curvature of individual gemma epidermal cells using the MorphoGraphX software. The average surface curvature of Mp*rop-1* gemma epidermal cells is significantly greater than that of WT, indicating that epidermal cell growth in Mp*rop-1* is not restricted to the plane parallel to the gemma surface, but occurs isotropically (Fig. 3.10). Moreover, a wider range of cell surface curvature values are observed for Mp*rop-1* gemma, which is consistent with a loss in regulation of cell growth orientation. Therefore, I conclude that MpROP contributes to gemma morphogenesis by regulating anisotropic cell growth orientation.

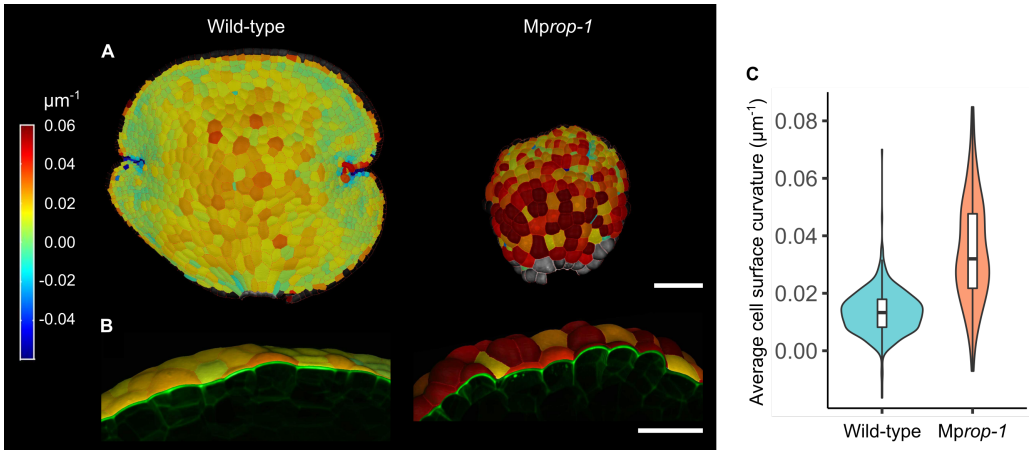

Figure 3.10 MpROP controls gemma morphogenesis by regulating anisotropic diffuse growth
(A, B) Heatmap displaying average surface curvature for a region 20μm in radius from the centre of each segmented cell surface. (A) surface view and (B) optical cross-sectional view. Scale bars, 100μm (A) and 50μm (B).
(C) Average cell surface curvature is significantly greater and more varied in Mp*rop-1* than in wild-type. Violin plots show distribution of curvature values and box plots within show median and interquartile range. This analysis was restricted to cells with an area > 150μm^2 as a region of 20μm in radius greatly exceeds the area of very small cells, meaning curvature values for very small cells represent the tissue curvature of a neighbourhood centred around the cell, rather than the surface curvature of the individual cell. Statistically significant difference in mean average cell curvature (Welch's t-test, $p < 2.2e^{-16}$) and variance (Levene's test, $p < 2.2e^{-16}$) between wild-type and Mp*rop-1*. n = 523 cells (1 gemma) for wild-type and 199 cells (1 gemma) for Mp*rop-1*.

3.4.10 Venus-MpROP proteins are polar localised in cells of developing air chambers

To investigate if MpROP contributes to tissue morphogenesis by regulating cell division pattern, I next characterised MpROP function in air chamber development as a series of oriented divisions is known to be important for their formation (Apostolakos et al., 1982). If MpROP controls air chamber morphogenesis, I hypothesised that the MpROP protein would mark the sites of polarised growth and cell division during air chamber development. To test this hypothesis, I determined Venus-MpROP subcellular localisation in cells of the developing air chamber. At a very early stage of air chamber development, cells which surround the initial aperture grow in a polarised fashion, inwards and slightly upwards towards the aperture entrance at the epidermal surface, effectively occluding the aperture entrance (Fig. 3.11C). In these aperture-surrounding cells, Venus-MpROP appears to be polarised to the cortical sites of growth, suggesting that MpROP promotes local polarised growth (Fig. 3.12A). Subsequently, these aperture-surrounding cells divide obliquely to form the roof mother cells (Fig. 3.11C). Venus-MpROP localised early to the new cell plate formed through this oblique division, consistent with the hypothesis that MpROP regulates cell division during air chamber development (Fig. 3.12B, cell marked with blue asterisk). The roof mother cell then divides anticlinally, giving rise to the roof cells of the air chamber (Fig. 3.11D). The roof cells which surround the closed aperture entrance, the air pore mother cells, undergo an oblique division to initiate air pore formation (Fig. 3.11E). During this oblique division, Venus-MpROP localises early to the new cell plate, suggesting that MpROP may be required for executing the switch in cell division orientation critical for air pore development (Fig. 3.12C, cell marked with blue asterisk). These data are therefore consistent with the hypothesis that MpROP regulates cell division pattern during air chamber morphogenesis.

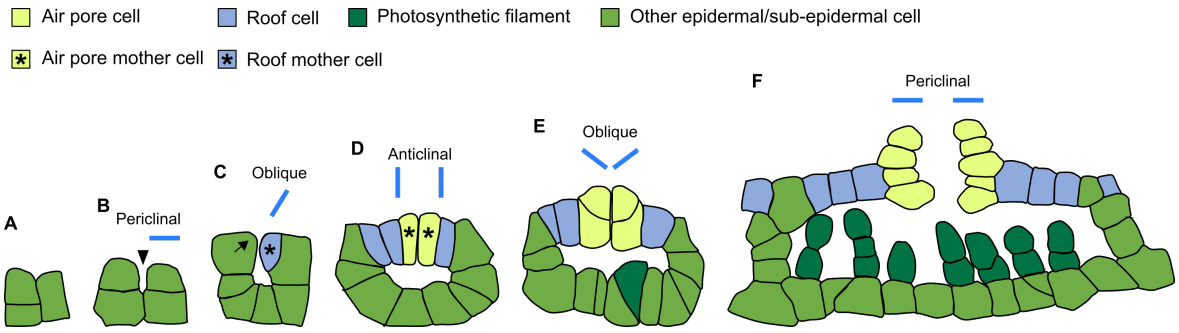

Figure 3.11 The air chamber is formed through a series of oriented cell divisions

Schematic representation of wild-type air chamber development in *Marchantia*, based on Apostolakos et al., 1982 and my own observations. Diagrams illustrate how air chambers appear in the cross-sectional plane, perpendicular to the dorsal epidermal surface.

(A, B) Air chamber development commences with the formation of the initial aperture (arrowhead in B) at the intersect of usually four epidermal cells close to the apical cell within the meristematic notch (see Figure 3.15A for epidermal surface view). This happens through the schizogenous separation of the anticlinal cell walls at the junction between the four cells.

(C) The epidermal cells surrounding the aperture entrance grow inwards and slightly upwards towards the aperture entrance at the epidermal surface. Arrow indicates cell growth orientation. This results in the closure of the aperture entrance. An oblique division follows producing the roof mother cell.

(D) The air chamber roof is formed through the anticlinal division of the roof mother cells. Simultaneously, the anticlinal division of the subepidermal cells which form the air chamber floor, expands the air chamber. Roof cells surrounding the aperture entrance elongate perpendicular to the epidermal surface to differentiate into air pore mother cells.

(E) Air pore formation initiates with the oblique division of the air pore mother cells. Development of photosynthetic filaments start at around the same time.

(F) Periclinal divisions complete air pore formation.

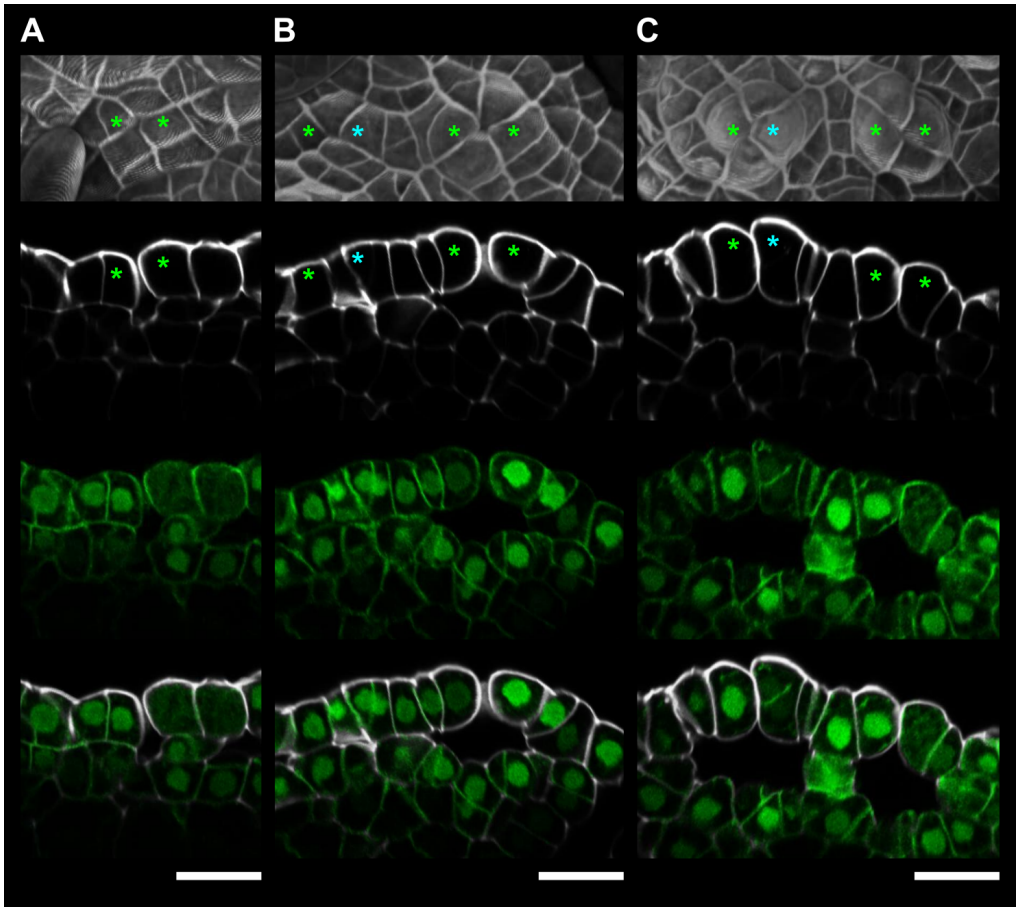

Figure 3.12 Polar localisation of Venus-MpROP in cells surrounding the aperture of immature air chambers

Immature air chambers of 6-day old gemmaling expressing $_{pro}$Mp*ROP:Venus*-Mp*ROP* fixed, cleared, and stained with the cell wall dye SR2200. Top row displays surface projection images (SR2200 fluorescence in grey). Second to forth rows show optical cross section images of SR2200 fluorescence (grey), Venus fluorescence (green) and the two channels merged. Asterisks mark cells surrounding the air chamber aperture entrance. Scale bar, 20µm.

In cells surrounding the initial aperture (A), Venus-MpROP appear to be polarised to the cortical region known to grow inwards and slightly upwards towards the entrance of the aperture. Venus-MpROP is potentially also polarised in a similar manner in aperture surrounding cells at a more advanced stage of air chamber development (B). Venus-MpROP observed early (before formation of cross-wall based on the absence of cell wall staining) at the new cell plate of cells dividing obliquely (marked with light blue asterisks) to give rise to the roof mother cell (B) and the air pore cells (C).

3.4.11 Mp*ROP* is required for air chamber morphogenesis

To test if Mp*ROP* is required for air chamber morphogenesis, I compared the dorsal thallus epidermis of WT and Mp*rop* mutants under the stereomicroscope. In WT, the dorsal thallus epidermis comprises a single layer of air chamber roof cells, regularly interspersed with air pores. An air pore complex together with surrounding roof cells constitute the epidermal surface of a single air chamber unit (epidermal boundary of one air chamber unit is demarcated in Fig. 3.13C). Neighbouring air chamber units are separated by a wall of cells (Fig. 3.11F). In the complete loss of function mutants, Mp*rop-1* and Mp*rop-3*, the walls separating the individual air chamber units are present, but the air chamber roof and the pores are missing (Fig. 3.13C). In the partial loss of function mutant, Mp*rop-2*, the separating walls are present, but only a partial roof develops, and air pore complexes are entirely absent. These mutant phenotypes indicate that Mp*ROP* is required for the formation of the air chamber roof and the air pore complex.

The dorsal thallus epidermis is also defective in the Mp*ren* mutant. However, unlike in Mp*rop* mutants, air pore complexes are present in the Mp*ren* mutant, but they appear ruptured in most cases (Fig. 3.13C). This suggests that modulation of ROP signalling by MpREN is necessary for air pore integrity.

The defective air chamber development in Mp*rop* mutants demonstrate that Mp*ROP* is required for air chamber formation and supports the hypothesis that MpROP influences tissue morphogenesis by controlling cell division. This is tested next.

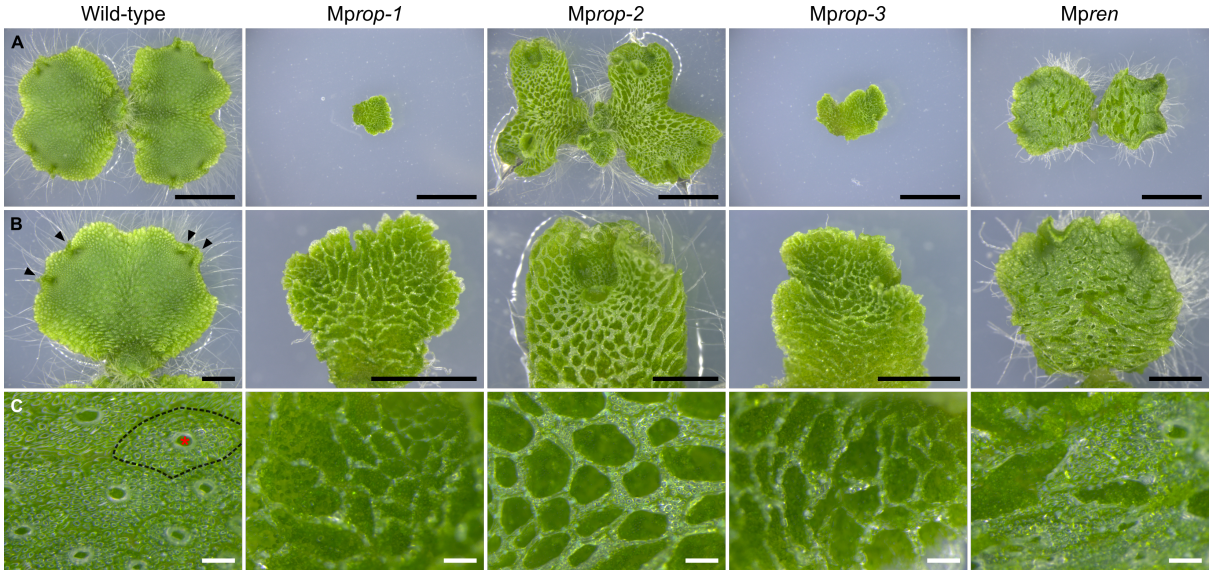

Figure 3.13 Mp*ROP* is required for air chamber morphogenesis
Stereomicroscope images of the dorsal thallus surface of 14-day old gemmalings.
(A) Whole gemmaling (scale bar, 5mm).
(B) Single thallus lobe (scale bar, 2mm). Arrow heads in the wild-type image point to the meristematic notches.
(C) Dorsal thallus epidermis (scale bar, 200µm). The dorsal thallus epidermis is composed of air pore cells and air chamber roof cells in wild-type. The boundary of one air chamber unit is demarcated with a black dashed line and the air pore of this air chamber is marked with a red asterisk. In Mp*rop-1* and Mp*rop-3*, air chamber boundaries are visible, but air chamber roofs, including the air pore complexes appear to be missing. In Mp*rop-2*, air chamber roofs are partially present, but air pore complexes are not visible. Consequently, in Mp*rop-1*, Mp*rop-2*, and Mp*rop-3*, photosynthetic filaments emanating from the floor of the air chamber are visible, unlike in wild-type. In Mp*ren*, air chamber roofs and air pore complexes are visible, however, many air pores are ruptured.

3.4.12 Mp*ROP* is required for the switch in cell division orientation during air chamber morphogenesis

To determine the cellular cause of the air chamber tissue defects of Mp*rop* mutants, I defined cellular organisation of air chambers in WT, Mp*rop-1*, and Mp*rop-2*. In *Mprop-1* a wall of cells which form the boundary between neighbouring air chamber units are present, however, neither roof cells nor air pore cells were found, confirming that a complete loss of Mp*ROP* function prevents the differentiation of these cell types (Fig. 3.14B, E). In WT, an oblique cell division gives rise to the roof mother cell (Fig. 3.11C). No evidence was found for this formative division taking place in Mp*rop-1*, suggesting that this is the cause for the absence of roof cells in Mp*rop-1*. Thus, Mp*ROP* is likely required for the oblique division to initiate air chamber roof formation.

Cellular organisation in the air chambers of Mp*rop-2* also indicates defect in cell division. Before air pore formation commences in WT, the roof cells surrounding the aperture entrance elongate perpendicular to the epidermal surface to differentiate into the air pore mother cells (Fig.3.11D). These then undergo oblique division to produce the first air pore cells, which continue to divide periclinally, to form the final air pore structure (Fig. 3.11E, F, 3.14D). Although there is evidence of anticlinal divisions of roof cells in Mp*rop-2*, neither oblique nor periclinal divisions of roof cells surrounding the aperture entrance were observed (Fig. 3.14F). Moreover, there was no indication of *Mprop-2* roof cells elongating perpendicular to the epidermal surface, as observed in WT, demonstrating that they do not differentiate into air pore mother cells. In WT, the oblique division of the air pore mother cells is followed by the emergence of photosynthetic filaments from the chamber floor (Fig. 3.14D). The absence of the air pore in Mp*rop-2* air chambers which have matured, indicated by the presence of photosynthetic filaments, further supports the hypothesis that the oblique division for initiating air pore formation does not take place in Mp*rop-2* (Fig. 3.14F). Therefore, Mp*ROP* is likely required for the oblique divisions to initiate air pore formation.

To summarise, a switch in cell division orientation to an oblique orientation that occurs during WT air chamber development does not occur in the Mp*rop* mutants. Thus, Mp*ROP* likely controls tissue morphogenesis through regulating cell division orientation.

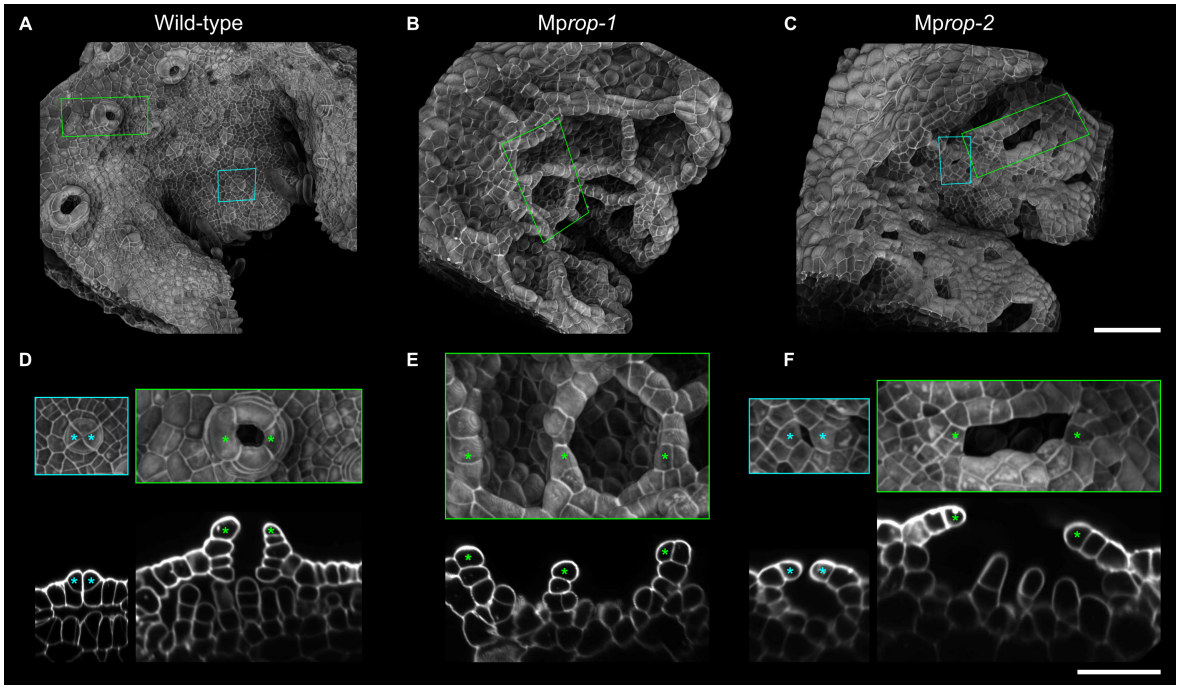

Figure 3.14 Mp*ROP* is required for switch in cell division orientation during air chamber morphogenesis

(A-C) 3D surface projection images of the dorsal thallus epidermis close to the meristematic notch from 6-day old gemmalings of wild-type, Mp*rop-1*, and Mp*rop-2* (fixed, cleared, and stained with the cell wall dye SR2200). Higher magnification images of boxed regions are shown in D-F. (D-F) Air chamber roof cells are absent in Mp*rop-1*, and air pore cells are absent in both Mp*rop-1* and Mp*rop-2*. Surface projection and optical cross section images of immature and mature air chambers from wild-type, Mp*rop-1*, and Mp*rop-2*. Cells forming the aperture boundary are marked with asterisks. In wild-type, anticlinal cell divisions form the air chamber roof. This takes place in Mp*rop-2* but not in Mp*rop-1*. In wild-type, a change in cell division orientation from anticlinal to periclinal facilitates air pore formation. This was not observed in Mp*rop-1* or Mp*rop-2*. Scale bars, 100µm (A-C) and 50µm (D-F).

3.4.13 Mp*ROP* is likely required for maintaining cell adhesion during air chamber morphogenesis

The absence of the oblique division required for air pore complex formation explains the absence of air pores in Mp*rop-2*, however, this does not explain the larger air chamber aperture of Mp*rop-2* compared to that of WT (Fig. 3.14C). A cell adhesion defect in Mp*rop-2* could cause the larger air chamber aperture. The first step in WT air chamber development is the formation of the initial

aperture at the intersect of usually four epidermal cells through schizogenous cell wall separation (Fig. 3.15A). This results in the separation of the anticlinal cell edge at the centre of the group of four cells. In other words, within the group of four cells, each cell only completely detaches from the cell diagonally opposite it and retains contact through their anticlinal cell faces with the two adjacent cells. This contact between adjacent cells at the aperture entrance is retained and consequently each air pore cell is connected to two adjacent air pore cells through their anticlinal walls in WT (Fig. 3.15A). In Mp*rop-2*, each of the four roof cells surrounding the aperture entrance are only in contact with one of their direct neighbours, suggesting a greater degree of cell wall separation than in WT (Fig. 3.15B). Continuation of cell wall separation during air chamber development could result in further expansion of the aperture entrance. I therefore speculate that MpROP also contributes to air chamber morphogenesis by maintaining cell adhesion.

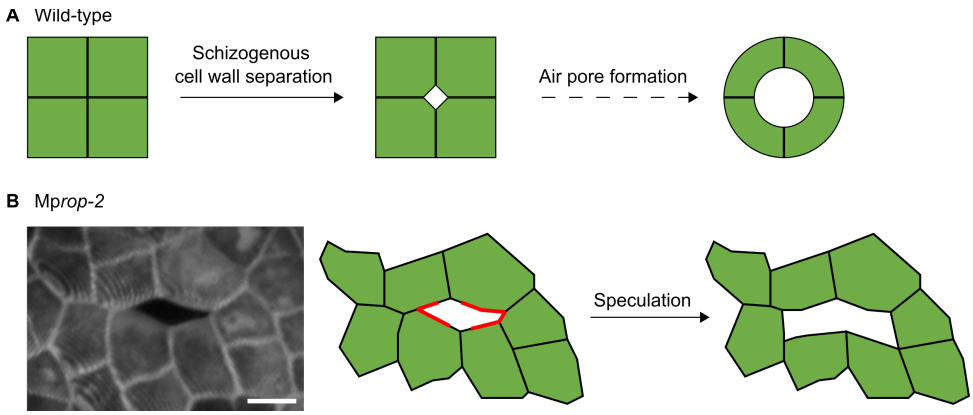

Figure 3.15 Mp*ROP* is likely required for maintaining cell adhesion during air chamber morphogenesis

(A) Schematic illustrating aperture formation (plane parallel to the epidermis) in wild-type, based on Apostolakos et al., 1982 and my own observations. The initial aperture forms at the junction of usually four epidermal cells. Following schizogenous cell wall separation, each cell surrounding the aperture entrance retains contact with their two adjacent neighbours and only completely detaches from the cell diagonally opposite it. This contact between cells at the aperture entrance is retained throughout air chamber development.

(B) Aperture entrance of immature air chamber of Mp*rop-2* (shown in Figure 3.14F). Each of the four epidermal cells surrounding the aperture entrance are in contact with only one neighbouring aperture cell. Anticlinal cell walls expected to remain adhered (if like wild-type) are highlighted in red. I speculate how the aperture entrance could expand further if cell wall separation continued. Scale bars, 10µm.

3.5 Discussion

3.5.1 ROP is required for orchestrating morphogenesis of complex tissues

ROP proteins in angiosperms are instrumental in cellular morphogenesis (Fu et al., 2005; Jones et al., 2002), however, how they influence morphogenesis at the tissue level has remained unclear. Recent work in the moss *P. patens* has indicated the requirement of ROP function in tissue patterning, although this is based on characterising ROP function in protonema, a relatively simple filamentous structure which forms before the more complex leafy gametophore (Cheng et al., 2020). In this chapter, I have demonstrated that ROP function is required for the morphogenesis of complex epidermal tissues in the liverwort *M. polymorpha*. As well as influencing cell growth and division orientation, I have shown that ROP function in modulating cell adhesion could be important for plant morphogenesis. The spatiotemporal coordination of these different cellular processes is critical for the proper formation of complex tissue, and ROP may represent a master regulator which ensures the coordination of different cellular processes to achieve tissue morphogenesis.

3.5.2 ROP function in regulating cellular processes important for tissue morphogenesis is conserved among land plants

In this chapter, I showed that MpROP coordinates tissue morphogenesis by regulating polarised cell growth, formative cell division associated with cell differentiation, and possibly cell adhesion. All three of these ROP functions have been described to varying extents in other land plants, notably in vascular plants, which suggests that these cellular ROP functions have remained conserved at least since the time bryophytes last shared a common ancestor with vascular plants.

Polarised diffuse growth of *A. thaliana* pavement cells is regulated by AtROP2, AtROP4, and AtROP6. AtROP2 and AtROP4 drives lobe outgrowth by promoting actin assembly, and AtROP6 restricts growth at indented neck regions by activating the microtubule severing enzyme Katanin, which promotes the formation of parallel microtubule arrays (Fu et al., 2005, 2009; Lin et al., 2013). In the moss *P. patens*, ROP has also been demonstrated to promote the cortical

accumulation of actin for polarised growth but its role in regulating microtubule organisation remains unclear (Burkart et al., 2015). The Mp*rop-1* mutant gemma epidermal cells resemble *A. thaliana* sepal epidermal cells treated with the microtubule depolymerising drug Oryzalin (Zhao et al., 2020). This suggests that like AtROP proteins, MpROP restricts anisotropic cell growth orientation through influencing cortical microtubule organisation. Therefore, the mechanism through which ROP regulates polarised diffuse cell growth is likely broadly conserved among land plants.

Mp*rop-1* and Mp*rop-2* are defective in specific formative cell divisions associated with cell differentiation, resulting in roof-less and pore-less air chambers in Mp*rop-1* and Mp*rop-2*, respectively. There is also some evidence that ROP function in regulating formative cell divisions is conserved among land plants. *Z. mays* and *P. patens rop* mutants have defects in asymmetric cell divisions, required for subsidiary cell differentiation and protonema branching, respectively (Humphries et al., 2011; Yi & Goshima, 2020). In both cases, ROP has been hypothesised to guide nuclear migration required for asymmetric cell division, although how ROP precisely regulates asymmetric cell divisions remains unclear. For example, formative divisions like that for *P. patens* protonema branching and *M. polymorpha* air chamber roof formation, are proceeded by polarised cell growth, for which ROP is required. It is therefore unclear to what extent the defects in cell division orientation are an indirect consequence of the defects in polarised cell growth of *rop* mutants. In symmetrically dividing *A. thaliana* root cells, there is evidence for direct involvement of ROP signalling in cell plate positioning (Stöckle et al., 2016). Based on this, it is likely that MpROP functions in determining formative cell division orientation, indirectly, by driving polarised growth of the mother cell, but also directly, by regulating cell plate positioning. A system in which asymmetric cell division takes place without prior polarised cell growth could help uncouple ROP function in asymmetric cell division from its role in polarised cell growth. Although mechanistic understanding is still limited, formative division defects in both vascular plant and bryophyte *rop* mutants suggest that ROP function in regulating formative cell division is conserved in land plants.

In Mp*rop-2,* the complete separation of the anticlinal walls between neighbouring aperture surrounding cells strongly suggests defect in cell adhesion, as this is not observed in WT. A cell adhesion defect has also been reported for the *P. patens* RNAi *rop* knock-down mutant, and this has been associated with reduced cellulose and callose content in the cell wall (Burkart et al., 2015). No *rop* mutants in other plant species have been shown to have a clear cell adhesion defect. However, the *A. thaliana* null mutant in *SPIKE1*, a single copy gene in *A. thaliana* which encodes a GEF (a positive regulator of RHO signalling) has gaps in between pavement cells, consistent with a cell adhesion defect (Qiu et al., 2002). This therefore suggests that ROP function in cell adhesion has remained conserved at least since bryophytes last shared a common ancestor with vascular plants.

Based on the conservation of cellular ROP functions between bryophytes and vascular plants, which are required for tissue morphogenesis, it is likely that ROP regulated tissue morphogenesis in the last common ancestor of land plants.

3.5.3 Tight regulation of ROP signalling is necessary for tissue morphogenesis

As well as Mp*rop* mutants, the Mp*ren* loss of function mutant is morphologically defective at the tissue level, highlighting the need for proper spatial regulation of ROP signalling for tissue morphogenesis. The wavy rhizoid phenotype of Mp*ren* resembles rhizoids treated with microtube stabilising or destabilising drugs, suggesting MpREN regulates MpROP function associated with microtubules (Champion et al., 2021). The ruptured air pores of Mp*ren* suggests MpREN also regulates MpROP function in cell adhesion. The less severe morphological defects of Mp*ren* compared to Mp*rop-1* indicate that the two other RhoGAPs in *M. polymorpha*, MpRopGAP and possibly MpRopGAPL, also regulate ROP function in tissue morphogenesis. This would be consistent with the requirement of RopGAP in *P. patens* protonema development (Bascom et al., 2019). The regulation of MpROP function in gemma formation and possibly gemma morphogenesis is mediated through MpRopGEF as a loss of MpRopGEF function results in plants with empty gemma cups (Hiwatashi et al., 2019). The very specific defect of Mp*ropgef* in just gemma formation, implies that the other GEF protein in *M. polymorpha*, SPIKE1, plays a more

significant role in regulating ROP function in tissue morphogenesis. With the lack of genetic redundancy not only in *ROP* but also within the genes encoding all the core ROP regulators, *M. polymorpha* would be an ideal system to further our understanding of how ROP signalling is regulated for cellular and tissue morphogenesis.

In this chapter, I have demonstrated that ROP orchestrates the morphogenesis of complex plant tissue. It achieves this, through controlling polarised cell growth, formative cell divisions, and possibly cell adhesion, which are all likely ancestral ROP functions which have remained conserved at least since the time early land plants existed. In the next chapter, I set out to determine when ROP function evolved.

Chapter 4: The conservation of *ROP* gene function from early in the streptophyte lineage

4.1 Abstract

The general increase in morphological complexity in the streptophyte linage is thought to have initiated with the transition from unicellular/colonial forms, like that of extant *Mesostigma* and *Chlorokybus*, to a multicellular filamentous body plan, like that of extant *Klebsormidium*. The genetic basis of this transition is unknown. Based on phylogenetic analyses, the timing of ROP signalling establishment coincides with this transition period in early streptophytes (chapter 2). The ROP protein sequence has remained highly conserved since its establishment, and it regulates cell growth, division, and adhesion for tissue morphogenesis in land plants (chapter 3). To determine since when ROP protein function has remained conserved and to gain further insight into the ancestral ROP function, a series of cross-species complementation experiments was designed. *ROP* homologues from *Coleochaete scutata* and *Klebsormidium nitens* fully and partially complement the Mp*rop-1* loss of function mutant, respectively. In contrast, the *ROP* homologue from *Chlorokybus atmophyticus* fails to complement Mp*rop-1*, indicating that ROP molecular function has remained largely conserved since the time land plants last shared a common ancestor with the Klebsormidiales. The establishment of ROP function could potentially be associated with morphological innovations which evolved after the divergence of the *Mesostigma*/*Chlorokybus* lineage, for example cortical microtubule mediated anisotropic diffuse cell growth.

4.2 Introduction

RHO GTPase proteins are conserved throughout most eukaryotes and play a fundamental role in signalling cellular morphogenesis. Their role in controlling cell shape and cell growth orientation, mainly through regulating the cytoskeleton, is ancient as this has been reported in a diverse range of eukaryotes, from animal and fungi to plants (Chiou et al., 2017; Feiguelman et al., 2018; Luo, 2000). However, RHO signalling in plants has evolved to become distinct in a variety of ways from RHO signalling in animals and fungi, and hence plant RHO proteins have been termed RHO Of Plants (ROPs). Moreover, the precise mechanisms through which RHO signalling orchestrates cellular morphogenesis differ across eukaryotes, in part because distinct components of the cytoskeleton have different significance for cellular morphogenesis in different eukaryotic lineages

(Fletcher & Mullins, 2010; Szymanski & Cosgrove, 2009). This raises the question – how did RHO signalling evolve to become distinct in plants, and what significance did it have on the evolution of morphological complexity in plants?

Viridiplantae, or the green plants, comprise two lineages, the chlorophytes and the streptophytes, which are thought to have shared a unicellular common ancestor roughly a billion years ago and subsequently evolved multicellularity independently (Umen, 2014). Chlorophytes consist entirely of green algae, whilst the streptophytes consist of the monophyletic group Embryophyta, or land plants, and the paraphyletic streptophyte algae. Within streptophytes, land plants are considered morphologically the most complex and this has been attributed to the evolution of apical cells with three or more cutting faces, which can give rise to complex 3D tissues (Moody, 2020). The paraphyletic streptophyte algae consists of five major lineages – Zygnematales, Coleochaetales, Charales, Klebsormidiales, and *Chlorokybus*/*Mesostigma* – in order of relatedness to land plants (Puttick et al., 2018). With the exception of Zygnematales, which secondarily lost morphological complexity, a higher degree of morphological complexity is generally observed in streptophyte lineages more closely related to land plants (Rensing, 2020). This has been associated with the evolution of novel features/traits. For example, the evolution of the phragmoplast in the common ancestor of land plants, Zygnematales, Coleochaetales, and Charales (collectively known as the Phragmoplastophyta), is thought to have given cells greater control over cell division orientation, facilitating the transition from filamentous body plans like that of extant Klebsormidiales, to parenchymatous (tissue-like) plant bodies like that of extant Coleochaetales (Buschmann, 2020). Based on *Mesostigma* and *Chlorokybus* being unicellular and colonial respectively, it can be hypothesised that polarised diffuse growth and cell adhesion evolved in the streptophytes sometime after the divergence of *Chlorokybus*/*Mesostigma* and before that of Klebsormidiales, however, it is unclear what mechanistic or genetic novelties contributed to this transition.

Phylogenetic analyses of ROP and ROP specific regulators I carried out (chapter 2) suggest that ROP signalling became established in the common ancestor of Klebsormidiales and land plants, after the divergence of the *Chlorokybus*/*Mesostigma* lineage. If this were true, one would

hypothesise that ROP function has remained conserved since the time land plants last shared a common ancestor with Klebsormidiales. To address if a particular gene function has remained conserved since two species last shared a common ancestor, cross-species complementation can be attempted to see if the gene from one species can functionally replace the homologous gene in the other (Delaux et al., 2019). Cross-species complementation studies have contributed to our understanding of genes which may have been important for land plant evolution. However, successful complementation of land plant mutants with streptophyte algal homologues, which could potentially indicate a genetic novelty associated with the morphological evolution in early streptophytes, has not been reported to date (Bonnot et al., 2017; Frangedakis et al., 2017; Liang et al., 2013; Zhang et al., 2020).

In this chapter, I present a cross-species complementation study, using the *Marchantia polymorpha rop-1* mutant as an experimental system, to determine when ROP function became established in the streptophyte lineage. The ability of *ROP* homologues from three algal species, representing three of the five major streptophyte algal lineages, to complement Mp*rop-1* was assayed. Consistent with the ROP phylogenetic analyses, I demonstrate that ROP function has remained largely conserved since the time land plants last shared a common ancestor with Klebsormidiales. This potentially signifies a role of ROP in the evolution of morphological complexity early in the streptophyte lineage.

4.3 Materials and Methods

4.3.1 Plant material and growth conditions

See chapter 2 for standard growth conditions and the generation of Mp*rop* mutants used in this chapter. Method for generating the complemented lines is described below.

4.3.2 Generation of complementation constructs

The OpenPlant Loop assembly toolkit and associated protocol provided by Sauret-Güeto et al., 2020 were used to generate four complementation constructs, encoding the coding sequence (CDS)

of Mp*ROP* or its homologues from *Coleochaete scutata*, *Klebsormidium nitens*, or *Chlorokybus atmophyticus*, all downstream of the Mp*ROP* promoter sequence.

The Mp*ROP* promoter sequence, corresponding to 4kb directly upstream of the Mp*ROP* start codon was PCR amplified from the $_{pro}$Mp*ROP:Venus*-Mp*ROP* construct (generated in chapter 3) in four separate fragments to domesticate internal *Bsa*I and *Sap*I recognition sites. Thermo Scientific Phusion Green High-Fidelity DNA Polymerase and primers listed in Appendix table 1 were used. The four PCR products were assembled into the pUAP4 vector through a *Sap*I assembly reaction, to generate L0_PROM5_MpROP.

The CDS for Mp*ROP* and its homologues from *C. scutata*, *K. nitens*, and *C. atmophyticus* were ordered as gBlocks Gene Fragments from IDT. No internal *Bsa*I and *Sap*I are present in the four CDS, hence no mutations were introduced into the sequences. The algal CDS were obtained from sources listed in Table 2.01**.** Appropriate overhang sequences were included in the gBlocks for *Sap*I assembly into the pUAP4 vector, to generate L0_CDS_MpROP, L0_CDS_CsROP, L0_CDS_KnROP, and L0_CDS_CaRHO.

Three L0 parts (L0_PROM5_MpROP, L0_CDS, and L0_3TERM_NOS-35S which encodes the Nos-35S terminator) were assembled into the pCk2 acceptor vector through the *Bsa*I assembly reaction to generate L1 plasmids encoding the transcriptional unit $_{pro}$Mp*ROP:RHO-Nos35S.* Finally, these L1 plasmids were combined with OP-062, OP-066, OP-012 and OP-005 (all provided in the OpenPlant Kit) in a L2 *Sap*I assembly reaction to generate expression vectors encoding the hygromycin phosphotransferase gene (for selection of transformants), $_{pro}$Mp*ROP:RHO* and $_{pro}$Mp*UBE2:mTurqoise-N7* (ubiquitous nuclear marker).

4.3.3 Plant transformation

Thallus transformation based on method developed by Kubota et al., 2013. First, plants were grown from gemmae or thallus clippings (as Mp*rop-1* produces very few gemmae) on Gamborg's medium under standard growth conditions (see chapter 3) for two weeks. Then, using a sterilised cork borer, disc shaped clippings (4mm diameter) were collected from the thallus, avoiding the

meristematic notch. Thallus discs were placed back on original media plates (making sure ventral side facing the agar surface) for 3 days of regeneration under standard growth conditions. Roughly 50 and 90 thallus discs were prepared per transformation for WT and Mp*rop* lines, respectively.

GV3101 *Agrobacterium tumefaciens* transformed with the desired expression construct was cultured from a single colony in 5ml of M51C medium (Honkanen et al., 2016; Ono et al., 1979) at 28°C in the dark with constant agitation (180rpm). After 2 days incubation, 2ml of the culture was spun down (3,000g, 10 minutes) and the pellet resuspended in 10ml of M51C containing 100µM acetosyringone. After a further 6 hours of incubation, 1ml of the induced *Agrobacterium* culture was added to a sterile 125ml Erlenmeyer flask containing 50ml M51C medium, together with acetosyringone (final concentration of 100µM) and 40–50 regenerating thallus discs. Flasks were left at 23°C under continuous white light (50–60µmol m^{-2} s^{-1}) with constant agitation (130 rpm) for 3-day co-cultivation.

Following 3 days of co-cultivation, thallus discs were washed in water then in 1mg/ml Cefotaxime as described by Kubota et al., 2013, and finally plated on standard Gamborg's medium containing 150µg/ml cefotaxime and 10µg/ml hygromycin and grown under standard condition (see chapter 3) for selection. Transformants were selected 2–3 weeks later. Thallus transformations carried out for this chapter are listed in the table below.

Line	**Construct**
Mp*rop-1 Cas9*-free T_1	$_{pro}$Mp*ROP:*Mp*ROP*$_{pro}$Mp*UBE2:mTurquoise2-N7*
Mp*rop-2 Cas9*-free T_1	$_{pro}$Mp*ROP:*Mp*ROP*$_{pro}$Mp*UBE2:mTurquoise2-N7*
WT *Cas9*-free T_1 (Mp*rop-2* T_1 sibling)	$_{pro}$Mp*ROP:*Mp*ROP* $_{pro}$Mp*UBE2:mTurquoise2-N7*
Mp*rop-1 Cas9*-free T_1	$_{pro}$Mp*ROP:Venus*-Mp*ROP*
Mp*rop-2 Cas9*-free T_1	$_{pro}$Mp*ROP:Venus*-Mp*ROP*
WT *Cas9*-free T_1 (Mp*rop-2* T_1 sibling)	$_{pro}$Mp*ROP:Venus*-Mp*ROP*
Mp*rop-1 Cas9*-free T_1	$_{pro}$Mp*ROP:*Cs*ROP* $_{pro}$Mp*UBE2:mTurquoise2-N7*
Mp*rop-1 Cas9*-free T_1	$_{pro}$Mp*ROP:*Kn*ROP* $_{pro}$Mp*UBE2:mTurquoise2-N7*
Mp*rop-1 Cas9*-free T_1	$_{pro}$Mp*ROP:*Ca*RHO*$_{pro}$Mp*UBE2:mTurquoise2-N7*

Table 4.01 Thallus transformations carried out in this study

4.3.4 Scoring complementation (tissue level assessment)

For phenotyping, successful transformants grown from gemmae (or thallus clipping) for 2–4 weeks under standard growth conditions were inspected under the Leica MZ16FA stereomicroscope. For each transformant, the extent of restoration of WT-like air pore/chamber morphology, gemma production, gemma cup morphology, and rhizoid growth was qualitatively assessed. Phenotyped transformants were propagated through gemma (or thallus clipping) to repeat phenotyping on clonal progeny, to validate the first round of phenotyping.

4.3.5 Imaging of live specimens

Images were acquired with the Leica MZ16FA stereomicroscope, equipped with the Leica DFC300 FX camera, or the Keyence VHX7000 digital microscope equipped with the VH-Z00R/Z00T and VH-ZST lenses and the VHX-7020 camera.

4.3.6 Rhizoid imaging and length measurement

See chapter 3 methods.

4.3.7 Gemma fixation, clearing, and staining

See chapter 3 methods.

4.3.8 Confocal microscopy of fixed gemmae

Same method was used as in chapter 3, with the following modifications – to acquire fluorescence images of mTurquoise2 and the cell wall dye SR2200 (in chapter 3, did not acquire mTurquoise2 fluorescence), sequential scanning was used to avoid bleed through. The following excitation laser wavelength and emission capture bandwidth were used: SR2200 (ex 405nm, em 420–500nm, based on Tofanelli et al., 2019), mTurquoise2 (ex 458nm, em 463–553nm).

4.3.9 Statistical analysis

Data plotted on graphs and statistically analysed in R and Excel.

4.4 Results

4.4.1 Mp*rop-1* and Mp*rop-2* are both loss of function mutants

To identify a genetic background in which to test if *RHO* genes from diverse streptophyte species could complement *ROP* function in *M. polymorpha*, I first set out to validate that the two Mp*rop* mutants generated in chapter 3 are recessive, loss of function mutants. Mp*rop-1* and Mp*rop-2* are expected to be complete and partial loss of function mutants, respectively, based on the nature of the mutations they harbour in the Mp*ROP* gene, and based on their phenotypes (chapter 3). If they are indeed loss of function mutants, as opposed to gain of function mutants, introducing a wild-type (WT) copy of the Mp*ROP* gene should restore WT development. To confirm that these two are loss of function mutants, *Cas9*-free Mp*rop-1* and Mp*rop-2* mutants were transformed with a construct encoding the *M. polymorpha ROP* coding sequence (CDS) downstream of the *M. polymorpha ROP* promoter sequence (Fig. 4.03A), and the phenotypes of the resulting transformants were examined.

There was full restoration of WT development in the majority (64%) of Mp*rop-1* mutants transformed with $_{pro}$Mp*ROP*:Mp*ROP* (Fig. 4.01). Air chamber development, gemma production, gemma development, and rhizoid growth were all restored (Fig. 4.01, 4.04, 4.07, 4.08). Partial restoration of WT development was observed in the remaining transformants (Fig. 4.01, 4.05). For example, some transformants appeared almost WT-like but developed ruptured air pores. This partial complementation in a minority of transformant lines could be due to the different T-DNA insertion sites of the transgene in different independent transformants, which can influence the expression level of the complementing *ROP* gene. Similarly, for Mp*rop-2*, there was full and partial restoration of WT development in 60% and 40% of transformants, respectively. As both Mp*rop-1* and Mp*rop-2* can be complemented by Mp*ROP*, I conclude that Mp*rop-1* and Mp*rop-2* are both loss of function mutants.

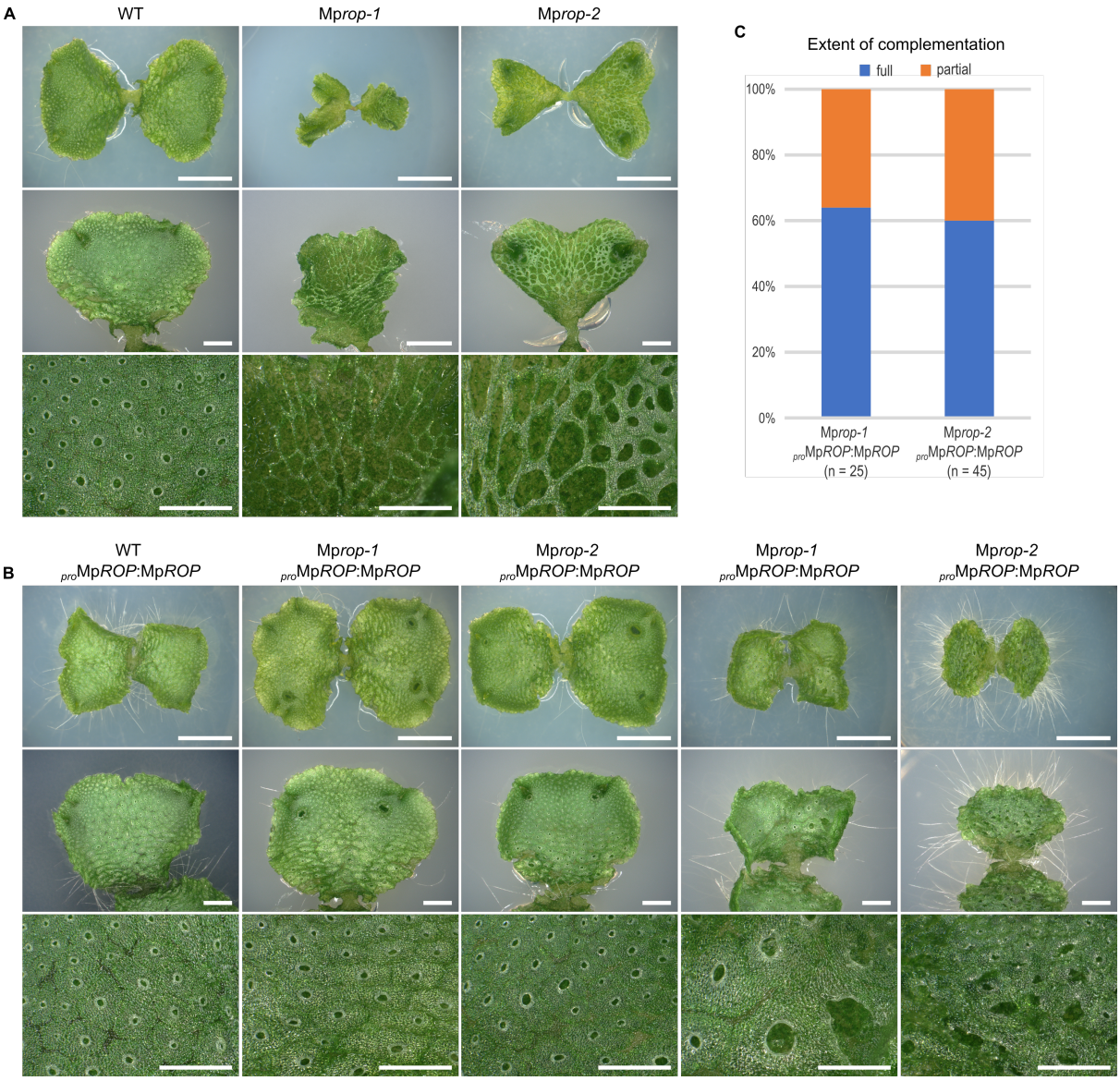

Figure 4.01 Mp*rop-1* and Mp*rop-2* are loss of function mutants

(A, B) Representative images of 14-day old gemmalings. Top row: whole plant (scale 5mm); middle row: thallus lobe (scale 2mm); bottom row: zoomed in dorsal epidermis composed of air pore and air chamber roof cells in WT (scale 1mm).

(A) Mp*rop-1* lack air pore and air chamber roof cells. Mp*rop-2* lack air pore cells and partially lack air chamber roof cells.

(B) Introduction of $_{pro}$Mp*ROP*:Mp*ROP* can restore WT air pore and air chamber roof development in Mp*rop-1* and Mp*rop-2*. Partial restoration was also observed.

(C) In the majority of Mp*rop-1* (64%) and Mp*rop-2* (60%) individuals transformed with $_{pro}$Mp*ROP*:Mp*ROP*, WT-like development was fully restored.

The use of a fluorophore tagged RHO in cross-species complementation experiments could potentially provide more information than a non-fluorophore tagged RHO, as it could also be used to test conservation of sub-cellular localisation patterns. However, a fused fluorophore could also compromise RHO function by hindering RHO interaction with its regulators and effectors (MpROP itself is only ~22kDa, whilst Venus is ~27kDa). To test if MpROP remains functional when N-terminally tagged with Venus, Mp*rop-1* and Mp*rop-2* were transformed with a construct encoding $_{pro}$Mp*ROP*:*Venus*-Mp*ROP* (Fig. 3.02A). Out of 16 Mp*rop-1* and 20 Mp*rop-2* individuals transformed, there was no transformant where WT development was fully restored (Fig. 4.02). For Mp*rop-1* $_{pro}$Mp*ROP*:*Venus*-Mp*ROP*, there were clear indications of partial complementation – the air chamber roof, gemma production and rhizoid growth were all at least partially restored, resembling the original Mp*rop-2*. For Mp*rop-2* $_{pro}$Mp*ROP*:*Venus*-Mp*ROP*, there were also some signs of complementation, for example, the air chamber roofs appeared more complete with smaller apertures compared to Mp*rop-2*. However these were less obvious than for Mp*rop-1* $_{pro}$Mp*ROP*:*Venus*-Mp*ROP* as Mp*rop-2* has less severe developmental defects compared to Mp*rop-1* in the first place. As $_{pro}$Mp*ROP*:*Venus*-Mp*ROP* can only partially complement Mp*rop-1* and Mp*rop-2*, I conclude that MpROP is only partially functional when N-terminally tagged with a fluorophore. Therefore, RHO N-terminally tagged with a fluorophore is not suitable for cross-species complementation experiments to test functional conservation.

Overall, these data demonstrate that the Mp*rop-1* mutant and Mp*ROP* homologues, without the fluorophore tag, should be used for cross-species complementation experiments.

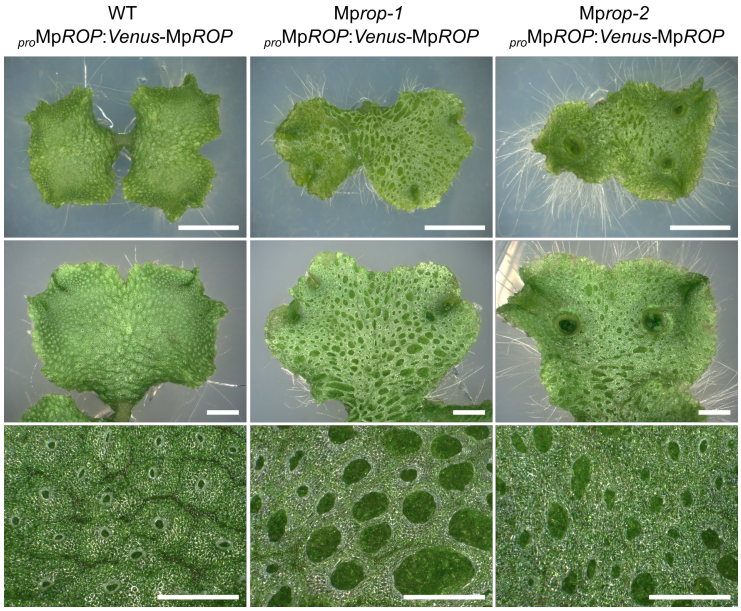

Figure 4.02 MpROP N-terminally tagged with Venus can only partially complement Mp*rop* mutants
Representative images of 14-day old gemmalings. Top row: whole plant (scale 5mm); middle row: thallus lobe (scale 2mm); bottom row: zoomed in dorsal epidermis composed of air pore and air chamber roof cells in WT (scale 1mm). In all Mp*rop-1* and Mp*rop-2* individuals transformed with $_{pro}$Mp*ROP*:*Venus*-Mp*ROP*, WT-like development was partially, but never fully, restored.

4.4.2 Cross-species complementation experiments were designed to study conservation of ROP function in the streptophyte lineage

The phylogenetic analyses (chapter 2) led to the hypothesis that ROP signalling became established early in the streptophyte lineage, sometime after the divergence of the *Chlorokybus* lineage and before the divergence of the Klebsormidiales (Fig. 4.03B). To test this hypothesis, I determined if *ROP* homologues from different streptophyte algal species could complement the defective phenotypes of the Mp*rop-1* mutant. Restoration of WT development following the introduction of an algal *ROP* homologue into the Mp*rop-1* background would indicate functional conservation of the *ROP* gene since the time *M. polymorpha* last shared a common ancestor with the particular algal species. To this end, three streptophyte algal species were selected – *Coleochaete scutata*, *Klebsormidium nitens*, and *Chlorokybus atmophyticus*, in order of relatedness to *M. polymorpha* (Fig. 4.03B). Homologues from *C. scutata*, *K. nitens*, and *C. atmophyticus* share 93%, 85%, and 66% amino acid sequence similarity respectively with MpROP (Fig. 4.03C). Based

on this and the phylogenetic and sequence analyses performed in chapter 2, I predicted that Mp*ROP* homologues from *C. scutata* and *K. nitens* would complement Mp*rop-1*, whilst that from *C. atmophyticus* would not. To test this hypothesis, complementation constructs were generated in which the coding sequence of Mp*ROP* homologues from each of the three algal species was cloned downstream of the Mp*ROP* promoter sequence (Fig. 4.03A). Following transformation of Mp*rop-1* with one of the three complementation constructs, complementation was assessed through phenotypic examinations.

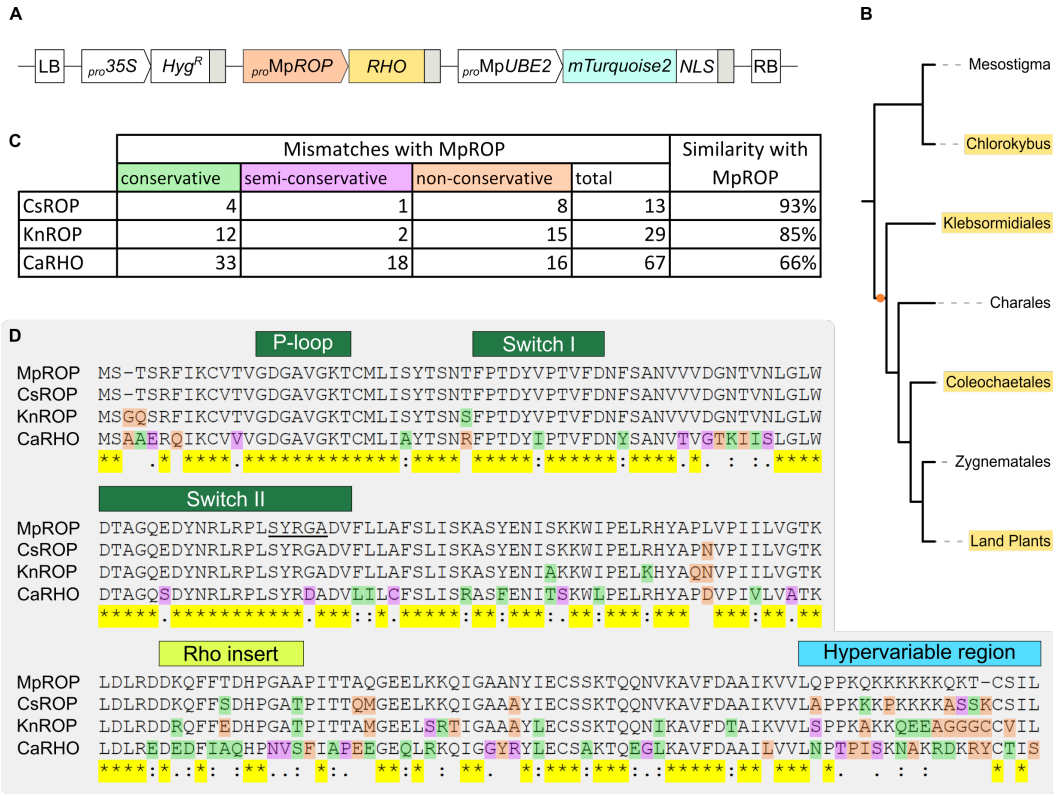

Figure 4.03 Complementation constructs encoding Mp*ROP*, Cs*ROP*, Kn*ROP*, or Ca*RHO* coding sequences were generated

(A) Schematic representation of the complementation construct design, showing only region flanked by left and right borders. Immediately downstream of the Mp*ROP* promoter sequence, the CDS for *M. polymorpha ROP* or its homologues from *C. scutata*, *K. nitens*, or *C. atmophyticus* was cloned (shown as RHO on the schematic). To aid selection of transformants, the complementing transgene was flanked by *pro35S:HPTII* and *pro*Mp*UBE2*:*mTurqoise2-N7*, to confer hygromycin resistance and label nuclei with CFP, respectively. Grey boxes indicate terminator sequences. See materials and methods for details on vector construction.

(B) Phylogenetic relationship of the five major streptophyte algal lineages with land plants. Orange dot marks when ROP signalling is predicted to have become established (chapter 2). Representatives from lineages highlighted in yellow are used in the cross-species complementation experiments.

(C) Summary comparison of amino acid sequence of MpROP with CsROP, KnROP, and CaRHO. (D) Amino acid sequence alignment with mismatches highlighted. Asterisks highlighted in yellow indicate conservation of residues across all four proteins. Residues highlighted are mismatches with MpROP residues. Colour coding: green (:) – conservative; purple (.) – semi-conservative; orange – non-conservative () mismatches with MpROP residue.

4.4.3 $_{pro}$Mp*ROP*:Cs*ROP* fully restores, $_{pro}$Mp*ROP*:Kn*ROP* partially restores, and $_{pro}$Mp*ROP*:Ca*RHO* does not restore wild-type tissue development in the Mp*rop-1* mutant

To determine if the *ROP* homologues from *C. scutata*, *K. nitens*, and *C. atmophyticus* could complement Mp*rop-1*, the phenotypes of all viable transformants (130 in total) were characterised. First, transformants were categorised based on their air chamber morphology, because the air chamber defect of Mp*rop-1* is one of its most distinctive phenotypes and because of the relative ease to inspect the dorsal side of the thallus. While the WT dorsal thallus epidermis is composed primarily of air chamber roof cells, interspersed with air pore complexes which mark the centre of each air chamber unit, Mp*rop-1* dorsal thallus epidermis lacks both air pore and roof cells (Fig. 4.04A). Cells which demarcate each air chamber unit are present in Mp*rop-1*, hence roof-less air chambers are visible. Gemmae production and gemma cup morphology, both of which are defective in Mp*rop-1*, were also then examined. WT gemma cups which protrude out of the dorsal thallus surface are full of gemmae and are radially symmetric with a serrated margin (Fig. 4.04A). By contrast, Mp*rop-1* gemma cups are either empty or contain very few gemmae and have an irregular margin which lacks clear serrations. Based on the evaluation of these phenotypes, transformants were categorised as fully complemented (indistinguishable from WT), not complemented (indistinguishable from Mp*rop-1*) or partially complemented (phenotype intermediate between WT and Mp*rop-1*).

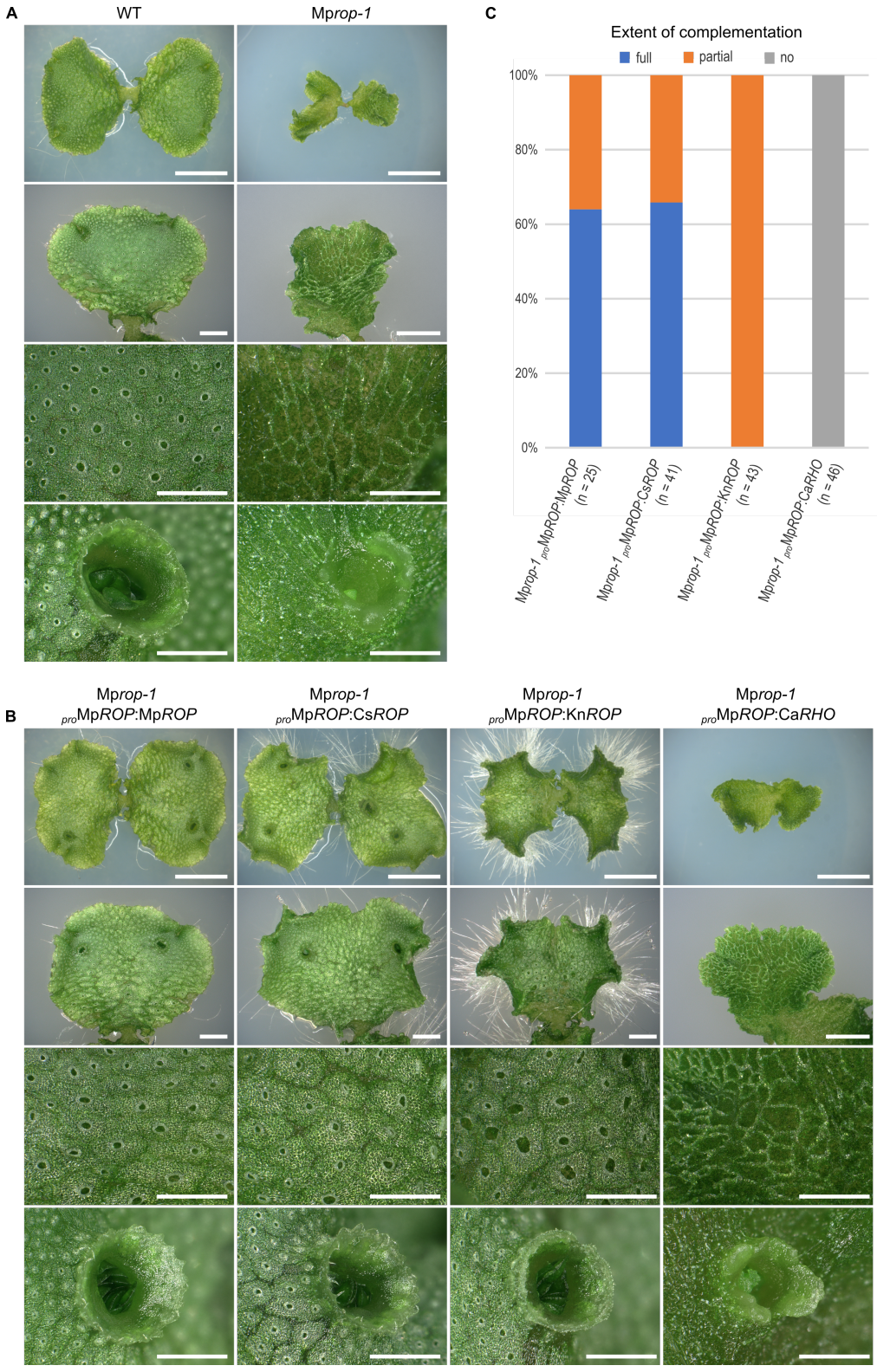

Figure 4.04 $_{pro}$Mp*ROP*:Cs*ROP* fully and $_{pro}$Mp*ROP*:Kn*ROP* partially restore wild-type tissue development in Mp*rop-1*

(A, B) Representative images of 14- (top three rows) and 21-day old (bottom row) plants, from gemmae. Top row: whole plant (scale 5mm); 2nd row: thallus lobe (scale 2mm); 3rd row: zoomed in dorsal epidermis (scale 1mm); bottom row: gemma cup (scale 1mm).

(C) In the majority (66%) of Mp*rop-1* individuals transformed with $_{pro}$Mp*ROP*:Cs*ROP*, WT-like development was fully restored. In all Mp*rop*-individuals transformed with $_{pro}$Mp*ROP*:Kn*ROP*, WT-like development was partially restored. All Mp*rop*-individuals transformed with $_{pro}$Mp*ROP*:Ca*RHO* were indistinguishable from Mp*rop-1*.

In the majority of cases (66%), introduction of $_{pro}$Mp*ROP*:Cs*ROP* into Mp*rop-1* resulted in full restoration of WT development (Fig. 4.04). Proportion of fully complemented individuals is similar to that observed when $_{pro}$Mp*ROP*:Mp*ROP* was introduced into Mp*rop-1* (64%). The range of thallus phenotypes observed among those partially complemented by $_{pro}$Mp*ROP*:Cs*ROP* is also similar to those partially complemented with $_{pro}$Mp*ROP*:Mp*ROP* (Fig. 405). Therefore, Cs*ROP* and Mp*ROP* equally restore WT tissue development in the Mp*rop-1* mutant.

In all cases, introduction of $_{pro}$Mp*ROP*:Kn*ROP* into Mp*rop-1* resulted in partial complementation (Fig. 4.04). Nearly 75% of transformants developed air pores that were ruptured to some extent (Fig. 4.05). This air chamber defect is however distinct from that of Mp*rop-1* or Mp*rop-2*. In Mp*rop-1* and Mp*rop-2*, the initial stages of air chamber morphogenesis, which take place within the apical notch, are defective (chapter 2 & Fig. 4.06). By contrast, in Mp*rop-1* $_{pro}$Mp*ROP*:Kn*ROP*, newly formed air chambers in and around the notch are WT-like in phenotype. However, the air pores are ruptured in the mature region of the thallus (Fig. 4.06). This suggests that KnROP can function in place of MpROP during early air chamber morphogenesis but cannot fully substitute MpROP function in maintaining air chamber integrity. The gemma cup phenotypes of Mp*rop-1* $_{pro}$Mp*ROP*:Kn*ROP* were also subtly different from WT. The serrations at the margin of WT gemma cups were absent or less prominent in all Mp*rop-1* $_{pro}$Mp*ROP*:Kn*ROP* gemma cups (Fig. 4.04, 4.05). However like WT, gemma cups of most Mp*rop-1* $_{pro}$Mp*ROP*:Kn*ROP* individuals are radially symmetric and filled with gemmae. Only 5% of Mp*rop-1* $_{pro}$Mp*ROP*:Kn*ROP* individuals were like Mp*rop-1* and developed irregular shaped gemma cups containing no or very few gemmae. Taken together these data indicate that although KnROP and MpROP are not completely interchangeable, there is a large degree of functional conservation.

To determine if $_{pro}$Mp*ROP*:Ca*RHO* could complement the Mp*rop-1* mutant, the phenotypes of transformed plants were characterised. All Mp*rop-1* $_{pro}$Mp*ROP*:Ca*RHO* individuals were indistinguishable from Mp*rop-1* at the tissue level, suggesting that MpROP and CaRHO are functionally different (Fig. 4.04). This is consistent with the hypothesis that MpROP and CaRHO functions have diverged since *M. polymorpha* last shared a common ancestor with *C. atmophyticus*.

Overall, these data are consistent with the hypothesis that ROP function in morphogenesis has remained largely conserved since the time land plants last shared a common ancestor with the Klebsormidiales.

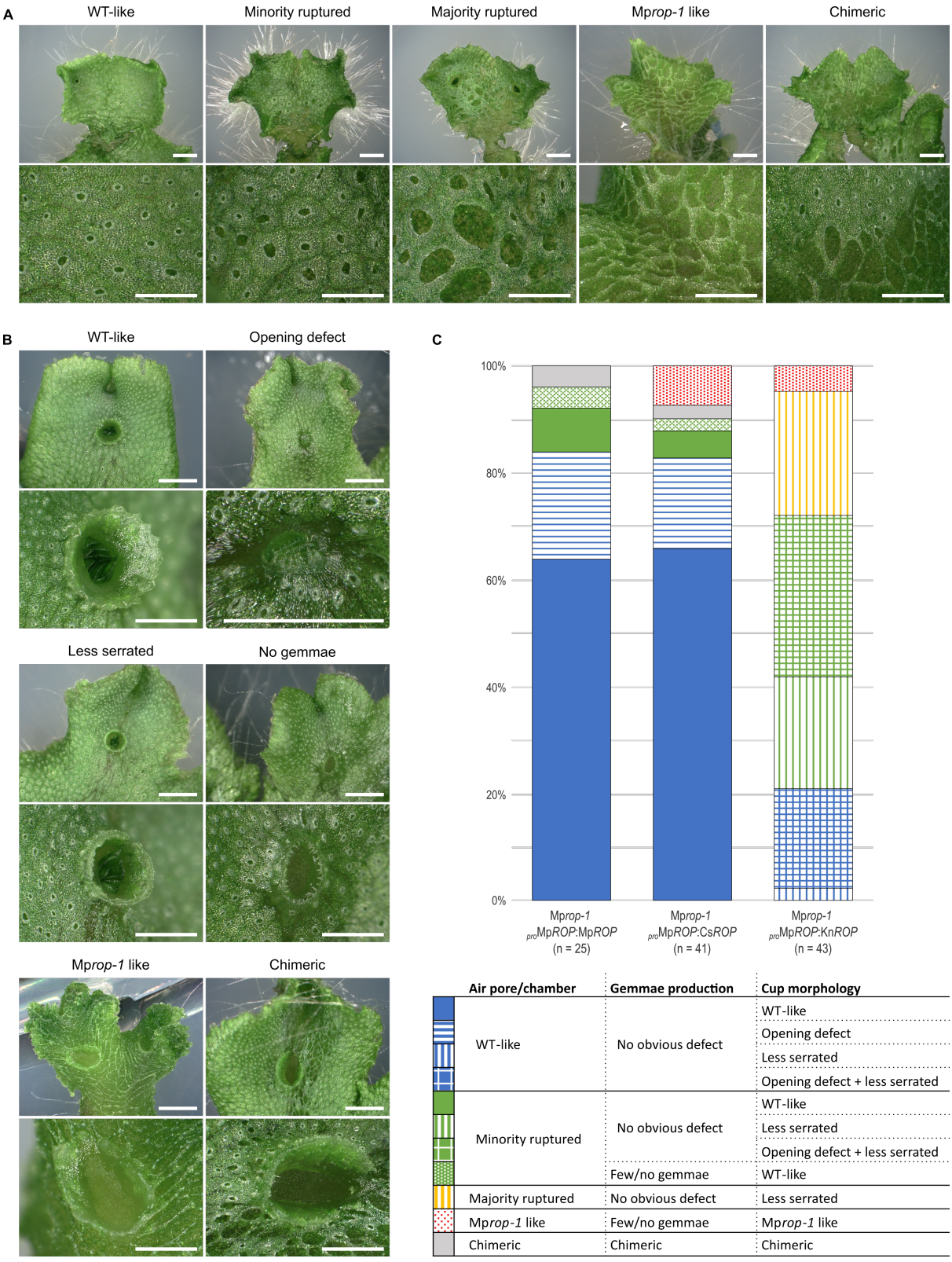

Figure 4.05 Phenotypes of partially complemented lines

A range of (A) air pore/chamber and (B) gemma cup phenotypes were observed amongst Mp*rop-1* transformed with $_{pro}$Mp*ROP*:Mp*ROP*, $_{pro}$Mp*ROP*:Cs*ROP*, or $_{pro}$Mp*ROP*:Kn*ROP*. Scale bar, 2mm and 1mm for top and bottom row images, respectively.

(C) Each transformant was categorised based on air pore/chamber morphology, gemma production, and gemma cup morphology. Solid blue represents full complementation whilst the others

represent different types of partial complementation. In all Mp*rop-1* individuals transformed with $_{pro}$Mp*ROP*:Mp*ROP*, $_{pro}$Mp*ROP*:Cs*ROP*, or $_{pro}$Mp*ROP*:Kn*ROP*, rhizoid growth was at least partially restored, hence even those with Mp*rop-1* like thallus morphology are considered partially complemented.

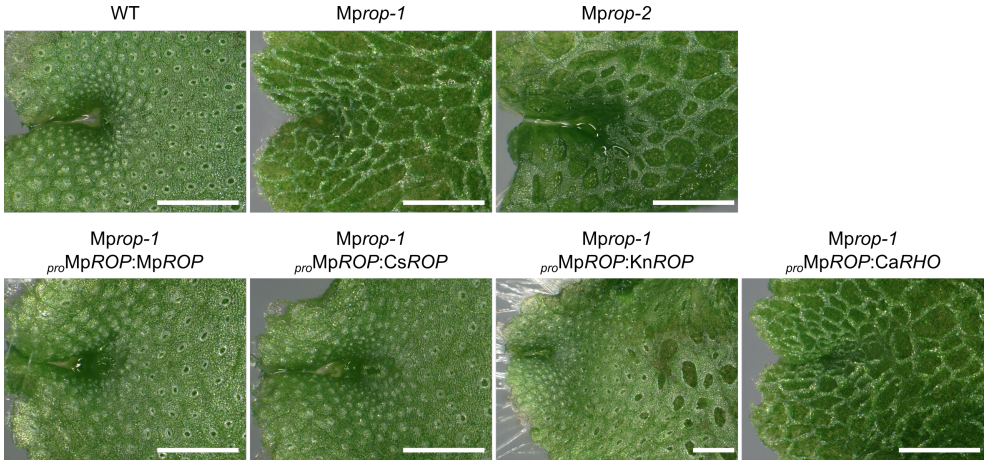

Figure 4.06 Defective air chambers observed in Mp*rop-1* $_{pro}$Mp*ROP*:Kn*ROP* lines is likely due to air pore rupture as opposed to defect in initial air chamber development
Representative dorsal thallus images of the meristematic notch region. Air chamber aperture of Mp*rop-2* is greater than that of WT in newly formed tissue around the meristematic notch, due to defect in initial air chamber development (chapter 3). Air chamber aperture of Mp*rop-1* $_{pro}$Mp*ROP*:Kn*ROP* is WT-like around the meristematic notch but larger in more mature tissue away from the notch. Scalebar, 1mm.

4.4.4 $_{pro}$Mp*ROP*:Cs*ROP* and $_{pro}$Mp*ROP*:Kn*ROP* restore polarised diffuse cell growth in the Mp*rop-1* mutant

ROP regulates polarised cell growth (diffuse as well as tip growth) in *M. polymorpha* and other land plants (chapter 2). To test if this cell polarity signalling function of MpROP is conserved among its homologues from *C. scutata*, *K. nitens*, and *C. atmophyticus*, complementation of the polarised growth defect in Mp*rop-1* mutants by $_{pro}$Mp*ROP*:Cs*ROP*, $_{pro}$Mp*ROP*:Kn*ROP*, and $_{pro}$Mp*ROP*:Ca*RHO* was tested.

Like Mp*rop-1* $_{pro}$Mp*ROP*:Mp*ROP*, both Mp*rop-1* $_{pro}$Mp*ROP*:Cs*ROP* and Mp*rop-1* $_{pro}$Mp*ROP*:Kn*ROP* produced WT-like gemmae, which appear disc like from above (when laid flat), with two meristematic notches on either side and an indented region at the base which is the stalk attachment point (Fig. 4.07A). By contrast, Mp*rop-1* $_{pro}$Mp*ROP*:Ca*RHO* gemmae resembled Mp*rop-1* mutant gemmae, which are globular and lack clear meristematic notches. The outer periclinal wall of WT gemma epidermal cells are flat and smooth, whilst the outer epidermal cells of Mp*rop-1* gemma swell out of the epidermal surface and the average cell depth (calculated as gemma thickness divided by number of cell layers) is greater (Fig. 4.07B). These data indicate that diffuse cell growth orientation is defective in the Mp*rop-1* mutant. The gemma epidermal surfaces of Mp*rop-1* expressing $_{pro}$Mp*ROP*:Mp*ROP*, $_{pro}$Mp*ROP*:Cs*ROP*, or $_{pro}$Mp*ROP*:Kn*ROP* are flat and smooth and indistinguishable from WT (Fig. 4.07A). Furthermore, the average gemma cell depth of Mp*rop-1* expressing $_{pro}$Mp*ROP*:Mp*ROP*, $_{pro}$Mp*ROP*:Cs*ROP*, or $_{pro}$Mp*ROP*:Kn*ROP* is indistinguishable from WT (Fig. 4.07B). By contrast, Mp*rop-1* $_{pro}$Mp*ROP*:Ca*RHO* gemmae are indistinguishable from Mp*rop-1* gemmae in terms of the epidermal cell swelling phenotype and average gemma cell depth. This suggests that CsROP and KnROP share the same function as MpROP in polarised diffuse growth, but CaRHO does not. Thus, these data are consistent with the hypothesis that ROP function in polarised cell growth has remained conserved since the time land plants last shared a common ancestor with the Klebsormidiales.

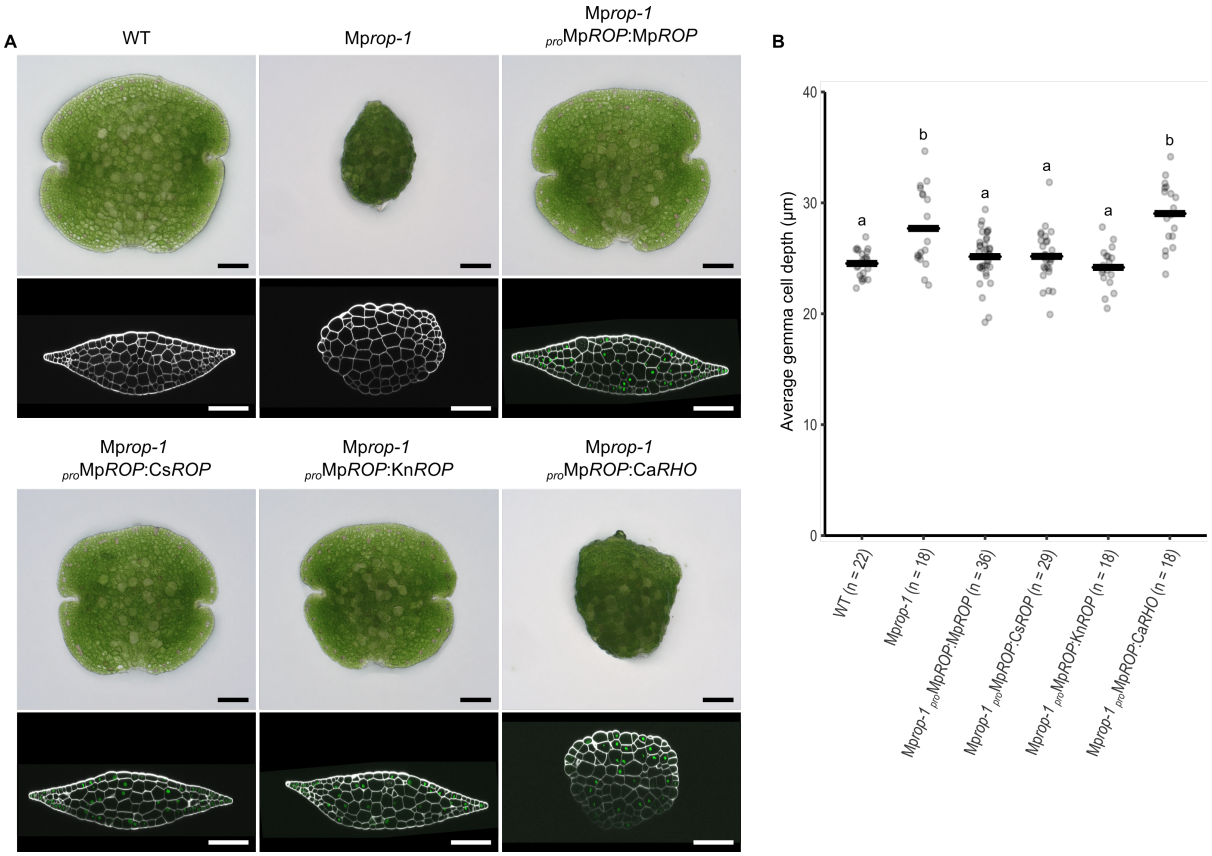

Figure 4.07 $_{pro}$Mp*ROP*:Cs*ROP* and $_{pro}$Mp*ROP*:Kn*ROP* restore polarised diffuse cell growth in Mp*rop-1*

(A) Representative images of 0-day old gemmae. Top row: surface view of live gemmae. Bottom row: confocal optical cross section images of fixed gemmae. SR2200 (cell wall dye) fluorescence in grey and mTurqoise2 fluorescence ($_{pro}$Mp*UBE2*:*mTurqoise2-N7*), indicating expression of the transgene, in green. Scale bar, 100µm.

(B) Average gemma cell depth is restored to WT-level in Mp*rop-1* transformed with $_{pro}$Mp*ROP*:Mp*ROP*, $_{pro}$Mp*ROP*:Cs*ROP*, or $_{pro}$Mp*ROP*:Kn*ROP*. Average cell depth for each gemma was calculated by dividing gemma depth with the number of cell layers at the thickest part of a gemma. For each genotype, gemma samples were taken from at least two independent lines. Main horizontal black bars represent mean. Each dot represents average cell depth for an individual gemma. Different lower-case letters indicate groups with significantly different means, based on one-way ANOVA followed by Tukey's HSD test ($p < 0.05$).

4.4.5 $_{pro}$Mp*ROP*:Cs*ROP* fully restores whilst $_{pro}$Mp*ROP*:Kn*ROP* partially restores tip growth in the Mp*rop-1* mutant

Based on the presence of tip growing rhizoid cells in *Chara braunii*, and the widespread presence of tip growing cells in land plants, tip growth in streptophytes is predicted to be a Phragmoplastophyta specific trait (Bonnot et al., 2019; Buschmann, 2020). Thus, I hypothesised that the tip growth promoting function of MpROP is conserved with CsROP but not with KnROP and CaRHO. To test this hypothesis, rhizoid phenotypes of *Mprop-1* transformed with $_{pro}$Mp*ROP*:Cs*ROP*, $_{pro}$Mp*ROP*:Kn*ROP*, or $_{pro}$Mp*ROP*:Ca*RHO* were characterised. As predicted, rhizoids were longer in all Mp*rop-1* $_{pro}$Mp*ROP*:Cs*ROP* individuals than in the Mp*rop-1* mutant (Fig. 4.08A). Unexpectedly, rhizoids were also visibly longer in all Mp*rop-1* $_{pro}$Mp*ROP*:Kn*ROP* individuals than in the Mp*rop-1* mutant. By contrast, rhizoids of Mp*rop-1* plants and *Mprop-1* $_{pro}$*MpROP*:Ca*RHO* were equally very short. To quantify the extent of complementation, I measured rhizoid length of 10-day old gemmalings in the complemented lines and WT. Rhizoid growth in Mp*rop-1* $_{pro}$Mp*ROP*:Mp*ROP* and Mp*rop-1* $_{pro}$Mp*ROP*:Cs*ROP* were indistinguishable from WT, indicating full complementation (Fig. 4.08B). Mp*rop-1* $_{pro}$Mp*ROP*:Kn*ROP* rhizoids were significantly longer than Mp*rop-1* rhizoids, however, they were also significantly shorter than WT rhizoids. These data indicate that ROP molecular function required for promoting tip growth has been fully or partially conserved since the time *M. polymorpha* last shared a common ancestor with *C. scutata* or *K. nitens*, respectively.

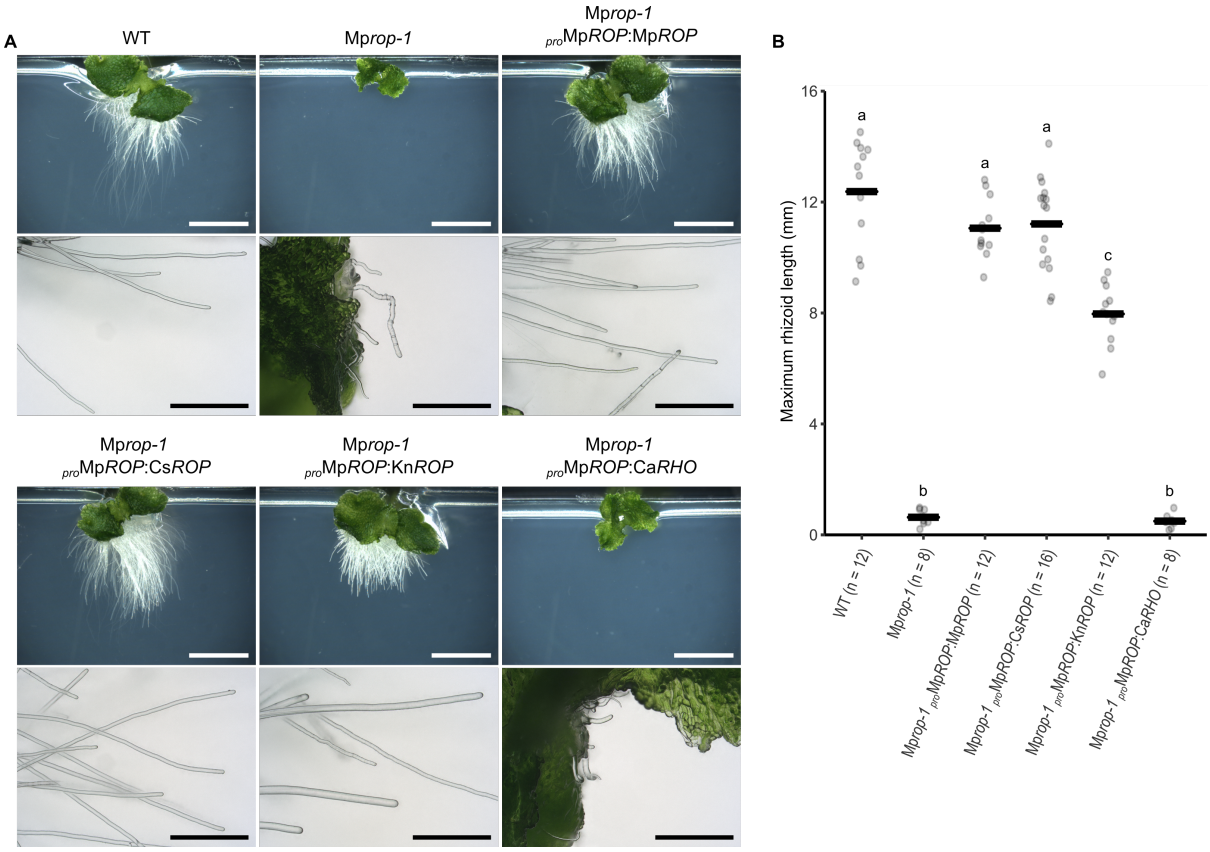

Figure 4.08 $_{pro}$Mp*ROP*:Cs*ROP* fully and $_{pro}$Mp*ROP*:Kn*ROP* partially restore tip growth in Mp*rop-1*

(A) Overall rhizoids of 10-day old gemmalings (top row) and zoomed in rhizoids of 7-day old gemmalings. Scale bar, 5mm and 500µm, for top and bottom rows respectively.

(B) Rhizoid growth is fully restored in Mp*rop-1* transformed with $_{pro}$Mp*ROP*:Mp*ROP* or $_{pro}$Mp*ROP*:Cs*ROP* and partially restored when transformed with $_{pro}$Mp*ROP*:Kn*ROP*. Maximum rhizoid length was measured for 10-day old gemmalings grown vertically on phytagel plates. Maximum rhizoid length was defined as the distance from the phytagel surface, on which the thallus sits, to the tip of the rhizoid which has grown the furthest away from the phytagel surface. At least two independent lines for each genotype were used for this assay. On the graph, each grey circle represents the maximum rhizoid length of a different plant, and the black horizontal bar represents the mean maximum rhizoid length of all the plants sampled within one genotype. Different letters indicate groups with significantly different means, based on one-way ANOVA followed by Tukey's HSD test ($p < 0.05$).

4.5 Discussion

In this chapter, I demonstrated that ROP protein function has remained conserved to a large extent since the time land plants last shared a common ancestor with the streptophyte alga *Klebsormidium nitens*. This was achieved through performing a series of cross-species complementation experiments where I tested the ability of *ROP* homologues from three streptophyte algal species (*C. scutata, K. nitens*, and *C. atmophyticus*) to complement the loss of function Mp*rop-1* mutant. This approach was possible because *M. polymorpha* encodes only a single *ROP* gene in its genome and Mp*rop-1* is a complete loss of function mutant with a characteristic, non-lethal phenotype. The most distinctive phenotype is the defective dorsal thallus epidermis, which is easy to screen by imaging with a stereomicroscope. This made it possible to phenotypically screen a large number of independent transformants and confidently score the complementing ability of each of the three algal *ROP* homologues. Moreover, quantitative assessment for the restoration of morphological defects, such as rhizoid tip growth, provided evidence for the different degrees of functional conservation between *ROP* homologues from *M. polymorpha, C. scutata*, and *K. nitens*. My discovery that the Cs*ROP* and Kn*ROP* genes complement the Mp*rop-1* mutant and that the *CaRHO* gene does not, suggests that a significant change in gene function occurred after the divergence of *C. atmophyticus.* The significance of the timing of ROP evolution in the context of plant evolution is discussed below.

4.5.1 Molecular ROP protein function has remained fully and largely conserved since land plants last shared a common ancestor with Coleochaetales and Klebsormidiales, respectively

Cross-species complementation experiments specifically test for conservation of the molecular or biochemical function, and not necessarily the cellular function, of a gene product (Delaux et al., 2019). This is highlighted by the ability of $_{pro}$Mp*ROP*:Kn*ROP* to partially restore rhizoid tip growth in Mp*rop-1*, even though tip growth in streptophytes are believed to have evolved after the divergence of the Klebsormidiales (Fig. 4.08). This piece of data specifically indicates that ROP capacity to interact with regulators and effectors required for promoting tip growth in *M.*

polymorpha has remained largely conserved since the time land plants last shared a common ancestor with *K. nitens*. Therefore, the overall ability of $_{pro}$Mp*ROP*:Kn*ROP* to largely complement Mp*rop-1* suggests that the precise molecular mechanism of ROP signalling has remained largely conserved at least since the time land plants last shared a common ancestor with the Klebsormidiales. Given that $_{pro}$Mp*ROP*:Cs*ROP* fully complements Mp*rop-1*, it is likely that further novel ROP regulators or effectors emerged (or existing ones acquired new features) specifically in the Phragmoplastophyta to fine tune ROP signalling for processes like tip growth. Some of the subtle phenotypes of Mp*rop-1* $_{pro}$Mp*ROP*:Kn*ROP* (e.g. less serrated gemma cup margin – Fig. 4.04, 4.05) may also signify the inability of KnROP to efficiently interact with regulators/effectors in *M. polymorpha* for fine tuning ROP mediated cellular morphogenesis.

The complete inability of $_{pro}$Mp*ROP*:Ca*RHO* to complement Mp*rop-1* indicates that the molecular functions of MpROP and CaRHO are not conserved. However, it does not indicate that CaRHO lacks cell polarity function in *C. atmophyticus*. Based on the widespread conservation of RHO polarity function throughout the eukaryotes, the origin of RHO polarity function is far more ancient than the origin of streptophytes, and therefore it is probable that CaRHO also regulates cell polarity in some form. My results suggest that the precise mechanism through which CaRHO and MpROP regulate cell polarity has diverged, and that this ROP-specific mechanism has remained largely and fully conserved since the time *M. polymorpha* last shared a common ancestor with *K. nitens* and *C. scutata*, respectively.

4.5.2 Speculating on the ancestral function of the ROP protein

How may the mechanisms through which ROPs and other RHO GTPases regulate polarised cell growth differ? To answer this question, we must consider how cellular morphogenesis is executed differently in plants and other eukaryotes. Unlike in animals where the actin cytoskeleton is the major determinant of cell shape, in plants, cortical microtubules play a more significant role as they guide the synthesis of the cellulose cell wall (Fletcher & Mullins, 2010; Paredez et al., 2006; Szymanski & Cosgrove, 2009). Anisotropy in cell wall stiffness is what ultimately governs turgor driven polarised growth, hence by local stiffening or loosening of the cell wall, growth can be

focussed to different parts of the cell cortex (Geitmann & Ortega, 2009). In polarised diffuse growing plant cells, cellulose microfibrils are aligned to parallel bundles of cortical microtubules, restricting growth along the microtubule/microfibril axis and promoting growth perpendicular to this axis (Hamada, 2014). ROP proteins in *A. thaliana* are known to coordinate polarised diffuse growth of pavement cells and hypocotyl cells via regulating cortical microtubule organisation (Fu et al., 2005, 2009). It is likely that MpROP also regulates diffuse cell growth orientation through acting on cortical microtubules as the diffuse growth defects of Mp*rop-1* gemma epidermal cells resemble *A. thaliana* sepal epidermal cells treated with the microtubule depolymerising drug Oryzalin (Zhao et al., 2020). Although RHOs in animals and fungi are also known to influence interphase microtubule organisation, this parallel arrangement of microtubules perpendicular to the growth axis is unique to plant cells, suggesting that this organisation of parallel cortical microtubules may be a ROP specific function.

Unlike the roundish cells of *Chlorokybus* and *Mesostigma*, *Klebsormidium* cells are elongated along a single axis, resembling land plant cells that undergo polarised diffuse growth. During interphase, parallel bundles of cortical microtubules are oriented perpendicular to the longitudinal axis of the *Klebsormidium* cells (Katsaros et al., 2011), suggesting that the role of cortical microtubules in orienting diffuse growth has remained conserved since land plants last shared a common ancestor with the Klebsormidiales. The importance of cortical microtubules for orienting diffuse growth has also been demonstrated in other streptophyte algae, such as in Charales (Green, 1962; Sommer et al., 2015; Wasteneys & Williamson, 1992) and Zygenmatales (Domozych et al., 2014). However, this does not appear to be the norm outside of streptophytes. In the chlorophyte algae *Chaetomorpha*, cortical microtubules are oriented parallel to the growth axis and not closely associated with the orientation of cellulose microfibrils (Kimura & Mizuta, 1994). In multicellular red algae, elongating cells grow through "band growth" as opposed to diffuse growth and no clear association has been described between cortical microtubule, cellulose microfibril, and cell growth orientations (Babuka & Pueschel, 1998; Tsekos, 1999; Waaland & Waaland, 1975). Brown algae, which share some morphological features with plants, albeit being very distantly related, lack

cortical microtubules in vegetative cells and actin rather than microtubules are responsible for orienting cellulose microfibrils (C. Katsaros et al., 2006). I therefore speculate that the organisation of cortical microtubules into parallel arrays perpendicular to the growth axis of diffuse growing cells may be an ancestral ROP-specific function, which has remained conserved since the time land plants last shared a common ancestor with Klebsormidiales.

As well as organising cortical microtubules into parallel arrays for polarised diffuse growth, it is possible to speculate a few other ways in which ROP signalling contributed to the morphological evolution in the streptophytes. Given its importance for a multicellular body plan, cell adhesion function is an obvious one. The large aperture of the Mp*rop-2* air chambers is expected to be due to a cell adhesion defect (Fig. 3.15). Compared to Mp*rop-2*, this cell adhesion defect is much less severe in most Mp*rop-1* $_{pro}$Mp*ROP:*Kn*ROP* plants and even absent in some, suggesting that KnROP, like MpROP, promotes cell adhesion (Fig. 4.06). This is consistent with cell adhesion being an ancestral ROP function, and therefore it may have facilitated the evolution of multicellular body plans in the streptophytes. It is also possible that the establishment of ROP signalling function in the last common ancestor of land plants and Klebsormidiales primed streptophytes for later innovations, such as tip growth and oriented cell divisions. The restoration of rhizoid tip growth and oriented cell divisions for air chamber roof and pore morphogenesis in Mp*rop-1* $_{pro}$Mp*ROP:*Kn*ROP*, is consistent with ROP signalling being preadapted for innovations associated with the Phragmoplastophyta (Fig. 4.06, 4.08). Therefore, the establishment of ROP signalling may have contributed to increased morphological complexity in the streptophyte lineage in several ways.

Chapter 5: General discussion

Plants have evolved mechanisms to form complex 3-dimensional tissues. Motivated to understand how such mechanisms regulate morphogenesis and how they evolved, I set out to investigate the function and evolution of cell polarity signalling, in particular ROP signalling, in the context of plant morphogenesis. I aimed to answer three specific questions. Below I summarise the findings from addressing these questions and their significance.

1. When and how did ROP signalling genes evolve? (Chapter 2)

Previous phylogenetic analyses for ROP signalling genes were heavily focussed on angiosperms and provided little insight into the early events in ROP signalling evolution (Christensen et al., 2003; Fowler, 2010). Taking advantage of the genome and transcriptome sequence data which have recently become available for a diverse range of plant taxa, I was able to evaluate the *ROP* gene phylogeny with much greater taxonomic breadth than any previous studies. I discovered that the *ROP* gene became established from the ancestral *RHO* gene early in the streptophyte lineage, in the period after the divergence of the *Mesostigma*/*Chlorokybus* lineage and before the divergence of the Klebsormidiales lineage. The establishment of the *ROP* gene was likely brought about by the emergence of two ROP specific regulators, RopGAP and REN. With all the core ROP regulators (known from studies in land plants) having emerged by this period (Elias, 2008; Garcia-Mata et al., 2011; Meller et al., 2005), this marks when ROP signalling became fully established. As *Mesostigma* and *Chlorokybus* are unicellular and colonial respectively, whilst all the other later diverging streptophyte lineages, including the Klebsormidiales, include multicellular species, the timing of ROP signalling establishment coincides with when multicellular body plan first evolved in the streptophytes. This led me to hypothesise that ROP function which became established early in the streptophyte lineage may have facilitated a major transition in plant body plan complexity.

2. How does ROP signalling contribute to plant morphogenesis? (Chapter 3)

Genetic studies, primarily in *A. thaliana*, but also in other species like *Z. mays* and *P. patens* have demonstrated the importance of ROP signalling function in regulating cell growth and division patterns, however, genetic redundancy has prevented understanding how ROP signalling

contributes to the morphogenesis of complex plant tissues (Burkart et al., 2015; Cheng et al., 2020; Fu et al., 2005; Gendre et al., 2019; Humphries et al., 2011). Through characterising ROP function in *M. polymorpha*, which encodes only a single *ROP* gene, I showed that ROP signalling is required for the morphogenesis of complex epidermal tissues. ROP orchestrates tissue morphogenesis through controlling cell growth, division, and possibly adhesion. Based on the conservation of these cellular ROP functions in bryophytes and vascular plants, it is likely that the *ROP* gene in the last common ancestor of land plants was also required for these cellular functions to orchestrate tissue morphogenesis.

3. What was the ancestral ROP function in the context of plant morphogenesis? (Chapter 4)

Leading on from my findings that the *ROP* gene sequence has remained highly conserved since the early streptophytes (chapter 2), and that ROP cellular functions required for tissue level morphogenesis are conserved among land plants (chapter 3), I set out to infer since when ROP function has remained conserved. To this end, the conservation of ROP function between *M. polymorpha* and three streptophyte algal species was tested through a cross-species complementation assay. The ability of Mp*ROP* homologues from *C. scutata* and *K. nitens* to complement the Mp*rop-1* mutant, fully and largely, respectively, and the inability of the homologue from *C. atmophyticus* to complement the Mp*rop-1* mutant indicated that molecular ROP function has remained largely conserved since land plants last shared a common ancestor with the Klebsormidiales, consist with findings from chapter 2.

This remarkable level of ROP signalling conservation suggests its establishment conferred a substantial selective advantage and may therefore be linked with the advent of a novel morphogenesis mechanism in the early streptophytes. Based on reviewing the literature for ROP regulated processes, which are specifically conserved amongst streptophytes, excluding *Mesostigma* and *Chlorokybus*, one possible ancestral ROP-specific function is the spatial regulation of cortical microtubules into parallel arrays for polarised diffuse cell growth. This is only one of many hypothetical ancestral ROP functions and further comparative studies, including

genetic studies directly in streptophyte algal species, are needed to test these hypotheses. Nevertheless, the results presented in this thesis clearly demonstrate that a signalling mechanism which evolved early in the streptophyte lineage is responsible for the morphogenesis of complex tissues in extant land plants. The broader implication of this finding is discussed below.

Alteration in spatial regulation at the sub-cellular level for streptophyte body plan evolution

The co-option of ancient genes for the evolution of novel morphological traits is a common theme reported for both animals and plants (Carroll, 2008; Pires & Dolan, 2012). Genes which are thought to have contributed to the elaboration of animal body plans, for example the *HOX* genes, are highly conserved even in morphologically primitive animals like the sea anemone, which are distantly related to more complex animals like insects and mammals (Technau & Genikhovich, 2018). This had led to the idea that the core "genetic toolkit" for developmental complexity was present in morphologically primitive ancestors, and the sequence (and hence the molecular function) of these core genes have changed very little since (Carroll, 2008). Rather than changes to the molecular function, alterations in the spatial regulation of gene activity (i.e. gene expression pattern) was proposed to have driven the evolution of novel morphological traits.

This model with an emphasis on gene expression pattern alteration may explain how elaborate animal and plant body plans emerged from primitive, yet already multicellular, body plans. It obviously cannot be applied to a single cell system and hence cannot explain the genetic basis for the morphological evolution in early streptophytes. In earlier events of body plan evolution, it is likely that alterations in mechanical cellular processes, like cell growth, division, and cell adhesion had a more significant impact than changes to gene regulatory networks. Nevertheless, alteration in spatial regulation would still have been critical. This would be at the subcellular level, to specify cell growth and division orientations, as opposed to at the gene expression pattern level to specify organ position. In this regard, the *ROP* gene may represent a member of the genetic toolkit, specific to streptophytes. As well as the evolution of ROP-specific regulators like RopGAP and REN, emergence of as of yet unidentified ROP specific effectors likely contributed to spatial

alternations in ROP signalling function, without altering ROP molecular function itself. Together with other toolkit genes, this may have contributed to the evolution of parallel cortical microtubule array organisation for polarised diffuse growth (as speculated in chapter 4), or ability to rotate division plane orientation for tissue formation. Even beyond the early streptophytes, I suspect enhanced spatial regulation of signalling at the sub-cellular level was important for plant body plan evolution, as the plant form is so tightly linked with cell growth and division patterns.

Conclusion

In this thesis, I have shown that ROP signalling became established early in the streptophyte lineage and that its molecular function has remained conserved ever since. This ancient signalling mechanism controls the morphogenesis of complex tissues in land plants. Enhanced spatial regulation of cell signalling to coordinate cell growth, division, and adhesion was undoubtedly required for body plan evolution in early streptophytes and the evolution of ROP signalling likely contributed to increased morphological complexity in the streptophytes.

References

Adami, C. (2002). What is complexity? In *BioEssays* (Vol. 24, Issue 12, pp. 1085–1094). John Wiley & Sons, Ltd. https://doi.org/10.1002/bies.10192

Adams, A. E. M., Johnson, D. I., Longnecker, R. M., Sloat, B. F., & Pringle, J. R. (1990). CDC42 and CDC43, two additional genes involved in budding and the establishment of cell polarity in the yeast Saccharomyces cerevisiae. *Journal of Cell Biology*, *111*(1), 131–142. https://doi.org/10.1083/jcb.111.1.131

Alberts, B., Johnson, A., Lewis, J., Morgan, D., Raff, M., Roberts, K., & Walter, P. (2015). Molecular Biology of the Cell. 6th Edition. In *New York: Garland Science*.

Amborella Genome Project. (2013). The Amborella Genome and the Evolution of Flowering Plants. *Science*, *342*(6165). https://doi.org/10.1126/science.1241089

Amin, E., Jaiswal, M., Derewenda, U., Reis, K., Nouri, K., Koessmeier, K. T., Aspenström, P., Somlyo, A. V., Dvorsky, R., & Ahmadian, M. R. (2016). Deciphering the molecular and functional basis of RHOGAP family proteins: A systematic approach toward selective inactivation of RHO family proteins. *Journal of Biological Chemistry*, *291*(39), 20353–20371. https://doi.org/10.1074/jbc.M116.736967

Aoyama, T., Hiwatashi, Y., Shigyo, M., Kofuji, R., Kubo, M., Ito, M., & Hasebe, M. (2012). AP2-type transcription factors determine stem cell identity in the moss physcomitrella patens. *Development*, *139*(17), 3120–3129. https://doi.org/10.1242/dev.076091

Apostolakos, P., Galatis, B., & Mitrakos, K. (1982). Studies on the Development of the Air Pores and Air Chambers of Marchantia paleacea 1 . Light Microscopy. *Annals of Botany*, *49*(3), 377–396. https://doi.org/10.1007/BF01276335

Atakhani, A., Bogdziewiez, L., & Verger, S. (2022). Characterising the mechanics of cell–cell adhesion in plants. *Quantitative Plant Biology*, *3*. https://doi.org/10.1017/qpb.2021.16

Babuka, S. J., & Pueschel, C. M. (1998). A freeze-substitution ultrastructural study of the cytoskeleton of the red alga Antithamnion kylinii (Ceramiales). *Phycologia*, *37*(4), 251–258. https://doi.org/10.2216/i0031-8884-37-4-251.1

Banks, J. A., Nishiyama, T., Hasebe, M., Bowman, J. L., Gribskov, M., DePamphilis, C., Albert, V. A., Aono, N., Aoyama, T., Ambrose, B. A., Ashton, N. W., Axtell, M. J., Barker, E., Barker, M. S., Bennetzen, J. L., Bonawitz, N. D., Chapple, C., Cheng, C., Correa, L. G. G., … Grigoriev, I. V. (2011). The Selaginella genome identifies genetic changes associated with the evolution of vascular plants. *Science*, *332*(6032), 960–963. https://doi.org/10.1126/science.1203810

Barbosa, M., Lefler, F., Berthold, D. E., & Laughinghouse, H. D. (2021). The Ecology of Charophyte Algae (Charales). *EDIS*, *1*. https://doi.org/10.32473/edis-ag448-2021

Bascom, C., Burkart, G. M., Mallett, D. R., O'sullivan, J. E., Tomaszewski, A. J., Walsh, K., & Bezanilla, M. (2019). Systematic survey of the function of ROP regulators and effectors during tip growth in the moss Physcomitrella patens. *Journal of Experimental Botany*, *70*(2), 447–457. https://doi.org/10.1093/jxb/ery376

Basu, D., Le, J., Zakharova, T., Mallery, E. L., & Szymanski, D. B. (2008). A SPIKE1 signaling complex controls actin-dependent cell morphogenesis through the heteromeric WAVE and ARP2/3 complexes. *Proceedings of the National Academy of Sciences of the United States of America*, *105*(10), 4044–4049. https://doi.org/10.1073/pnas.0710294105

Bender, A., & Pringle, J. R. (1989). Multicopy suppression of the cdc24 budding defect in yeast by CDC42 and three newly identified genes including the ras-related gene RSR1. *Proceedings of the National Academy of Sciences of the United States of America*, *86*(24), 9976–9980. https://doi.org/10.1073/pnas.86.24.9976

Bennett, T. (2015). PIN proteins and the evolution of plant development. In *Trends in Plant Science* (Vol. 20, Issue 8, pp. 498–507). Elsevier Current Trends. https://doi.org/10.1016/j.tplants.2015.05.005

Bennett, T., Brockington, S. F., Rothfels, C., Graham, S. W., Stevenson, D., Kutchan, T., Rolf, M., Thomas,

P., Wong, G. K. S., Leyser, O., Glover, B. J., & Harrison, C. J. (2014). Paralogous radiations of PIN proteins with multiple origins of noncanonical PIN structure. *Molecular Biology and Evolution*, *31*(8), 2042–2060. https://doi.org/10.1093/molbev/msu147

Berken, A. (2006). ROPs in the spotlight of plant signal transduction. *Cellular and Molecular Life Sciences*, *63*(21), 2446–2459. https://doi.org/10.1007/s00018-006-6197-1

Berken, A., Thomas, C., & Wittinghofer, A. (2005). A new family of RhoGEFs activates the Rop molecular switch in plants. *Nature*, *436*(7054), 1176–1180. https://doi.org/10.1038/nature03883

Berken, A., & Wittinghofer, A. (2008). Structure and function of Rho-type molecular switches in plants. *Plant Physiology and Biochemistry*, *46*(3), 380–393. https://doi.org/10.1016/j.plaphy.2007.12.008

Bi, E., & Park, H. O. (2012). Cell polarization and cytokinesis in budding yeast. *Genetics*, *191*(2), 347–387. https://doi.org/10.1534/genetics.111.132886

Blanc-Mathieu, R., Verhelst, B., Derelle, E., Rombauts, S., Bouget, F. Y., Carré, I., Château, A., Eyre-Walker, A., Grimsley, N., Moreau, H., Piégu, B., Rivals, E., Schackwitz, W., Van de Peer, Y., & Piganeau, G. (2014). An improved genome of the model marine alga Ostreococcus tauri unfolds by assessing Illumina de novo assemblies. *BMC Genomics*, *15*(1), 1–12. https://doi.org/10.1186/1471-2164-15-1103

Blanc, G., Agarkova, I., Grimwood, J., Kuo, A., Brueggeman, A., Dunigan, D. D., Gurnon, J., Ladunga, I., Lindquist, E., Lucas, S., Pangilinan, J., Pröschold, T., Salamov, A., Schmutz, J., Weeks, D., Yamada, T., Lomsadze, A., Borodovsky, M., Claverie, J. M., … Van Etten, J. L. (2012). The genome of the polar eukaryotic microalga Coccomyxa subellipsoidea reveals traits of cold adaptation. *Genome Biology*, *13*(5), 1–12. https://doi.org/10.1186/gb-2012-13-5-r39

Blanc, G., Duncan, G., Agarkova, I., Borodovsky, M., Gurnon, J., Kuo, A., Lindquist, E., Lucas, S., Pangilinan, J., Polle, J., Salamov, A., Terry, A., Yamada, T., Dunigan, D. D., Grigoriev, I. V., Claverie, J. M., & van Etten, J. L. (2010). The Chlorella variabilis NC64A genome reveals adaptation to photosymbiosis, coevolution with viruses, and cryptic sex. *Plant Cell*, *22*(9), 2943–2955. https://doi.org/10.1105/tpc.110.076406

Bonnot, C., Hetherington, A. J., Champion, C., Breuninger, H., Kelly, S., & Dolan, L. (2019). Neofunctionalisation of basic helix−loop−helix proteins occurred when embryophytes colonised the land. *New Phytologist*, *223*(2), 993–1008. https://doi.org/10.1111/nph.15829

Bonnot, C., Proust, H., Pinson, B., Colbalchini, F. P. L., Lesly-Veillard, A., Breuninger, H., Champion, C., Hetherington, A. J., Kelly, S., & Dolan, L. (2017). Functional PTB phosphate transporters are present in streptophyte algae and early diverging land plants. *New Phytologist*, *214*(3), 1158–1171. https://doi.org/10.1111/nph.14431

Boureux, A., Vignal, E., Faure, S., & Fort, P. (2007). Evolution of the Rho family of Ras-like GTPases in eukaryotes. *Molecular Biology and Evolution*, *24*(1), 203–216. https://doi.org/10.1093/molbev/msl145

Braidwood, L., Breuer, C., & Sugimoto, K. (2014). My body is a cage: Mechanisms and modulation of plant cell growth. *New Phytologist*, *201*(2), 388–402. https://doi.org/10.1111/nph.12473

Brembu, T., Winge, P., Bones, A. M., & Yang, Z. (2006). A RHOse by any other name: A comparative analysis of animal and plant Rho GTPases. *Cell Research*, *16*(5), 435–445. https://doi.org/10.1038/sj.cr.7310055

Burkart, G. M., Baskin, T. I., & Bezanilla, M. (2015). A family of ROP proteins that suppresses actin dynamics, and is essential for polarized growth and cell adhesion. *Journal of Cell Science*, *128*(14), 2553–2564. https://doi.org/10.1242/jcs.172445

Buschmann, H. (2020). Into another dimension: How streptophyte algae gained morphological complexity. In *Journal of Experimental Botany* (Vol. 71, Issue 11, pp. 3279–3286). Oxford Academic. https://doi.org/10.1093/jxb/eraa181

Buschmann, H., & Zachgo, S. (2016). The Evolution of Cell Division: From Streptophyte Algae to Land Plants. In *Trends in Plant Science* (Vol. 21, Issue 10, pp. 872–883). Elsevier Ltd. https://doi.org/10.1016/j.tplants.2016.07.004

Butty, A. C., Perrinjaquet, N., Petit, A., Jaquenoud, M., Segall, J. E., Hofmann, K., Zwahlen, C., & Peter, M.

(2002). A positive feedback loop stabilizes the guanine-nucleotide exchange factor Cdc24 at sites of polarization. *EMBO Journal*, *21*(7), 1565–1576. https://doi.org/10.1093/emboj/21.7.1565

Butty, A. C., Pryciak, P. M., Huang, L. S., Herskowitz, I., & Peter, M. (1998). The role of Far1p in linking the heterotrimeric G protein to polarity establishment proteins during yeast mating. *Science*, *282*(5393), 1511–1516. https://doi.org/10.1126/science.282.5393.1511

Campos, R., Goff, J., Rodriguez-Furlan, C., & Van Norman, J. M. (2020). The Arabidopsis Receptor Kinase IRK Is Polarized and Represses Specific Cell Divisions in Roots. *Developmental Cell*, *52*(2), 183–195. https://doi.org/10.1016/j.devcel.2019.12.001

Carol, R. J., Takeda, S., Linstead, P., Durrant, M. C., Kakesova, H., Derbyshire, P., Drea, S., Zarsky, V., & Dolan, L. (2005). A RhoGDP dissociation inhibitor spatially regulates growth in root hair cells. *Nature*, *438*(7070), 1013–1016. https://doi.org/10.1038/nature04198

Carroll, S. B. (2008). Evo-Devo and an Expanding Evolutionary Synthesis: A Genetic Theory of Morphological Evolution. In *Cell* (Vol. 134, Issue 1, pp. 25–36). Cell Press. https://doi.org/10.1016/j.cell.2008.06.030

Champion, C., Lamers, J., Shivas Jones, V. A., Morieri, G., Honkanen, S., & Dolan, L. (2021). Microtubule associated protein WAVE DAMPENED2-LIKE (WDL) controls microtubule bundling and the stability of the site of tip-growth in Marchantia polymorpha rhizoids. *PLoS Genetics*, *17*(6), e1009533. https://doi.org/10.1371/journal.pgen.1009533

Chant, J., & Herskowitz, I. (1991). Genetic control of bud site selection in yeast by a set of gene products that constitute a morphogenetic pathway. *Cell*, *65*(7), 1203–1212. https://doi.org/10.1016/0092-8674(91)90015-Q

Cheng, S., Xian, W., Fu, Y., Marin, B., Keller, J., Wu, T., Sun, W., Li, X., Xu, Y., Zhang, Y., Wittek, S., Reder, T., Günther, G., Gontcharov, A., Wang, S., Li, L., Liu, X., Wang, J., Yang, H., … Melkonian, M. (2019). Genomes of Subaerial Zygnematophyceae Provide Insights into Land Plant Evolution. *Cell*, *179*(5), 1057-1067.e14. https://doi.org/10.1016/j.cell.2019.10.019

Cheng, X., Mwaura, B. W., Chang Stauffer, S. R., & Bezanilla, M. (2020). A Fully Functional ROP Fluorescent Fusion Protein Reveals Roles for this GTPase in Subcellular and Tissue-level Patterning. *The Plant Cell*, tpc.00440.2020. https://doi.org/10.1105/tpc.20.00440

Chiou, J., Balasubramanian, M. K., & Lew, D. J. (2017). Cell Polarity in Yeast. *Annual Review of Cell and Developmental Biology*, *33*(1), 77–101. https://doi.org/10.1146/annurev-cellbio-100616-060856

Christensen, T. M., Vejlupkova, Z., Sharma, Y. K., Arthur, K. M., Spatafora, J. W., Albright, C. A., Meeley, R. B., Duvick, J. P., Quatrano, R. S., & Fowler, J. E. (2003). Conserved subgroups and developmental regulation in the monocot rop gene family. *Plant Physiology*, *133*(4), 1791–1808. https://doi.org/10.1104/pp.103.029900

Clark, J. W., & Donoghue, P. C. J. (2018). Whole-Genome Duplication and Plant Macroevolution. In *Trends in Plant Science* (Vol. 23, Issue 10, pp. 933–945). Elsevier Ltd. https://doi.org/10.1016/j.tplants.2018.07.006

Collén, J., Porcel, B., Carré, W., Ball, S. G., Chaparro, C., Tonon, T., Barbeyron, T., Michel, G., Noel, B., Valentin, K., Elias, M., François Artiguenave, Arun, A., Aury, J. M., Barbosa-Neto, J. F., Bothwell, J. H., Bouget, F. Y., Brillet, L., Cabello-Hurtado, F., … Boyen, C. (2013). Genome structure and metabolic features in the red seaweed Chondrus crispus shed light on evolution of the Archaeplastida. *Proceedings of the National Academy of Sciences of the United States of America*, *110*(13), 5247–5252. https://doi.org/10.1073/PNAS.1221259110/SUPPL_FILE/SAPP.PDF

Cooper, E., & Delwiche, C. (2016). *Green algal transcriptomes for phylogenetics and comparative genomics*. Figshare. https://dx.doi.org/10.6084/m9.figshare.1604778

Crooks, G. E., Hon, G., Chandonia, J. M., & Brenner, S. E. (2004). WebLogo: A sequence logo generator. *Genome Research*, *14*(6), 1188–1190. https://doi.org/10.1101/gr.849004

de Castro, E., Sigrist, C. J. A., Gattiker, A., Bulliard, V., Langendijk-Genevaux, P. S., Gasteiger, E., Bairoch, A., & Hulo, N. (2006). ScanProsite: Detection of PROSITE signature matches and ProRule-associated functional and structural residues in proteins. *Nucleic Acids Research*, *34*(WEB. SERV. ISS.), W362–W365. https://doi.org/10.1093/nar/gkl124

De Clerck, O., Kao, S. M., Bogaert, K. A., Blomme, J., Foflonker, F., Kwantes, M., Vancaester, E., Vanderstraeten, L., Aydogdu, E., Boesger, J., Califano, G., Charrier, B., Clewes, R., Del Cortona, A., D'Hondt, S., Fernandez-Pozo, N., Gachon, C. M., Hanikenne, M., Lattermann, L., … Bothwell, J. H. (2018). Insights into the Evolution of Multicellularity from the Sea Lettuce Genome. *Current Biology*, *28*(18), 2921-2933.e5. https://doi.org/10.1016/j.cub.2018.08.015

De Juan, D., Pazos, F., & Valencia, A. (2013). Emerging methods in protein co-evolution. In *Nature Reviews Genetics* (Vol. 14, Issue 4, pp. 249–261). Nature Publishing Group. https://doi.org/10.1038/nrg3414

de Reuille, P. B., Routier-Kierzkowska, A. L., Kierzkowski, D., Bassel, G. W., Schüpbach, T., Tauriello, G., Bajpai, N., Strauss, S., Weber, A., Kiss, A., Burian, A., Hofhuis, H., Sapala, A., Lipowczan, M., Heimlicher, M. B., Robinson, S., Bayer, E. M., Basler, K., Koumoutsakos, P., … Smith, R. S. (2015). MorphoGraphX: A platform for quantifying morphogenesis in 4D. *ELife*, *4*(MAY), 1–20. https://doi.org/10.7554/eLife.05864

de Vries, J., Fischer, A. M., Roettger, M., Rommel, S., Schluepmann, H., Bräutigam, A., Carlsbecker, A., & Gould, S. B. (2016). Cytokinin-induced promotion of root meristem size in the fern Azolla supports a shoot-like origin of euphyllophyte roots. *New Phytologist*, *209*(2), 705–720. https://doi.org/10.1111/nph.13630

Delaux, P. M., Hetherington, A. J., Coudert, Y., Delwiche, C., Dunand, C., Gould, S., Kenrick, P., Li, F. W., Philippe, H., Rensing, S. A., Rich, M., Strullu-Derrien, C., & de Vries, J. (2019). Reconstructing trait evolution in plant evo–devo studies. In *Current Biology* (Vol. 29, Issue 21, pp. R1110–R1118). Cell Press. https://doi.org/10.1016/j.cub.2019.09.044

Denninger, P., Reichelt, A., Schmidt, V. A. F., Mehlhorn, D. G., Asseck, L. Y., Stanley, C. E., Keinath, N. F., Evers, J. F., Grefen, C., & Grossmann, G. (2019). Distinct RopGEFs Successively Drive Polarization and Outgrowth of Root Hairs. *Current Biology*, *29*(11), 1854-1865.e5. https://doi.org/10.1016/j.cub.2019.04.059

Domozych, D. S., Sørensen, I., Sacks, C., Brechka, H., Andreas, A., Fangel, J. U., Rose, J. K. C., Willats, W. G. T., & Popper, Z. A. (2014). Disruption of the microtubule network alters cellulose deposition and causes major changes in pectin distribution in the cell wall of the green alga, Penium margaritaceum. *Journal of Experimental Botany*, *65*(2), 465–479. https://doi.org/10.1093/jxb/ert390

Dong, J. H., Wen, J. F., & Tian, H. F. (2007). Homologs of eukaryotic Ras superfamily proteins in prokaryotes and their novel phylogenetic correlation with their eukaryotic analogs. *Gene*, *396*(1), 116–124. https://doi.org/10.1016/j.gene.2007.03.001

Dong, J., MacAlister, C. A., & Bergmann, D. C. (2009). BASL Controls Asymmetric Cell Division in Arabidopsis. *Cell*, *137*(7), 1320–1330. https://doi.org/10.1016/j.cell.2009.04.018

Donoghue, P. C. J., Harrison, C. J., Paps, J., & Schneider, H. (2021). The evolutionary emergence of land plants. In *Current Biology* (Vol. 31, Issue 19, pp. R1281–R1298). https://doi.org/10.1016/j.cub.2021.07.038

Dorer, R., Pryciak, P. M., & Hartwell, L. H. (1995). Saccharomyces cerevisiae cells execute a default pathway to select a mate in the absence of pheromone gradients. *Journal of Cell Biology*, *131*(4), 845–861. https://doi.org/10.1083/jcb.131.4.845

Eklund, D. M., Svensson, E. M., & Kost, B. (2010). Physcomitrella patens: A model to investigate the role of RAC/ROP GTPase signalling in tip growth. In *Journal of Experimental Botany*. https://doi.org/10.1093/jxb/erq080

Elias, M. (2008). The guanine nucleotide exchange factors Sec2 and PRONE: Candidate synapomorphies for the Opisthokonta and the Archaeplastida. *Molecular Biology and Evolution*, *25*(8), 1526–1529. https://doi.org/10.1093/molbev/msn113

Eliáš, M., & Klimeš, V. (2012). Rho GTPases: Deciphering the evolutionary history of a complex protein family. In *Methods in Molecular Biology* (Vol. 827). Springer, New York, NY. https://doi.org/10.1007/978-1-61779-442-1_2

Engel, S. R., Dietrich, F. S., Fisk, D. G., Binkley, G., Balakrishnan, R., Costanzo, M. C., Dwight, S. S., Hitz, B. C., Karra, K., Nash, R. S., Weng, S., Wong, E. D., Lloyd, P., Skrzypek, M. S., Miyasato, S. R., Simison, M., & Cherry, J. M. (2014). The Reference Genome Sequence of Saccharomyces cerevisiae: Then and Now. *G3: Genes, Genomes, Genetics*, *4*(3), 389–398. https://doi.org/10.1534/g3.113.008995

Etienne-Manneville, S., & Hall, A. (2002). Rho GTPases in cell biology. *Nature*, *420*(6916), 629–635. https://doi.org/10.1038/nature01148

Evangelista, M., Blundell, K., Longtine, M. S., Chow, C. J., Adames, N., Pringle, J. R., Peter, M., & Boone, C. (1997). Bni1p, a yeast formin linking Cdc42p and the actin cytoskeleton during polarized morphogenesis. *Science*, *276*(5309), 118–122. https://doi.org/10.1126/science.276.5309.118

Evangelista, M., Pruyne, D., Amberg, D. C., Boone, C., & Bretscher, A. (2002). Formins direct Arp2/3-independent actin filament assembly to polarize cell growth in yeast. *Nature Cell Biology*, *4*(3), 260–269. https://doi.org/10.1038/ncb718

Feiguelman, G., Fu, Y., & Yalovsky, S. (2018). ROP GTPases structure-function and signaling pathways. *Plant Physiology*, *176*(January), 57–79. https://doi.org/10.1104/pp.17.01415

Fletcher, D. A., & Mullins, R. D. (2010). Cell mechanics and the cytoskeleton. *Nature*, *463*(7280), 485–492. https://doi.org/10.1038/nature08908

Fodor-Dunai, C., Fricke, I., Potocký, M., Dorjgotov, D., Domoki, M., Jurca, M. E., Ötvös, K., Ẑárský, V., Berken, A., & Fehér, A. (2011). The phosphomimetic mutation of an evolutionarily conserved serine residue affects the signaling properties of Rho of plants (ROPs). *Plant Journal*, *66*(4), 669–679. https://doi.org/10.1111/j.1365-313X.2011.04528.x

Fort, P., & Blangy, A. (2017). The evolutionary landscape of Dbl-like RhoGEF families: Adapting eukaryotic cells to environmental signals. *Genome Biology and Evolution*, *9*(6), 1471–1486. https://doi.org/10.1093/gbe/evx100

Fowler, J. E. (2010). Evolution of the ROP GTPase Signaling Module. In *Integrated G Proteins Signaling in Plants* (pp. 305–327). Springer, Berlin, Heidelberg. https://doi.org/10.1007/978-3-642-03524-1_15

Frangedakis, E., Saint-Marcoux, D., Moody, L. A., Rabbinowitsch, E., & Langdale, J. A. (2017). Nonreciprocal complementation of KNOX gene function in land plants. *New Phytologist*, *216*(2), 591–604. https://doi.org/10.1111/nph.14318

Fricke, I., & Berken, A. (2009). Molecular basis for the substrate specificity of plant guanine nucleotide exchange factors for ROP. *FEBS Letters*, *583*(1), 75–80. https://doi.org/10.1016/j.febslet.2008.12.008

Friml, J., Vieten, A., Sauer, M., Weijers, D., Schwarz, H., Hamann, T., Offringa, R., & Jürgens, G. (2003). Efflux-dependent auxin gradients establish the apical-basal axis of Arabidopsis. *Nature*, *426*(6963), 147–153. https://doi.org/10.1038/nature02085

Fu, Y., Gu, Y., Zheng, Z., Wasteneys, G., & Yang, Z. (2005). Arabidopsis interdigitating cell growth requires two antagonistic pathways with opposing action on cell morphogenesis. *Cell*, *120*(5), 687–700. https://doi.org/10.1016/j.cell.2004.12.026

Fu, Y., Li, H., & Yang, Z. (2002). The ROP2 GTPase controls the formation of cortical fine F-actin and the early phase of directional cell expansion during arabidopsis organogenesis. *Plant Cell*, *14*(4), 777–794. https://doi.org/10.1105/tpc.001537

Fu, Y., Wu, G., & Yang, Z. (2001). Rop GTPase-dependent dynamics of tip-localized F-actin controls tip growth in pollen tubes. *Journal of Cell Biology*, *152*(5), 1019–1032. https://doi.org/10.1083/jcb.152.5.1019

Fu, Y., Xu, T., Zhu, L., Wen, M., & Yang, Z. (2009). A ROP GTPase Signaling Pathway Controls Cortical Microtubule Ordering and Cell Expansion in Arabidopsis. *Current Biology*, *19*(21), 1827–1832. https://doi.org/10.1016/j.cub.2009.08.052

Garcia-Mata, R., Boulter, E., & Burridge, K. (2011). The "invisible hand": Regulation of RHO GTPases by RHOGDIs. *Nature Reviews Molecular Cell Biology*, *12*(8), 493–504. https://doi.org/10.1038/nrm3153

Geitmann, A., & Emons, A. M. C. (2000). The cytoskeleton in plant and fungal cell tip growth. *Journal of Microscopy*, *198*(3), 218–245. https://doi.org/10.1046/j.1365-2818.2000.00702.x

Geitmann, A., & Ortega, J. K. E. (2009). Mechanics and modeling of plant cell growth. In *Trends in Plant Science* (Vol. 14, Issue 9, pp. 467–478). Elsevier Current Trends. https://doi.org/10.1016/j.tplants.2009.07.006

Gendre, D., Baral, A., Dang, X., Esnay, N., Boutte, Y., Stanislas, T., Vain, T., Claverol, S., Gustavsson, A.,

Lin, D., Grebe, M., & Bhalerao, R. P. (2019). Rho-of-plant activated root hair formation requires arabidopsis YIP4a/b gene function. *Development*, *146*(5), dev168559. https://doi.org/10.1242/dev.168559

Goldstein, B., & Macara, I. G. (2007). The PAR Proteins: Fundamental Players in Animal Cell Polarization. In *Developmental Cell* (Vol. 13, Issue 5, pp. 609–622). https://doi.org/10.1016/j.devcel.2007.10.007

Goryachev, A. B., & Pokhilko, A. V. (2008). Dynamics of Cdc42 network embodies a Turing-type mechanism of yeast cell polarity. *FEBS Letters*, *582*(10), 1437–1443. https://doi.org/10.1016/j.febslet.2008.03.029

Graham, L. E., Arancibia-Avila, P., Taylor, W. A., Strother, P. K., & Cook, M. E. (2012). Aeroterrestrial Coleochaete (Streptophyta, Coleochaetales) models early plant adaptation to land. *American Journal of Botany*, *99*(1), 130–144. https://doi.org/10.3732/ajb.1100245

Graham, L. E., Cook, M. E., & Busse, J. S. (2000). The origin of plants: Body plan changes contributing to a major evolutionary radiation. In *Proceedings of the National Academy of Sciences of the United States of America* (Vol. 97, Issue 9, pp. 4535–4540). https://doi.org/10.1073/pnas.97.9.4535

Green, P. B. (1962). *Mechanism for Plant Cellular Morphogenesis. 138*(3548), 1404–1405. https://doi.org/10.1126/science.138.3548.1404

Gu, Y., Fu, Y., Dowd, P., Li, S., Vernoud, V., Gilroy, S., & Yang, Z. (2005). A Rho family GTPase controls actin dynamics and tip growth via two counteracting downstream pathways in pollen tubes. *Journal of Cell Biology*, *169*(1), 127–138. https://doi.org/10.1083/jcb.200409140

Guan, R., Zhao, Y., Zhang, H., Fan, G., Liu, X., Zhou, W., Shi, C., Wang, J., Liu, W., Liang, X., Fu, Y., Ma, K., Zhao, L., Zhang, F., Lu, Z., Lee, S., Xu, X., Wang, J., Yang, H., … Chen, W. (2019). *Updated genome assembly of Ginkgo biloba*. GigaScience Database. http://dx.doi.org/10.5524/100613

Guindon, S., Dufayard, J. F., Lefort, V., Anisimova, M., Hordijk, W., & Gascuel, O. (2010). New algorithms and methods to estimate maximum-likelihood phylogenies: Assessing the performance of PhyML 3.0. *Systematic Biology*, *59*(3), 307–321. https://doi.org/10.1093/sysbio/syq010

Gulli, M. P., Jaquenoud, M., Shimada, Y., Niederhäuser, G., Wiget, P., & Peter, M. (2000). Phosphorylation of the Cdc42 exchange factor Cdc24 by the PAK-like kinase Cla4 may regulate polarized growth in yeast. *Molecular Cell*, *6*(5), 1155–1167. https://doi.org/10.1016/S1097-2765(00)00113-1

Haigler, C. H., & Roberts, A. W. (2019). Structure/function relationships in the rosette cellulose synthesis complex illuminated by an evolutionary perspective. In *Cellulose* (Vol. 26, Issue 1, pp. 227–247). https://doi.org/10.1007/s10570-018-2157-9

Hall, A. (1998). Rho GTPases and the Actin Cytoskeleton. *Science*, *279*(5350), 509–514. https://doi.org/10.1126/science.279.5350.509

Hall, T. A. (1999). BioEdit: a user-friendly biological sequence alignment editor and analysis program for Windows 95/98/NT. *Nucleic Acids Symposium Series*, *41*, 95–98.

Hamada, T. (2014). Microtubule organization and microtubule-associated proteins in plant cells. In *International Review of Cell and Molecular Biology* (Vol. 312, pp. 1–52). Elsevier Inc. https://doi.org/10.1016/B978-0-12-800178-3.00001-4

Harkins, H. A., Pagé, N., Schenkman, L. R., De Virgilio, C., Shaw, S., Bussey, H., & Pringle, J. R. (2001). Bud8p and Bud9p, proteins that may mark the sites for bipolar budding in yeast. *Molecular Biology of the Cell*, *12*(8), 2497–2518. https://doi.org/10.1091/mbc.12.8.2497

Harris, B. J., Harrison, C. J., Hetherington, A. M., & Williams, T. A. (2020). Phylogenomic Evidence for the Monophyly of Bryophytes and the Reductive Evolution of Stomata. *Current Biology*. https://doi.org/10.1016/j.cub.2020.03.048

Harrison, C. J. (2017). Development and genetics in the evolution of land plant body plans. In *Philosophical Transactions of the Royal Society B: Biological Sciences* (Vol. 372, Issue 1713). The Royal Society. https://doi.org/10.1098/rstb.2015.0490

Hartwell, L. H., Mortimer, R. K., Culotti, J., & Culotti, M. (1973). Genetic control of the cell division cycle in yeast: V. Genetic analysis of cdc mutants. *Genetics*, *74*(2), 267–286. https://doi.org/74(2): 267–286.

Hirano, T., Konno, H., Takeda, S., Dolan, L., Kato, M., Aoyama, T., Higaki, T., Takigawa-Imamura, H., & Sato, M. H. (2018). PtdIns(3,5)P2 mediates root hair shank hardening in Arabidopsis. In *Nature Plants* (Vol. 4, Issue 11, pp. 888–897). https://doi.org/10.1038/s41477-018-0277-8

Hiwatashi, T., Quan, K. L., Yasui, Y., Takami, H., Kajikawa, M., Kirita, H., Sato, M., Wakazaki, M., Yamaguchi, K., Shigenobu, S., Fukaki, H., Mimura, T., Yamato, K. T., Toyooka, K., Sawa, S., Urano, D., Kohchi, T., & Ishizaki, K. (2019). The RopGEF KARAPPO is Essential for the Initiation of Vegetative Reproduction in Marchantia. *Current Biology*, *29*, 1–7. https://doi.org/10.2139/ssrn.3236486

Honkanen, S., Jones, V. A. S., Morieri, G., Champion, C., Hetherington, A. J., Kelly, S., Proust, H., Saint-Marcoux, D., Prescott, H., & Dolan, L. (2016). The Mechanism Forming the Cell Surface of Tip-Growing Rooting Cells Is Conserved among Land Plants. *Current Biology*, *26*(20), 3238–3244. https://doi.org/10.1016/j.cub.2017.09.062

Honkanen, S., Thamm, A., Arteaga-Vazquez, M. A., & Dolan, L. (2018). Negative regulation of conserved RSL class I bHLH transcription factors evolved independently among land plants. *ELife*, *7*, 1–21. https://doi.org/10.7554/eLife.38529

Hori, K., Maruyama, F., Fujisawa, T., Togashi, T., Yamamoto, N., Seo, M., Sato, S., Yamada, T., Mori, H., Tajima, N., Moriyama, T., Ikeuchi, M., Watanabe, M., Wada, H., Kobayashi, K., Saito, M., Masuda, T., Sasaki-Sekimoto, Y., Mashiguchi, K., … Ohta, H. (2014). Klebsormidium flaccidum genome reveals primary factors for plant terrestrial adaptation. *Nature Communications*, *5*(1), 1–9. https://doi.org/10.1038/ncomms4978

Howell, A. S., Jin, M., Wu, C. F., Zyla, T. R., Elston, T. C., & Lew, D. J. (2012). Negative feedback enhances robustness in the yeast polarity establishment circuit. *Cell*, *149*(2), 322–333. https://doi.org/10.1016/j.cell.2012.03.012

Humphries, J. A., Vejlupkova, Z., Luo, A., Meeley, R. B., Sylvester, A. W., Fowler, J. E., & Smith, L. G. (2011). ROP GTPases Act with the Receptor-Like Protein PAN1 to Polarize Asymmetric Cell Division in Maize. *The Plant Cell*, *23*(6), 2273–2284. https://doi.org/10.1105/tpc.111.085597

Hwang, J. U., Vernoud, V., Szumlanski, A., Nielsen, E., & Yang, Z. (2008). A Tip-Localized RhoGAP Controls Cell Polarity by Globally Inhibiting Rho GTPase at the Cell Apex. *Current Biology*, *18*(24), 1907–1916. https://doi.org/10.1016/j.cub.2008.11.057

Hwang, J. U., Wu, G., Yan, A., Lee, Y. J., Grierson, C. S., & Yang, Z. (2010). Pollen-tube tip growth requires a balance of lateral propagation and global inhibition of Rho-family GTPase activity. *Journal of Cell Science*, *123*(3), 340–350. https://doi.org/10.1242/jcs.039180

Irazoqui, J. E., Gladfelter, A. S., & Lew, D. J. (2003). Scaffold-mediated symmetry breaking by Cdc42p. *Nature Cell Biology*, *5*(12), 1062–1070. https://doi.org/10.1038/ncb1068

Irisarri, I., Darienko, T., Pröschold, T., Fürst-Jansen, J. M. R., Jamy, M., & De Vries, J. (2021). Unexpected cryptic species among streptophyte algae most distant to land plants. *Proceedings of the Royal Society B: Biological Sciences*, *288*(1963). https://doi.org/10.1098/rspb.2021.2168

Irisarri, I., Strassert, J. F. H., & Burki, F. (2022). Phylogenomic Insights into the Origin of Primary Plastids. *Systematic Biology*, *71*(1), 105–120. https://doi.org/10.1093/sysbio/syab036

Ishizaki, K., Chiyoda, S., Yamato, K. T., & Kohchi, T. (2008). Agrobacterium-mediated transformation of the haploid liverwort Marchantia polymorpha L., an emerging model for plant biology. *Plant and Cell Physiology*, *49*(7), 1084–1091. https://doi.org/10.1093/pcp/pcn085

Iwase, M., Luo, J., Nagaraj, S., Longtine, M., Kim, H. B., Haarer, B. K., Caruso, C., Tong, Z., Pringle, J. R., & Bi, E. (2006). Role of a Cdc42p effector pathway in recruitment of the yeast septins to the presumptive bud site. *Molecular Biology of the Cell*, *17*(3), 1110–1125. https://doi.org/10.1091/mbc.E05-08-0793

Jiao, C., Sørensen, I., Sun, X., Sun, H., Behar, H., Alseekh, S., Philippe, G., Palacio Lopez, K., Sun, L., Reed, R., Jeon, S., Kiyonami, R., Zhang, S., Fernie, A. R., Brumer, H., Domozych, D. S., Fei, Z., & Rose, J. K. C. (2020). The Penium margaritaceum Genome: Hallmarks of the Origins of Land Plants. *Cell*, *0*(0), 1097-1111.e12. https://doi.org/10.1016/j.cell.2020.04.019

Jiao, Y., Peluso, P., Shi, J., Liang, T., Stitzer, M. C., Wang, B., Campbell, M. S., Stein, J. C., Wei, X., Chin,

C. S., Guill, K., Regulski, M., Kumari, S., Olson, A., Gent, J., Schneider, K. L., Wolfgruber, T. K., May, M. R., Springer, N. M., … Ware, D. (2017). Improved maize reference genome with single-molecule technologies. *Nature*, *546*(7659), 524–527. https://doi.org/10.1038/nature22971

Johnson, D. I., & Pringle, J. R. (1990). Molecular characterization of CDC42, a Saccharomyces cerevisiae gene involved in the development of cell polarity. *Journal of Cell Biology*, *111*(1), 143–152. https://doi.org/10.1083/jcb.111.1.143

Jones, M. A., Shen, J.-J., Fu, Y., Li, H., Yang, Z., & Grierson, C. S. (2002). The Arabidopsis Rop2 GTPase Is a Positive Regulator of Both Root Hair Initiation and Tip Growth. *The Plant Cell*, *14*, 763–776. https://doi.org/10.1105/tpc.010359

Ju, C., Van De Poel, B., Cooper, E. D., Thierer, J. H., Gibbons, T. R., Delwiche, C. F., & Chang, C. (2015). Conservation of ethylene as a plant hormone over 450 million years of evolution. *Nature Plants*, *1*. https://doi.org/10.1038/nplants.2014.4

Kalyaanamoorthy, S., Minh, B. Q., Wong, T. K. F., Von Haeseler, A., & Jermiin, L. S. (2017). ModelFinder: Fast model selection for accurate phylogenetic estimates. *Nature Methods*, *14*(6), 587–589. https://doi.org/10.1038/nmeth.4285

Kang, P. J., Sanson, A., Lee, B., & Park, H. O. (2001). A GDP/GTP exchange factor involved in linking a spatial landmark to cell polarity. *Science*, *292*(5520), 1376–1378. https://doi.org/10.1126/science.1060360

Kapli, P., Yang, Z., & Telford, M. J. (2020). Phylogenetic tree building in the genomic age. In *Nature Reviews Genetics* (Vol. 21, Issue 7, pp. 428–444). Nature Publishing Group. https://doi.org/10.1038/s41576-020-0233-0

Katoh, K., & Standley, D. M. (2013). MAFFT multiple sequence alignment software version 7: Improvements in performance and usability. *Molecular Biology and Evolution*, *30*(4), 772–780. https://doi.org/10.1093/molbev/mst010

Katsaros, C. I., Varvarigos, V., Gachon, C. M. M., Brand, J., Motomura, T., Nagasato, C., & Küpper, F. C. (2011). Comparative Immunofluorescence and Ultrastructural Analysis of Microtubule Organization in Uronema sp., Klebsormidium flaccidum, K. subtilissimum, Stichococcus bacillaris and S. chloranthus (Chlorophyta). *Protist*, *162*(2), 315–331. https://doi.org/10.1016/j.protis.2010.10.004

Katsaros, C., Karyophyllis, D., & Galatis, B. (2006). Cytoskeleton and morphogenesis in brown algae. In *Annals of Botany* (Vol. 97, Issue 5, pp. 679–693). Oxford Academic. https://doi.org/10.1093/aob/mcl023

Kawahara, Y., de la Bastide, M., Hamilton, J. P., Kanamori, H., McCombie, W. R., Ouyang, S., Schwartz, D. C., Tanaka, T., Wu, J., Zhou, S., Childs, K. L., Davidson, R. M., Lin, H., Quesada-Ocampo, L., Vaillancourt, B., Sakai, H., Lee, S. S., Kim, J., Numa, H., … Matsumoto, T. (2013). Improvement of the Oryza sativa Nipponbare reference genome using next generation sequence and optical map data. *Rice*, *6*(1), 1–10. https://doi.org/10.1186/1939-8433-6-1

Kimura, S., & Mizuta, S. (1994). Role of the microtubule cytoskeleton in alternating changes in cellulose-microfibril orientation in the coenocytic green alga, Chaetomorpha moniligera. *Planta*, *193*(1), 21–31. https://doi.org/10.1007/BF00191602

Kirchhelle, C., Chow, C. M., Foucart, C., Neto, H., Stierhof, Y. D., Kalde, M., Walton, C., Fricker, M., Smith, R. S., Jérusalem, A., Irani, N., & Moore, I. (2016). The Specification of Geometric Edges by a Plant Rab GTPase Is an Essential Cell-Patterning Principle During Organogenesis in Arabidopsis. *Developmental Cell*, *36*(4), 386–400. https://doi.org/10.1016/j.devcel.2016.01.020

Kirchhelle, C., & Moore, I. (2017). A simple chamber for long-term confocal imaging of root and hypocotyl development. *Journal of Visualized Experiments*, *2017*(123), 1–9. https://doi.org/10.3791/55331

Klahre, U., & Kost, B. (2006). Tobacco RhoGTPase activating protein1 spatially restricts signaling of RAC/Rop to the apex of pollen tubes. *Plant Cell*, *18*(11), 3033–3046. https://doi.org/10.1105/tpc.106.045336

Knoll, A. H. (2011). The multiple origins of complex multicellularity. *Annual Review of Earth and Planetary Sciences*, *39*, 217–239. https://doi.org/10.1146/annurev.earth.031208.100209

Kosami, K. I., Ohki, I., Nagano, M., Furuita, K., Sugiki, T., Kawano, Y., Kawasaki, T., Fujiwara, T., Nakagawa, A., Shimamoto, K., & Kojima, C. (2014). The crystal structure of the plant small GTPase OsRac1 reveals its mode of binding to NADPH oxidase. *Journal of Biological Chemistry*, *289*(41), 28569–28578. https://doi.org/10.1074/jbc.M114.603282

Kozminski, K. G., Chen, A. J., Rodal, A. A., & Drubin, D. G. (2000). Functions and Functional Domains of the GTPase Cdc42p. *Molecular Biology of the Cell*, *11*, 339–354. https://www.ncbi.nlm.nih.gov/pmc/articles/PMC14778/pdf/mk000339.pdf

Kozubowski, L., Saito, K., Johnson, J. M., Howell, A. S., Zyla, T. R., & Lew, D. J. (2008). Symmetry-Breaking Polarization Driven by a Cdc42p GEF-PAK Complex. *Current Biology*, *18*(22), 1719–1726. https://doi.org/10.1016/j.cub.2008.09.060

Kubota, A., Ishizaki, K., Hosaka, M., & Kohchi, T. (2013). Efficient Agrobacterium -Mediated Transformation of the Liverwort Marchantia polymorpha Using Regenerating Thalli. *Bioscience, Biotechnology and Biochemistry*, *77*(1), 167–172. https://doi.org/10.1271/bbb.120700

Kurihara, D., Mizuta, Y., Nagahara, S., & Higashiyama, T. (2021). ClearSeeAlpha: Advanced Optical Clearing for Whole-Plant Imaging. *Plant & Cell Physiology*. https://doi.org/10.1093/pcp/pcab033

Kwon, T., Kwon, D. Y., Chun, J., Kim, J. H., & Kang, S. S. (2000). Akt protein kinase inhibits Rac1-GTP binding through phosphorylation at serine 71 of Rac1. *Journal of Biological Chemistry*, *275*(1), 423–428. https://doi.org/10.1074/jbc.275.1.423

Lamesch, P., Berardini, T. Z., Li, D., Swarbreck, D., Wilks, C., Sasidharan, R., Muller, R., Dreher, K., Alexander, D. L., Garcia-Hernandez, M., Karthikeyan, A. S., Lee, C. H., Nelson, W. D., Ploetz, L., Singh, S., Wensel, A., & Huala, E. (2012). The Arabidopsis Information Resource (TAIR): improved gene annotation and new tools. *Nucleic Acids Research*, *40*(D1), D1202–D1210. https://doi.org/10.1093/NAR/GKR1090

Lang, D., Ullrich, K. K., Murat, F., Fuchs, J., Jenkins, J., Haas, F. B., Piednoel, M., Gundlach, H., Van Bel, M., Meyberg, R., Vives, C., Morata, J., Symeonidi, A., Hiss, M., Muchero, W., Kamisugi, Y., Saleh, O., Blanc, G., Decker, E. L., … Rensing, S. A. (2018). The Physcomitrella patens chromosome-scale assembly reveals moss genome structure and evolution. *Plant Journal*, *93*(3), 515–533. https://doi.org/10.1111/TPJ.13801

Lauster, T., Stöckle, D., Gabor, K., Haller, T., Krieger, N., Lotz, P., Mayakrishnan, R., Späth, E., Zimmermann, S., Livanos, P., & Müller, S. (2022). Arabidopsis pavement cell shape formation involves spatially confined ROPGAP regulators. *Current Biology*, *32*(3), 532-544.e7. https://doi.org/10.1016/j.cub.2021.12.042

Lee, J. M., Kim, D., Bhattacharya, D., & Yoon, H. S. (2019). Expansion of phycobilisome linker gene families in mesophilic red algae. *Nature Communications*, *10*(1), 1–10. https://doi.org/10.1038/s41467-019-12779-1

Leebens-Mack, J. H., Barker, M. S., Carpenter, E. J., Deyholos, M. K., Gitzendanner, M. A., Graham, S. W., Grosse, I., Li, Z., Melkonian, M., Mirarab, S., Porsch, M., Quint, M., Rensing, S. A., Soltis, D. E., Soltis, P. S., Stevenson, D. W., Ullrich, K. K., Wickett, N. J., DeGironimo, L., … Wong, G. K. S. (2019). One thousand plant transcriptomes and the phylogenomics of green plants. *Nature*, *574*(7780), 679–685. https://doi.org/10.1038/s41586-019-1693-2

Lefort, V., Longueville, J. E., & Gascuel, O. (2017). SMS: Smart Model Selection in PhyML. *Molecular Biology and Evolution*, *34*(9), 2422–2424. https://doi.org/10.1093/molbev/msx149

Lemieux, C., Otis, C., & Turmel, M. (2007). A clade uniting the green algae Mesostigma viride and Chlorokybus atmophyticus represents the deepest branch of the Streptophyta in chloroplast genome-based phylogenies. *BMC Biology*, *5*(1), 1–17. https://doi.org/10.1186/1741-7007-5-2

Lemieux, C., Turmel, M., Otis, C., & Pombert, J. F. (2019). A streamlined and predominantly diploid genome in the tiny marine green alga Chloropicon primus. *Nature Communications*, *10*(1), 1–13. https://doi.org/10.1038/s41467-019-12014-x

Letunic, I., & Bork, P. (2007). Interactive Tree Of Life (iTOL): An online tool for phylogenetic tree display and annotation. *Bioinformatics*, *23*(1), 127–128. https://doi.org/10.1093/bioinformatics/btl529

Letunic, I., & Bork, P. (2018). 20 years of the SMART protein domain annotation resource. *Nucleic Acids*

Research, *46*(D1), D493–D496. https://doi.org/10.1093/nar/gkx922

Li, F. W., Brouwer, P., Carretero-Paulet, L., Cheng, S., De Vries, J., Delaux, P. M., Eily, A., Koppers, N., Kuo, L. Y., Li, Z., Simenc, M., Small, I., Wafula, E., Angarita, S., Barker, M. S., Bräutigam, A., Depamphilis, C., Gould, S., Hosmani, P. S., … Pryer, K. M. (2018). Fern genomes elucidate land plant evolution and cyanobacterial symbioses. *Nature Plants*, *4*(7), 460–472. https://doi.org/10.1038/s41477-018-0188-8

Li, F. W., Nishiyama, T., Waller, M., Frangedakis, E., Keller, J., Li, Z., Fernandez-Pozo, N., Barker, M. S., Bennett, T., Blázquez, M. A., Cheng, S., Cuming, A. C., de Vries, J., de Vries, S., Delaux, P. M., Diop, I. S., Harrison, C. J., Hauser, D., Hernández-García, J., … Szövényi, P. (2020). Anthoceros genomes illuminate the origin of land plants and the unique biology of hornworts. *Nature Plants*, *6*(3), 259–272. https://doi.org/10.1038/s41477-020-0618-2

Li, H., Lin, Y., Heath, R. M., Zhu, M. X., & Yang, Z. (1999). Control of pollen tube tip growth by a Rop GTPase-dependent pathway that leads to tip-localized calcium influx. *Plant Cell*, *11*(9), 1731–1742. https://doi.org/10.1105/tpc.11.9.1731

Li, H., Shen, J. J., Zheng, Z. L., Lin, Y., & Yang, Z. (2001). The Rop GTPase switch controls multiple developmental processes in Arabidopsis. *Plant Physiology*, *126*(June), 670–684. https://doi.org/10.1104/pp.126.2.670

Liang, Z., Demko, V., Wilson, R. C., Johnson, K. A., Ahmad, R., Perroud, P. F., Quatrano, R., Zhao, S., Shalchian-Tabrizi, K., Otegui, M. S., Olsen, O. A., & Johansen, W. (2013). The catalytic domain CysPc of the DEK1 calpain is functionally conserved in land plants. *The Plant Journal*, *75*(5), 742–754. https://doi.org/10.1111/tpj.12235

Liang, Z., Geng, Y., Ji, C., Du, H., Wong, C. E., Zhang, Q., Zhang, Y., Zhang, P., Riaz, A., Chachar, S., Ding, Y., Wen, J., Wu, Y., Wang, M., Zheng, H., Wu, Y., Demko, V., Shen, L., Han, X., … Yu, H. (2020). Mesostigma viride Genome and Transcriptome Provide Insights into the Origin and Evolution of Streptophyta. *Advanced Science*, *7*(1), 1901850. https://doi.org/10.1002/advs.201901850

Lin, D., Cao, L., Zhou, Z., Zhu, L., Ehrhardt, D., Yang, Z., & Fu, Y. (2013). Rho GTPase signaling activates microtubule severing to promote microtubule ordering in arabidopsis. *Current Biology*, *23*(4), 290–297. https://doi.org/10.1016/j.cub.2013.01.022

Lin, Y, Wang, Y., Zhu, J., & Yang, Z. (1996). Localization of a Rho GTPase Implies a Role in Tip Growth and Movement of the Generative Cell in Pollen Tubes. *The Plant Cell*, *8*(February), 293–303. https://doi.org/10.1105/tpc.8.2.293

Lin, Yakang, & Yang, Z. (1997). Inhibition of pollen tube elongation by microinjected anti-Rop1Ps antibodies suggests a crucial role for Rho-type GTPases in the control of tip growth. *Plant Cell*, *9*(9), 1647–1659. https://doi.org/10.1105/tpc.9.9.1647

Livanos, P., & Müller, S. (2019). Division Plane Establishment and Cytokinesis. In *Annual Review of Plant Biology* (Vol. 70, Issue 1, pp. 239–267). Annual Reviews Inc. https://doi.org/10.1146/annurev-arplant-050718-100444

Luo, L. (2000). RHO GTPASES in neuronal morphogenesis. *Nature Reviews Neuroscience*, *1*(3), 173–180. https://doi.org/10.1038/35044547

Luo, N., Yan, A., Liu, G., Guo, J., Rong, D., Kanaoka, M. M., Xiao, Z., Xu, G., Higashiyama, T., Cui, X., & Yang, Z. (2017). Exocytosis-coordinated mechanisms for tip growth underlie pollen tube growth guidance. *Nature Communications*, *8*(1). https://doi.org/10.1038/s41467-017-01452-0

Madaule, P., & Axel, R. (1985). A novel ras-related gene family. *Cell*, *41*(1), 31–40. https://doi.org/10.1016/0092-8674(85)90058-3

Manton, I., & Ettl, H. (1965). Observations on the fine structure of Mesostigma viride Lauterborn. *Journal of the Linnean Society of London, Botany*, *59*(378), 175–184. https://doi.org/10.1111/j.1095-8339.1965.tb00056.x

Marchesi, S., Montani, F., Deflorian, G., D'Antuono, R., Cuomo, A., Bologna, S., Mazzoccoli, C., Bonaldi, T., DiFiore, P. P., & Nicassio, F. (2014). DEPDC1B coordinates de-adhesion events and cell-cycle progression at mitosis. *Developmental Cell*, *31*(4), 420–433. https://doi.org/10.1016/j.devcel.2014.09.009

Marks, R. A., Smith, J. J., Cronk, Q., Grassa, C. J., & McLetchie, D. N. (2019). Genome of the tropical plant Marchantia inflexa: implications for sex chromosome evolution and dehydration tolerance. *Scientific Reports*, *9*(1), 1–13. https://doi.org/10.1038/s41598-019-45039-9

Meinhardt, H. (2012). Turing's theory of morphogenesis of 1952 and the subsequent discovery of the crucial role of local self enhancement and long-range inhibition. In *Interface Focus* (Vol. 2, Issue 4, pp. 407–416). Royal Society. https://doi.org/10.1098/rsfs.2011.0097

Meller, N., Merlot, S., & Guda, C. (2005). CZH proteins: A new family of Rho-GEFs. In *Journal of Cell Science* (Vol. 118, Issue 21, pp. 4937–4946). The Company of Biologists. https://doi.org/10.1242/jcs.02671

Merchant, S. S., Prochnik, S. E., Vallon, O., Harris, E. H., Karpowicz, S. J., Witman, G. B., Terry, A., Salamov, A., Fritz-Laylin, L. K., Maréchal-Drouard, L., Marshall, W. F., Qu, L. H., Nelson, D. R., Sanderfoot, A. A., Spalding, M. H., Kapitonov, V. V., Ren, Q., Ferris, P., Lindquist, E., … Zhou, K. (2007). The Chlamydomonas genome reveals the evolution of key animal and plant functions. *Science*, *318*(5848), 245–251. https://doi.org/10.1126/science.1143609

Merlini, L., Dudin, O., & Martin, S. G. (2013). Mate and fuse: How yeast cells do it. *Open Biology*, *3*(MAR). https://doi.org/10.1098/rsob.130008

Mikhailyuk, T., Holzinger, A., Massalski, A., & Karsten, U. (2014). Morphology and ultrastructure of Interfilum and Klebsormidium (Klebsormidiales, Streptophyta) with special reference to cell division and thallus formation. *European Journal of Phycology*, *49*(4), 395–412. https://doi.org/10.1080/09670262.2014.949308

Mikkelsen, M. D., Harholt, J., Westereng, B., Domozych, D., Fry, S. C., Johansen, I. E., Fangel, J. U., Łężyk, M., Feng, T., Nancke, L., Mikkelsen, J. D., Willats, W. G. T., & Ulvskov, P. (2021). Ancient origin of fucosylated xyloglucan in charophycean green algae. *Communications Biology*, *4*(1), 1–12. https://doi.org/10.1038/s42003-021-02277-w

Minh, B. Q., Nguyen, M. A. T., & Von Haeseler, A. (2013). Ultrafast approximation for phylogenetic bootstrap. *Molecular Biology and Evolution*, *30*(5), 1188–1195. https://doi.org/10.1093/molbev/mst024

Molendijk, A. J., Bischoff, F., Rajendrakumar, C. S. V., Friml, J., Braun, M., Gilroy, S., & Palme, K. (2001). Arabidopsis thaliana Rop GTPases are localized to tips of root hairs and control polar growth. *EMBO Journal*, *20*(11), 2779–2788. https://doi.org/10.1093/emboj/20.11.2779

Montgomery, S. A., Tanizawa, Y., Galik, B., Wang, N., Ito, T., Mochizuki, T., Akimcheva, S., Bowman, J. L., Cognat, V., Maréchal-Drouard, L., Ekker, H., Hong, S. F., Kohchi, T., Lin, S. S., Liu, L. Y. D., Nakamura, Y., Valeeva, L. R., Shakirov, E. V., Shippen, D. E., … Berger, F. (2020). Chromatin Organization in Early Land Plants Reveals an Ancestral Association between H3K27me3, Transposons, and Constitutive Heterochromatin. *Current Biology*, *30*(4), 573-588.e7. https://doi.org/10.1016/j.cub.2019.12.015

Moody, L. A. (2019). The 2D to 3D growth transition in the moss Physcomitrella patens. In *Current Opinion in Plant Biology* (Vol. 47, pp. 88–95). https://doi.org/10.1016/j.pbi.2018.10.001

Moody, L. A. (2020). Three-dimensional growth: a developmental innovation that facilitated plant terrestrialization. *Journal of Plant Research*, *133*(3), 283–290. https://doi.org/10.1007/s10265-020-01173-4

Moody, L. A., Kelly, S., Rabbinowitsch, E., & Langdale, J. A. (2018). Genetic Regulation of the 2D to 3D Growth Transition in the Moss Physcomitrella patens. *Current Biology*, *28*(3), 473-478.e5. https://doi.org/10.1016/j.cub.2017.12.052

Moreau, H., Verhelst, B., Couloux, A., Derelle, E., Rombauts, S., Grimsley, N., Van Bel, M., Poulain, J., Katinka, M., Hohmann-Marriott, M. F., Piganeau, G., Rouzé, P., Da Silva, C., Wincker, P., Van de Peer, Y., & Vandepoele, K. (2012). Gene functionalities and genome structure in Bathycoccus prasinos reflect cellular specializations at the base of the green lineage. *Genome Biology*, *13*(8), R74. https://doi.org/10.1186/gb-2012-13-8-r74

Morris, J. L., Puttick, M. N., Clark, J. W., Edwards, D., Kenrick, P., Pressel, S., Wellman, C. H., Yang, Z., Schneider, H., & Donoghue, P. C. J. (2018). The timescale of early land plant evolution. *Proceedings of the National Academy of Sciences of the United States of America*, *115*(10), E2274–E2283.

https://doi.org/10.1073/pnas.1719588115

Muroyama, A., & Bergmann, D. (2019). Plant Cell Polarity: Creating Diversity from Inside the Box. *Annual Review of Cell and Developmental Biology*, *35*(1), 309–336. https://doi.org/10.1146/annurev-cellbio-100818-125211

Nagawa, S., Xu, T., & Yang, Z. (2010). RHO GTPase in plants: Conservation and invention of regulators and effectors. In *Small GTPases* (Vol. 1, Issue 2, pp. 78–88). Taylor and Francis Inc. https://doi.org/10.4161/sgtp.1.2.14544

Nir, I., Amador, G., Gong, Y., Smoot, N. K., Cai, L., Shohat, H., & Bergmann, D. C. (2022). Evolution of polarity protein BASL and the capacity for stomatal lineage asymmetric divisions. *Current Biology*, *32*(2), 329-337.e5. https://doi.org/10.1016/j.cub.2021.11.013

Nishiyama, T., Sakayama, H., de Vries, J., Buschmann, H., Saint-Marcoux, D., Ullrich, K. K., Haas, F. B., Vanderstraeten, L., Becker, D., Lang, D., Vosolsobě, S., Rombauts, S., Wilhelmsson, P. K. I., Janitza, P., Kern, R., Heyl, A., Rümpler, F., Villalobos, L. I. A. C., Clay, J. M., … Rensing, S. A. (2018). The Chara Genome: Secondary Complexity and Implications for Plant Terrestrialization. *Cell*, *174*(2), 448-464.e24. https://doi.org/10.1016/j.cell.2018.06.033

Nozaki, H., Takano, H., Misumi, O., Terasawa, K., Matsuzaki, M., Maruyama, S., Nishida, K., Yagisawa, F., Yoshida, Y., Fujiwara, T., Takio, S., Tamura, K., Chung, S. J., Nakamura, S., Kuroiwa, H., Tanaka, K., Sato, N., & Kuroiwa, T. (2007). A 100%-complete sequence reveals unusually simple genomic features in the hot-spring red alga Cyanidioschyzon merolae. *BMC Biology*, *5*(1), 1–8. https://doi.org/10.1186/1741-7007-5-28

Nystedt, B., Street, N. R., Wetterbom, A., Zuccolo, A., Lin, Y. C., Scofield, D. G., Vezzi, F., Delhomme, N., Giacomello, S., Alexeyenko, A., Vicedomini, R., Sahlin, K., Sherwood, E., Elfstrand, M., Gramzow, L., Holmberg, K., Hällman, J., Keech, O., Klasson, L., … Jansson, S. (2013). The Norway spruce genome sequence and conifer genome evolution. *Nature*, *497*(7451), 579–584. https://doi.org/10.1038/nature12211

O'Rourke, C., Gregson, T., Murray, L., Sadler, I. H., & Fry, S. C. (2015). Sugar composition of the pectic polysaccharides of charophytes, the closest algal relatives of land-plants: Presence of 3-O-methyl-d-galactose residues. *Annals of Botany*, *116*(2), 225–236. https://doi.org/10.1093/aob/mcv089

Ono, K., Ohyama, K., & Gamborg, O. L. (1979). Regeneration of the liverwort Marchantia polymorpha L. From protoplasts isolated from cell suspension culture. *Plant Science Letters*, *14*(3), 225–229. https://doi.org/https://doi.org/10.1016/0304-4211(79)90074-9

Palenik, B., Grimwood, J., Aerts, A., Rouzé, P., Salamov, A., Putnam, N., Dupont, C., Jorgensen, R., Derelle, E., Rombauts, S., Zhou, K., Otillar, R., Merchant, S. S., Podell, S., Gaasterland, T., Napoli, C., Gendler, K., Manuell, A., Tai, V., … Grigoriev, I. V. (2007). The tiny eukaryote Ostreococcus provides genomic insights into the paradox of plankton speciation. *Proceedings of the National Academy of Sciences of the United States of America*, *104*(18), 7705–7710. https://doi.org/10.1073/pnas.0611046104

Paredez, A. R., Somerville, C. R., & Ehrhardt, D. W. (2006). Visualization of cellulose synthase demonstrates functional association with microtubules. *Science*, *312*(5779), 1491–1495. https://doi.org/10.1126/science.1126551

Payne, R. J. H., & Grierson, C. S. (2009). A theoretical model for ROP localisation by auxin in arabidopsis root hair cells. *PLoS ONE*, *4*(12), e8337. https://doi.org/10.1371/journal.pone.0008337

Perroud, P. F., Demko, V., Johansen, W., Wilson, R. C., Olsen, O. A., & Quatrano, R. S. (2014). Defective Kernel 1 (DEK1) is required for three-dimensional growth in Physcomitrella patens. *New Phytologist*, *203*(3), 794–804. https://doi.org/10.1111/nph.12844

Pickett-Heaps, J. D., Gunning, B. E. S., Brown, R. C., Lemmon, B. E., & Cleary, A. L. (1999). The cytoplast concept in dividing plant cells: Cytoplasmic domains and the evolution of spatially organized cell division. *American Journal of Botany*, *86*(2), 153–172. https://doi.org/10.2307/2656933

Pires, N. D., & Dolan, L. (2012). Morphological evolution in land plants: New designs with old genes. In *Philosophical Transactions of the Royal Society B: Biological Sciences* (Vol. 367, Issue 1588, pp. 508–518). https://doi.org/10.1098/rstb.2011.0252

Price, D. C., Goodenough, U. W., Roth, R., Lee, J. H., Kariyawasam, T., Mutwil, M., Ferrari, C., Facchinelli, F., Ball, S. G., Cenci, U., Chan, C. X., Wagner, N. E., Yoon, H. S., Weber, A. P. M., & Bhattacharya, D. (2019). Analysis of an improved Cyanophora paradoxa genome assembly. *DNA Research*, *26*(4), 287–299. https://doi.org/10.1093/dnares/dsz009

Prochnik, S. E., Umen, J., Nedelcu, A. M., Hallmann, A., Miller, S. M., Nishii, I., Ferris, P., Kuo, A., Mitros, T., Fritz-Laylin, L. K., Hellsten, U., Chapman, J., Simakov, O., Rensing, S. A., Terry, A., Pangilinan, J., Kapitonov, V., Jurka, J., Salamov, A., … Rokhsar, D. S. (2010). Genomic analysis of organismal complexity in the multicellular green alga volvox carteri. *Science*, *329*(5988), 223–226. https://doi.org/10.1126/science.1188800

Puttick, M. N., Morris, J. L., Williams, T. A., Cox, C. J., Edwards, D., Kenrick, P., Pressel, S., Wellman, C. H., Schneider, H., Pisani, D., & Donoghue, P. C. J. (2018). The Interrelationships of Land Plants and the Nature of the Ancestral Embryophyte. *Current Biology*, *28*(5), 733-745.e2. https://doi.org/10.1016/j.cub.2018.01.063

Qiu, J. L., Jilk, R., Marks, M. D., & Szymanski, D. B. (2002). The Arabidopsis SPIKE1 gene is required for normal cell shape control and tissue development. *Plant Cell*, *14*(1), 101–118. https://doi.org/10.1105/tpc.010346

Ramalho, J. J., Jones, V. A. S., Mutte, S., & Weijers, D. (2022). Pole position: How plant cells polarize along the axes. In *Plant Cell* (Vol. 34, Issue 1, pp. 174–192). Oxford Academic. https://doi.org/10.1093/plcell/koab203

Rasmussen, M. D., & Kellis, M. (2007). Accurate gene-tree reconstruction by learning gene- and species-specific substitution rates across multiple complete genomes. *Genome Research*, *17*(12), 1932–1942. https://doi.org/10.1101/gr.7105007

Ren, H., Dang, X., Yang, Y., Huang, D., Liu, M., Gao, X., & Lin, D. (2016). SPIKE1 activates ROP GTPase to modulate petal growth and shape. *Plant Physiology*, *172*(1), 358–371. https://doi.org/10.1104/pp.16.00788

Rensing, S. A. (2020). How Plants Conquered Land. *Cell*, *181*(5), 964–966. https://doi.org/10.1016/j.cell.2020.05.011

Sánchez-Baracaldo, P., Raven, J. A., Pisani, D., & Knoll, A. H. (2017). Early photosynthetic eukaryotes inhabited low-salinity habitats. *Proceedings of the National Academy of Sciences of the United States of America*, *114*(37), E7737–E7745. https://doi.org/10.1073/pnas.1620089114

Sauret-Güeto, S., Frangedakis, E., Silvestri, L., Rebmann, M., Tomaselli, M., Markel, K., Delmans, M., West, A., Patron, N. J., & Haseloff, J. (2020). Systematic Tools for Reprogramming Plant Gene Expression in a Simple Model, Marchantia polymorpha. *ACS Synthetic Biology*, *9*(4), 864–882. https://doi.org/10.1021/acssynbio.9b00511

Schaefer, A., Reinhard, N. R., & Hordijk, P. L. (2014). Toward understanding RhoGTPase specificity: Structure, function and local activation. *Small GTPases*, *5*(2). https://doi.org/10.4161/21541248.2014.968004

Scheffzek, K., Ahmadian, M. R., & Wittinghofer, A. (1998). GTPase-activating proteins: Helping hands to complement an active site. In *Trends in Biochemical Sciences* (Vol. 23, Issue 7, pp. 257–262). Elsevier Current Trends. https://doi.org/10.1016/S0968-0004(98)01224-9

Schepetilnikov, M., Makarian, J., Srour, O., Geldreich, A., Yang, Z., Chicher, J., Hammann, P., & Ryabova, L. A. (2017). GTPase ROP 2 binds and promotes activation of target of rapamycin, TOR , in response to auxin. *The EMBO Journal*, *36*(7), 886–903. https://doi.org/10.15252/embj.201694816

Schott, D. H., Collins, R. N., & Bretscher, A. (2002). Secretory vesicle transport velocity in living cells depends on the myosin-V lever arm length. *Journal of Cell Biology*, *156*(1), 35–39. https://doi.org/10.1083/jcb.200110086

Shimamura, M. (2016). Marchantia polymorpha: Taxonomy, phylogeny and morphology of a model system. *Plant and Cell Physiology*, *57*(2), 230–256. https://doi.org/10.1093/pcp/pcv192

Skokan, R., Medvecká, E., Viaene, T., Vosolsobě, S., Zwiewka, M., Müller, K., Skůpa, P., Karady, M., Zhang, Y., Janacek, D. P., Hammes, U. Z., Ljung, K., Nodzyński, T., Petrášek, J., & Friml, J. (2019). PIN-driven auxin transport emerged early in streptophyte evolution. *Nature Plants*, *5*(11), 1114–1119.

https://doi.org/10.1038/s41477-019-0542-5

Sommer, A., Hoeftberger, M., Hoepflinger, M. C., Schmalbrock, S., Bulychev, A., & Foissner, I. (2015). Convoluted plasma membrane domains in the green alga chara are depleted of microtubules and actin filaments. *Plant and Cell Physiology*, *56*(10), 1981–1996. https://doi.org/10.1093/pcp/pcv119

Sorek, N., Gutman, O., Bar, E., Abu-Abied, M., Feng, X., Running, M. P., Lewinsohn, E., Ori, N., Sadot, E., Henis, Y. I., & Yalovsky, S. (2011). Differential effects of prenylation and S-acylation on type I and II ROPS membrane interaction and function. *Plant Physiology*, *155*(2), 706–720. https://doi.org/10.1104/pp.110.166850

Sørensen, I., Pettolino, F. A., Bacic, A., Ralph, J., Lu, F., O'Neill, M. A., Fei, Z., Rose, J. K. C., Domozych, D. S., & Willats, W. G. T. (2011). The charophycean green algae provide insights into the early origins of plant cell walls. *Plant Journal*, *68*(2), 201–211. https://doi.org/10.1111/j.1365-313X.2011.04686.x

Stöckle, D., Herrmann, A., Lipka, E., Lauster, T., Gavidia, R., Zimmermann, S., & Müller, S. (2016). Putative RopGAPs impact division plane selection and interact with kinesin-12 POK1. *Nature Plants*, *2*(9). https://doi.org/10.1038/nplants.2016.120

Sugano, S. S., Nishihama, R., Shirakawa, M., Takagi, J., Matsuda, Y., Ishida, S., Shimada, T., Hara-Nishimura, I., Osakabe, K., & Kohchi, T. (2018). Efficient CRISPR/Cas9-based genome editing and its application to conditional genetic analysis in Marchantia polymorpha. *PLoS ONE*, *13*(10), e0205117. https://doi.org/10.1371/journal.pone.0205117

Szymanski, D. B., & Cosgrove, D. J. (2009). Dynamic Coordination of Cytoskeletal and Cell Wall Systems during Plant Cell Morphogenesis. *Current Biology*, *19*(17), R800–R811. https://doi.org/10.1016/j.cub.2009.07.056

Takeuchi, H., & Higashiyama, T. (2016). Tip-localized receptors control pollen tube growth and LURE sensing in Arabidopsis. *Nature*, *531*(7593), 245–248. https://doi.org/10.1038/nature17413

Technau, U., & Genikhovich, G. (2018). Evolution: Directives from Sea Anemone Hox Genes. *Current Biology*, *28*(22), R1303–R1305. https://doi.org/10.1016/j.cub.2018.09.040

The Tomato Genome Consortium. (2012). The tomato genome sequence provides insights into fleshy fruit evolution. *Nature*, *485*(7400), 635–641. https://doi.org/10.1038/nature11119

Thole, J. M., Perroud, P. F., Quatrano, R. S., & Running, M. P. (2014). Prenylation is required for polar cell elongation, cell adhesion, and differentiation in Physcomitrella patens. *Plant Journal*, *78*(3), 441–451. https://doi.org/10.1111/tpj.12484

Tofanelli, R., Vijayan, A., Scholz, S., & Schneitz, K. (2019). Protocol for rapid clearing and staining of fixed Arabidopsis ovules for improved imaging by confocal laser scanning microscopy. *Plant Methods*, *15*(1), 120. https://doi.org/10.1186/s13007-019-0505-x

Tolliday, N., VerPlank, L., & Li, R. (2002). Rho1 directs formin-mediated actin ring assembly during budding yeast cytokinesis. *Current Biology*, *12*(21), 1864–1870. https://doi.org/10.1016/S0960-9822(02)01238-1

Trifinopoulos, J., Nguyen, L. T., von Haeseler, A., & Minh, B. Q. (2016). W-IQ-TREE: a fast online phylogenetic tool for maximum likelihood analysis. *Nucleic Acids Research*, *44*(W1), W232–W235. https://doi.org/10.1093/NAR/GKW256

Tsekos, I. (1999). The sites of cellulose synthesis in algae: Diversity and evolution of cellulose-synthesizing enzyme complexes. In *Journal of Phycology* (Vol. 35, Issue 4, pp. 635–655). John Wiley & Sons, Ltd. https://doi.org/10.1046/j.1529-8817.1999.3540635.x

Turing, A. M. (1952). The chemical basis of morphogenesis. *Philosophical Transactions of the Royal Society of London. Series B, Biological Sciences*, *237*(641), 37–72. https://doi.org/10.1098/rstb.1952.0012

Umen, J. G. (2014). Green Algae and the Origins of Multicellularity in the Plant Kingdom. *Cold Spring Harbor Perspectives in Biology*, *6*(11), a016170. https://doi.org/10.1101/cshperspect.a016170

Ursache, R., Andersen, T. G., Marhavý, P., & Geldner, N. (2018). A protocol for combining fluorescent proteins with histological stains for diverse cell wall components. *Plant Journal*, *93*(2), 399–412. https://doi.org/10.1111/tpj.13784

Valentine, J. W., Collins, A. G., & Meyer, C. P. (1994). Morphological complexity increase in metazoans. *Paleobiology*, *20*(2), 131–142. https://doi.org/10.1017/S0094837300012641

van Baren, M. J., Bachy, C., Reistetter, E. N., Purvine, S. O., Grimwood, J., Sudek, S., Yu, H., Poirier, C., Deerinck, T. J., Kuo, A., Grigoriev, I. V., Wong, C. H., Smith, R. D., Callister, S. J., Wei, C. L., Schmutz, J., & Worden, A. Z. (2016). Evidence-based green algal genomics reveals marine diversity and ancestral characteristics of land plants. *BMC Genomics*, *17*(1), 1–22. https://doi.org/10.1186/s12864-016-2585-6

van Dop, M., Fiedler, M., Mutte, S., de Keijzer, J., Olijslager, L., Albrecht, C., Liao, C. Y., Janson, M. E., Bienz, M., & Weijers, D. (2020). DIX Domain Polymerization Drives Assembly of Plant Cell Polarity Complexes. *Cell*, *180*(3), 427-439.e12. https://doi.org/10.1016/j.cell.2020.01.011

Vetter, I. R., & Wittinghofer, A. (2001). The guanine nucleotide-binding switch in three dimensions. In *Science* (Vol. 294, Issue 5545, pp. 1299–1304). American Association for the Advancement of Science. https://doi.org/10.1126/science.1062023

Villarreal A., J. C., Crandall-Stotler, B. J., Hart, M. L., Long, D. G., & Forrest, L. L. (2016). Divergence times and the evolution of morphological complexity in an early land plant lineage (Marchantiopsida) with a slow molecular rate. *New Phytologist*, *209*(4), 1734–1746. https://doi.org/10.1111/nph.13716

Waaland, S. D., & Waaland, J. R. (1975). Analysis of cell elongation in red algae by fluorescent labelling. *Planta*, *126*(2), 127–138. https://doi.org/10.1007/BF00380616

Wang, S., Li, L., Li, H., Sahu, S. K., Wang, H., Xu, Y., Xian, W., Song, B., Liang, H., Cheng, S., Chang, Y., Song, Y., Çebi, Z., Wittek, S., Reder, T., Peterson, M., Yang, H., Wang, J., Melkonian, B., … Liu, X. (2020). Genomes of early-diverging streptophyte algae shed light on plant terrestrialization. *Nature Plants*, *6*(2), 95–106. https://doi.org/10.1038/s41477-019-0560-3

Wasteneys, G. O., & Williamson, R. E. (1992). Microtubule organization differs between acid and alkaline bands in internodal cells of Chara but bands can develop in the absence of microtubules. *Planta*, *188*(1), 99–105. https://doi.org/10.1007/BF01160718

Wennerberg, K., Rossman, K. L., & Der, C. J. (2005). The Ras superfamily at a glance. *Journal of Cell Science*, *118*(5), 843–846. https://doi.org/10.1242/jcs.01660

Whitewoods, Chris D., Cammarata, J., Nemec Venza, Z., Sang, S., Crook, A. D., Aoyama, T., Wang, X. Y., Waller, M., Kamisugi, Y., Cuming, A. C., Szövényi, P., Nimchuk, Z. L., Roeder, A. H. K., Scanlon, M. J., & Harrison, C. J. (2018). CLAVATA Was a Genetic Novelty for the Morphological Innovation of 3D Growth in Land Plants. *Current Biology*, 2365–2376. https://doi.org/10.1016/j.cub.2018.05.068

Whitewoods, Christopher D., & Coen, E. (2017). Growth and Development of Three-Dimensional Plant Form. In *Current Biology* (Vol. 27, Issue 17, pp. R910–R918). Elsevier. https://doi.org/10.1016/j.cub.2017.05.079

Winge, P., Brembu, T., Kristensen, R., & Bones, A. M. (2000). Genetic structure and evolution of RAC-GTPases in Arabidopsis thaliana. *Genetics*, *156*(4), 1959–1971.

Wloka, C., & Bi, E. (2012). Mechanisms of cytokinesis in budding yeast. *Cytoskeleton*, *69*(10), 710–726. https://doi.org/10.1002/cm.21046

Woods, B., & Lew, D. J. (2019). Polarity establishment by Cdc42: Key roles for positive feedback and differential mobility. *Small GTPases*, *10*(2), 130–137. https://doi.org/10.1080/21541248.2016.1275370

Worden, A. Z., Lee, J. H., Mock, T., Rouzé, P., Simmons, M. P., Aerts, A. L., Allen, A. E., Cuvelier, M. L., Derelle, E., Everett, M. V., Foulon, E., Grimwood, J., Gundlach, H., Henrissat, B., Napoli, C., McDonald, S. M., Parker, M. S., Rombauts, S., Salamov, A., … Grigoriev, I. V. (2009). Green evolution and dynamic adaptations revealed by genomes of the marine picoeukaryotes micromonas. *Science*, *324*(5924), 268–272. https://doi.org/10.1126/science.1167222

Wu, C.-F., Chiou, J.-G., Minakova, M., Woods, B., Tsygankov, D., Zyla, T. R., Savage, N. S., Elston, T. C., & Lew, D. J. (2015). Role of competition between polarity sites in establishing a unique front. *ELife*, *4*. https://doi.org/10.7554/elife.11611

Wu, G., Li, H., & Yang, Z. (2000). Arabidopsis RopGAPs are a novel family of Rho GTPase-activating proteins that require the Cdc42/Rac-interactive binding motif for Rop-specific GTPase stimulation.

Plant Physiology, *124*(4), 1625–1636. https://doi.org/10.1104/pp.124.4.1625

Wu, H., Turner, C., Gardner, J., Temple, B., & Brennwald, P. (2010). The Exo70 subunit of the exocyst is an effector for both Cdc42 and Rho3 function in polarized exocytosis. *Molecular Biology of the Cell*, *21*(3), 430–442. https://doi.org/10.1091/mbc.E09-06-0501

Xu, T., Wen, M., Nagawa, S., Fu, Y., Chen, J. G., Wu, M. J., Perrot-Rechenmann, C., Friml, J., Jones, A. M., & Yang, Z. (2010). Cell surface- and Rho GTPase-based auxin signaling controls cellular interdigitation in Arabidopsis. *Cell*, *143*(1), 99–110. https://doi.org/10.1016/j.cell.2010.09.003

Yanagisawa, M., Alonso, J. M., & Szymanski, D. B. (2018). Microtubule-Dependent Confinement of a Cell Signaling and Actin Polymerization Control Module Regulates Polarized Cell Growth. *Current Biology*, *28*(15), 2459-2466.e4. https://doi.org/10.1016/j.cub.2018.05.076

Yang, Z., & Watson, J. C. (1993). Molecular cloning and characterization of rho, a ras-related small GTP-binding protein from the garden pea. *Proceedings of the National Academy of Sciences of the United States of America*, *90*(18), 8732–8736. https://doi.org/10.1073/pnas.90.18.8732

Yi, P., & Goshima, G. (2020). Rho of Plants GTPases and Cytoskeletal Elements Control Nuclear Positioning and Asymmetric Cell Division during Physcomitrella patens Branching. *Current Biology*, *30*(14), 2860-2868.e3. https://doi.org/10.1016/j.cub.2020.05.022

Yoshida, S., van der Schuren, A., van Dop, M., van Galen, L., Saiga, S., Adibi, M., Möller, B., ten Hove, C. A., Marhavy, P., Smith, R., Friml, J., & Weijers, D. (2019). A SOSEKI-based coordinate system interprets global polarity cues in Arabidopsis. In *Nature Plants* (Vol. 5, Issue 2, pp. 160–166). Palgrave Macmillan Ltd. https://doi.org/10.1038/s41477-019-0363-6

You, C., Cui, J., Wang, H., Qi, X., Kuo, L. Y., Ma, H., Gao, L., Mo, B., & Chen, X. (2017). Conservation and divergence of small RNA pathways and microRNAs in land plants. *Genome Biology*, *18*(1), 1–19. https://doi.org/10.1186/s13059-017-1291-2

Zhang, J., Fu, X. X., Li, R. Q., Zhao, X., Liu, Y., Li, M. H., Zwaenepoel, A., Ma, H., Goffinet, B., Guan, Y. L., Xue, J. Y., Liao, Y. Y., Wang, Q. F., Wang, Q. H., Wang, J. Y., Zhang, G. Q., Wang, Z. W., Jia, Y., Wang, M. Z., … Chen, Z. D. (2020). The hornwort genome and early land plant evolution. *Nature Plants*, *6*(2), 107–118. https://doi.org/10.1038/s41477-019-0588-4

Zhang, Y., Rodriguez, L., Li, L., Zhang, X., & Friml, J. (2020). Functional innovations of PIN auxin transporters mark crucial evolutionary transitions during rise of flowering plants. *Science Advances*, *6*(50), 8895–8906. https://doi.org/10.1126/sciadv.abc8895

Zhao, F., Du, F., Oliveri, H., Zhou, L., Ali, O., Chen, W., Feng, S., Wang, Q., Lü, S., Long, M., Schneider, R., Sampathkumar, A., Godin, C., Traas, J., & Jiao, Y. (2020). Microtubule-Mediated Wall Anisotropy Contributes to Leaf Blade Flattening. *Current Biology*, *30*(20), 3972-3985.e6. https://doi.org/10.1016/j.cub.2020.07.076

Zheng, Z. L., & Yang, Z. (2000). The Rop GTPase: An emerging signaling switch in plants. *Plant Molecular Biology*, *44*(1), 1–9. https://doi.org/10.1023/A:1006402628948

Appendices

Name	ID	Sequence (5' to 3')	Category	Description
sgRNA1_MpROP_Fw	HM03	CTCGCTGAAGTTATCGAACACGG	cloning CRISPR constructs to mutagenise Mp *ROP*	sgRNA1 target sequence
sgRNA1_MpROP_Rv	HM04	AAACCCGTGTTCGATAACTTCAG		sgRNA1 target sequence
sgRNA2_MpROP_Fw	HM05	CTCGTTGTGATAGGAGCAGCGCC		sgRNA2 target sequence
sgRNA2_MpROP_Rv	HM06	AAACGGCGCTGCTCCTATCACAA		sgRNA2 target sequence
sgRNA3_MpROP_Fw	HM07	CTCGGGCTGCAGAACGACCTTTA		sgRNA3 target sequence
sgRNA3_MpROP_Rv	HM08	AAACTAAAGGTCGTTCTGCAGCC		sgRNA3 target sequence
SacI-NOS_Fw	HM09	GATCCCCGGGTACCGAGCTCGAATTTCCCCGATCGTTCAA	cloning MpROP transcriptional and translational reporter constructs	amplify NOS terminator for *proMpROP:NLS-Venus*
NOS-EcoRI_Rv	HM10	CCATGATTACGAATTCAGTTAGCTCACTCATTAGGC		amplify NOS terminator for *proMpROP:NLS-Venus*
MpROP_NOS_Fw	HM16	ATTTTGTTCAAAAGGAGCTCGAATTTCCCCGATCGTTCAA		amplify NOS terminator for *proMpROP:Venus-MpROP*
NOS-EcoRI_Rv	HM17	TATGACCATGATTACGAATTCAGTTAGCTCACTCATTAGGC		amplify NOS terminator for *proMpROP:Venus-MpROP*
BsrGI-MpROP_Fw	HM14	TAGAGGATCCCCGGGTACCGCTGTACAAGATGAGTACTTCCAGGTTTAT		amplify MpROP for *proMpROP:Venus-MpROP*
MpROP-SacI_Rv	HM15	GAGCTCCTTTTGAACAAAATCACAGG		amplify MpROP for *proMpROP:Venus-MpROP*
SalI-pMpROP_Fw	HM18	CTTGCATGCCTGCAGGTCGACGTCACATCCTTTTCTCGCAC		amplify MpROP promoter (4.9kb)
pMpROP_Rv	HM19	TGTTCACTCCTAAAAGAACTTTGGC		amplify MpROP promoter (4.9kb)
pMpROP-YFP_Fw	HM20	AGTTCTTTTAGGAGTGAACAATGGTGAGCAAGGGCGAGGA		amplify Venus YFP for *proMpROP:Venus-MpROP*
YFP-BsrGI_Rv	HM21	TGGAAGTACTCATCTTGTACAGCTCGTCCATGC		amplify Venus YFP for *proMpROP:Venus-MpROP*
pMpROP-NLS-YFP_Fw	HM39	AGTTCTTTTAGGAGTGAACAATGGCTCCCAAGAAGAAGAG		amplify NLS-YFP for *proMpROP:NLS-Venus*
NOS-SacI-YFP_Rv	HM40	TGAACGATCGGGGAAATTCGAGCTCTTACTTGTACAGCTCGTCCA		amplify NLS-YFP for *proMpROP:NLS-Venus*
pMpROP_fragment1_Fw	HM67	AGGCTCTTCGTCTCGGGAGATTCAGGTTCAAGGTAAAAATC	cloning complementation constructs	amplify Mp *ROP* promoter sequence (4kb) in four fragments to domesticate internal *Bsa* I and *Sap* I sites
pMpROP_fragment1_Rv	HM55	CAGCTCTTCGGTCGCCTTTCCAGATTTTGTCC		
pMpROP_fragment2_Fw	HM56	CTGCTCTTCAGACCTGCCCGTTGGTCGACATAAC		
pMpROP_fragment2_Rv	HM57	ACGCTCTTCACACGAGTGTCAAAGCT		
pMpROP_fragment3_Fw	HM58	CTGCTCTTCCGTGTGAATAGCGTGGTATCCCTC		
pMpROP_fragment3_Rv	HM76	CAGCTCTTCCAATGAAGAACAATAGCAACCGGCA		
pMpROP_fragment4_Fw	HM75	TTGCTCTTCAATTGTCTCTTTCTGTGACAC		
pMpROP_fragment4_Rv	HM63	CTGCTCTTCGTCTCCCATTGTTCACTCCTAAAAGAACTTTGGC		
MpROP Seq1_Rv	HM26	TTACTCACTGTGGGGAAGGT	colony PCR & Sanger sequencing plasmids	to validate successful cloning and confirm sequence
MpROP Seq2_Fw	HM32	GCCAGAAGACCTTGTTTTCC		
MpROP Seq3_Rv	HM33	CCACCTGTTCGAATGTCAAC		
MpROP Seq4_Fw	HM27	ACACTCAAGCTTCTGGCACA		
pMpROP Seq1_Rv	HM28	CTTGACGAATGTACGCATGG		
pMpROP Seq2_Fw	HM29	TCGTCTCCGAAGTTCTGCTT		
pMpROP Seq3_Fw	HM35	AGGGGCCATGCTAATCTTCT		
pMpROP Seq4_Fw	HM36	AGATAACGACACCTGCCAAG		
pMpROP Seq5_Fw	HM37	GCCGAATGCCATGACTTTAT		
pMpROP Seq6_Fw	HM38	GCGTGTGGGTAACGGTTAGT		
pMpROP Seq7_Rv	HM74	CGGAAGAAGCTGTGTCCAATCTCT		
pMpROP Seq8_Rv	HM73	CGCGAGCCTTCAATTATTTC		
NOS-Seq_Rv	HM13	GACCGGCAACAGGATTCAAT		
pMpUBR2_Seq Rv	HM77	CGGTTTCGCATTTAGTGGTTG		
M13F	-	TGTAAAACGACGGCCAGT		
M13R	-	CAGGAAACAGCTATGAC		
UAP_F	-	CTCGAGTGCCACCTGACGTCTAAGAAAC		
UAP_R	-	CGAGGAAGCCTGCATAACGCGAAGTAATC		
pC_F	-	GCAACGCTCTGTCATCGTTAC		
pC_R	-	GTAACTTAGGACTTGTGCGACATGTC		
sgRNA1_PCR_Fw	HM41	CGTCACAGGTCGTAGATCTTCT	Mp *rop* genotyping	amplify genomic region targeted by sgRNA1
sgRNA1_PCR_Rv	HM42	GCCTTACTGATAAGGGAGAAGG		amplify genomic region targeted by sgRNA1
sgRNA1_Seq_Fw	HM43	TCCGAAGTTCTGCTTGAAGG		sequence genomic region targeted by sgRNA1
sgRNA2_PCR_Fw	HM45	TGAGACACTATGCACCTCTGGT		amplify genomic region targeted by sgRNA2
sgRNA2_PCR_Rv	HM46	ACAGTTTATGTCTCCCGACGAG		amplify genomic region targeted by sgRNA2
sgRNA2_Seq_Fw	HM47	AGCCTGCCCTTCACATTGTA		sequence genomic region targeted by sgRNA2
sgRNA3_PCR_Fw	HM48	CAGGAGAGTTAGCGTCCTTCAT		amplify genomic region targeted by sgRNA3
sgRNA3_PCR_Rv	HM49	CCTCCTGGGCTTTACATCCTAT		amplify genomic region targeted by sgRNA3
sgRNA3_Seq_Fw	HM50	CGTGCCAAGAACGCTAGATT		sequence genomic region targeted by sgRNA3
MpROP_cDNA_Fw	HM78	GTGAACAATGAGTACTTCCAGG		amplify whole Mp *ROP* CDS from cDNA
MpROP_cDNA_Rv	HM79	CTTCACAGGATGGAACATGTC		amplify whole Mp *ROP* CDS from cDNA
MpROP_cDNA_Fw2	HM80	CTGTTGGGAAGACATGTATGC		sequence Mp *ROP* cDNA

Table A1 Primers used in this thesis

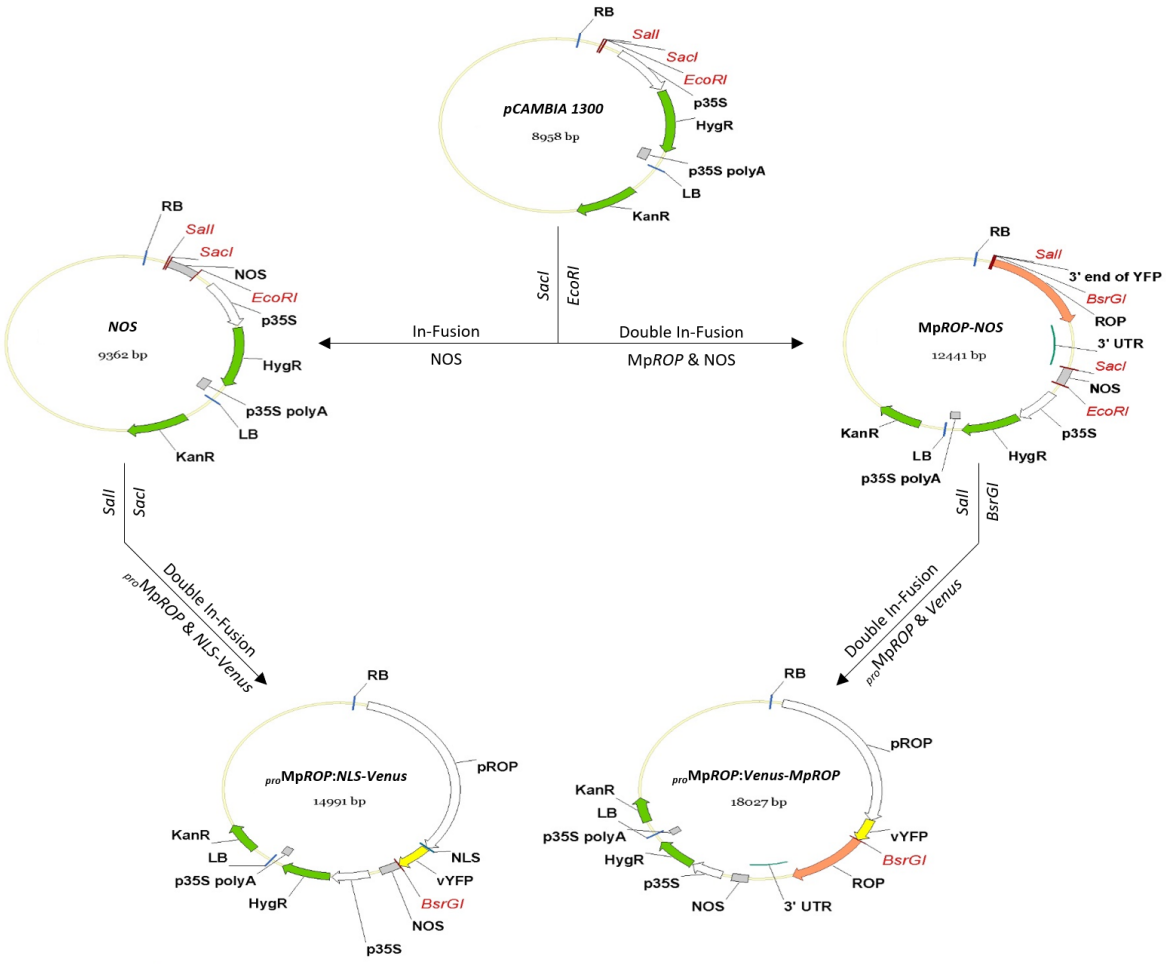

Figure A1 Cloning of Mp*ROP* transcriptional and translational reporter constructs